NELSON MANDELA

UNIVERSITY

Combined Additive Manufacturing and Machining for Large-Scale Prototyping for Minimising Material Wastage

Masters Research Dissertation

For the qualification

Master of Engineering (Mechanical)

Department of Mechanical Engineering

Faculty of Engineering, the Built Environment and Technology

Nelson Mandela University

By

Kyle Joshua Taylor

Student Number: 215293509

-

March 2022

Supervisor: Professor Russell Phillips

NELSON MANDELA

UNIVERSITY

DECLARATION BY CANDIDATE

NAME: *KYLE JOSHUA TAYLOR*

STUDENT NUMBER: *215293509*

QUALIFICATION: *MASTER OF ENGINEERING (MECHANICAL)*

TITLE OF PROJECT: *COMBINED ADDITIVE MANUFACTURING AND MACHINING FOR LARGE-SCALE PROTOTYPING FOR MINIMISING MATERIAL WASTAGE*

DECLARATION:

In accordance with Rule G5.6.3, I hereby declare that the above-mentioned treatise/ dissertation/ thesis is my own work and that it has not previously been submitted for assessment to another University or for another qualification.

SIGNATURE: *KTaylor*

DATE: 16/03/2022

Acknowledgements

I would like to thank the following people:

My supervisor, Professor Russell Phillips, for his support and guidance throughout this research. When faced with a challenge, you would help derive a solution to overcome the obstacle and move forward. Your determination and "never give up" attitude has inspired me significantly.

MerSETA and Karl du Preez for providing the funding for this research project, without which the necessary tools and equipment could not have been obtained.

Damian Mooney for providing me with an alternative solution each time I ran into a problem. Your patience and enthusiasm towards all projects in the lab create a constructive and positive work environment. Thanks to you, I now know how to *correctly* use a hot glue gun.

SPD - Jacques Welgemoed, Kabelo Mpurwana, Jan Hendrik de Jongh, Jarryd Steele, James Sewell. Thank you for all your contributions and the much appreciated constructive criticism during this research. Our end of the week board meetings were instrumental in the completion of this research.

My parents, Russell and Olga Taylor, for your constant support (technical, emotional & financial), love and encouragement throughout this research. My sister, Kelly Louw, for always believing in me and constantly checking in on how things were going. Dave Foaden, for your suggestions and technical advice towards the research.

Raechel Thompson, for your years of unconditional love and support, without which I may never have concluded this research project. You motivated me to focus on one thing at a time and not let the fear of failure prevent me from achieving the final goal.

Abstract

This research project aimed to develop a combined additive and subtractive manufacturing platform capable of rapidly producing large-scale prototypes for minimising material wastage. A design conceptualisation process led to the design and development of a system to deposit the additive material. The developed system was mounted to a large-scale CNC milling machine. This combination of additive and subtractive manufacturing into a single system integrated the separate benefits of the two independent technologies. Mastercam was selected as the preferred CAD/CAM software package to generate toolpaths for the additive and subtractive processes. The Beckhoff HMI provided a user-friendly interface to interpret the generated G-code files, set the Work Coordinate System, and control user-defined parameters such as the feed rate. An in-depth statistical analysis of the developed platform's dimensional accuracy, repeatability, stability, and material wastage was performed. In addition, the effects of the independent adjustment of the subtractive manufacturing process parameters such as the spindle speed, feed rate, depth of cut and stepover distance were considered. Finally, a cycle time comparison was performed in producing a working prototype between the developed HM system and a commercially available 3D printer. This research provided a platform for further investigation into the ever-expanding applications and benefits of rapid prototyping.

Contents

List of Figures

List of Tables

List of Abbreviations

ISO	International Organization for Standardization
CNC	Computer Numerical Control
CAD	Computer-Aided Design
CAM	Computer-Aided Manufacturing
GDP	Gross Domestic Product
RP	Rapid Prototyping
RT	Rapid Tooling
RM	Rapid Manufacturing
SLA	Stereolithography
UV	Ultraviolet
STL	Standard Tessellation Language
FDM	Fused Deposition Modelling
SLS	Selective Laser Sintering
3DP	Three-Dimensional Printing
LOM	Laminated Object Manufacturing
AM	Additive Manufacturing
HM	Hybrid Manufacturing
R_{MR}	Material Removal Rate
HMI	Human-Machine Interface
PU	Polyurethane
MDF	Medium-Density Fibreboard
EDM	Electrical Discharge Machining
PPS	Pulses per Second
PCB	Printed Circuit Board
DAC	Digital-to-Analog Converter
ADC	Analog-to-Digital Converter
IDE	Integrated Development Environment
STP	Standard Temperature and Pressure
FSD	Full-Scale Deflection
WCS	Work Coordinate System
PBM	Parts by Mass
VFD	Variable-Frequency Drive
VTOL	Vertical Take-off and Landing
I/O	Input/Output

PLC	Programmable Logic Controller
CMOS	Complementary Metal-Oxide-Semiconductor
RC	Radio-Control
PW	Pulse Width
DMLS	Direct Metal Laser Sintering
PBF	Powder Bed Fusion

Chapter 1

Research Proposal and Overview

1.1 Introduction

This research project provided a suitable and cost-effective solution to the rising need for rapid prototyping by developing a platform capable of efficiently producing real-life models that may be used to obtain feedback regarding proposed designs. The proposed system combined additive and subtractive manufacturing into a one-setup system which removed the cost and additional space requirements of using two separate machines. The abilities of rapid prototyping to enhance product development are countless as new techniques and materials are continuously being researched. This research focused on the design conceptualisation and development of a hybrid manufacturing system to enhance the rapid prototyping capabilities of the Renewable Energy Research Group (RERG). This chapter discussed the research proposal and provided an overview of the dissertation structure.

1.2 Research Objective

The research objective was defined as the development of a combined additive and subtractive manufacturing platform capable of rapidly producing large-scale prototypes for minimising material wastage. This development was achieved by analysing existing hybrid manufacturing systems, determining a suitable deposition method for the additive material, and experimenting with parameters to produce repeatable products that complied with applicable standards (e.g., ISO 2768). These parameters included the flow rate of the additive material and the machining parameters.

1.3 Sub-Problems

The system's design included as many off-the-shelf components as possible to ensure interchangeability and reduce downtime if maintenance was required. The overall cost was kept to a minimum, and the operation did not endanger the operator or anyone within proximity to the machine. Listed below are the sub-problems that were considered to achieve the aim of this research project.

1.3.1 Sub-Problem 1

The material properties of the additive material were investigated to understand how the material would flow and cure to ensure that the material flowed in a controllable manner during the deposition processes. Then, a practical means of depositing this additive material with as minimal material wastage as possible was established.

1.3.2 Sub-Problem 2

The effects of various process parameters on the produced products were quantified. These parameters included, but were not limited to, the spindle rotational speed, feed rate, cutting depth, and the width of cut.

1.3.3 Sub-Problem 3

The necessary measurements to be taken were determined, and an appropriate experimental procedure was established to produce data that could be assessed and quantified.

1.3.4 Sub-Problem 4

A thorough statistical analysis of the data obtained from Sub-Problem 3 was performed to evaluate and quantify the overall performance of the developed platform. Finally, the findings were presented, and conclusions were drawn from these findings.

1.4 Hypothesis

It is envisaged that a large-scale rapid prototyping platform can be developed. This platform would be capable of repeatedly producing full-scale models which are dimensionally accurate, cost-effective, and stable. Furthermore, these full-scale models would reduce material wastage and cycle time by combining additive manufacturing and conventional manufacturing processes according to industry standards.

1.5 Delimitations

The following delimitations applied to this research project:

- ➢ Polyurethane foam was used as the additive material, and the research falls within the ambit of Polymer Additive Manufacturing.
- ➢ An existing large-scale CNC milling machine was used for the subtractive platform, and this research project did not focus on the design thereof. Therefore, the dimensional accuracy and repeatability of the developed hybrid platform were limited by the CNC machine's positional accuracy.
- ➢ The machining parameters depended on the CNC machine's capabilities (maximum spindle rotational speed and feed rate of 18000 RPM and 5m/min, respectively).

➢ Instead of a volume comparison, a mass comparison was computed to determine the material wastage of the developed system.

➢ Although the developed platform was capable of producing large-scale parts of up to 1600x1000x1500 mm in X, Y and Z, the parts produced to evaluate the system's overall performance for this research did not exceed 260 mm in dimension.

1.6 Significance of the Research

The findings obtained from this research project sought to contribute to the following:

➢ Industry

With refinement, the platform developed in this research project and the data used to analyse the effectiveness of such a large-scale, hybrid system could provide an opportunity for a more efficient and cost-effective alternative than current methods of rapid prototyping used in industry.

➢ Nelson Mandela University

This hybrid manufacturing method yielded minimised material wastage and holds potential benefits for development projects conducted within the Renewable Energy Research Group (RERG). In addition, once refined, the university may use the system to further expand its research into rapid prototyping due to the potential design capabilities offered by such a system.

1.7 Research Methodology

The following list detailed the research methodology:

1.7.1 Preliminary Research

A literature review regarding existing conventional manufacturing processes, AM technologies, and related research (academic and commercial) was conducted to understand how researchers in the field of rapid prototyping had overcome challenges encountered when implementing such a system.

1.7.2 Design Development and Construction

Once the preliminary research was complete, the design concepts of the system were developed and finalised. Once the design had been finalised, components were sourced, and the construction of the final design commenced. The final design was determined and evaluated through a design conceptualisation process.

1.7.3 Testing and Modifications

Various models were created using CAD software to test both the additive and subtractive capabilities of the system whilst adjusting the necessary parameters to obtain a prototype that could be compared to a set of pre-determined evaluation criteria. Changes to the physical design of the developed system were implemented if an optimal prototype was not achieved.

1.7.4 Analysis of Data

The dimensional accuracy, repeatability, stability, material wastage, and cycle time of the produced prototypes were recorded. Next, relationships were deduced based on the parameters used to arrive at the final product. Finally, the obtained results were used to improve the system further to achieve optimal performance.

1.8 Chapter Conclusion

This chapter provided an outline of what is to be expected from the research project. First, the research objective was to develop a combined additive and subtractive manufacturing platform for large-scale rapid prototyping for minimising material wastage. Next, the sub-problems, hypothesis, delimitations, and the significance of the research were discussed. Finally, a research methodology was defined as a guideline to meet the proposed research objective for this research project. Chapter 2 conducted a literature review pertaining to topics relevant to this research, as briefly outlined in Section 1.7.1.

Chapter 2

Literature Review

This chapter detailed the topics covered to compile the literature review for this research project. Commercially available systems, as well as relevant literature from authors in the same field, were reviewed.

2.1 Manufacturing and its Impact on the Economy

Statistics South Africa (Stats SA) defined the real GDP as "the total value of goods and services that are produced in an economy in a certain time period, with the term "real" indicating that the GDP has been adjusted to remove the effects of inflation."[1] These produced goods and services are divided into three sectors, namely [2]:

- ➢ Primary - agriculture and mining.
- ➢ Secondary - manufacturing, electricity, and construction.
- ➢ Tertiary - trade, transport, finance, government, and personal services.

Manufacturing is the fourth largest economic industry in South Africa, as shown in Figure 2.1 and contributes substantially to the overall Gross Domestic Product (GDP) of South Africa. It plays a crucial role in job creation and skills development in a struggling economy where the country's official unemployment rate is at its lowest value in the past 11 years – 23.3% [3].

Zalk [4] stated that South Africa achieved its highest rates of GDP growth post-World War II when the rate of real manufacturing growth was more significant than the rate of real GDP growth. The real manufacturing growth experienced was driven by three factors that have gradually fallen away over the years: inexpensive labour, competitive electricity supply due to an abundance of raw materials and government-backed incentives such as tariffs and subsidies [5] [6]. In addition, the introduction of globalisation created opportunities for other developing countries to develop internationally, which placed further strain on the South African economy to adapt and compete.
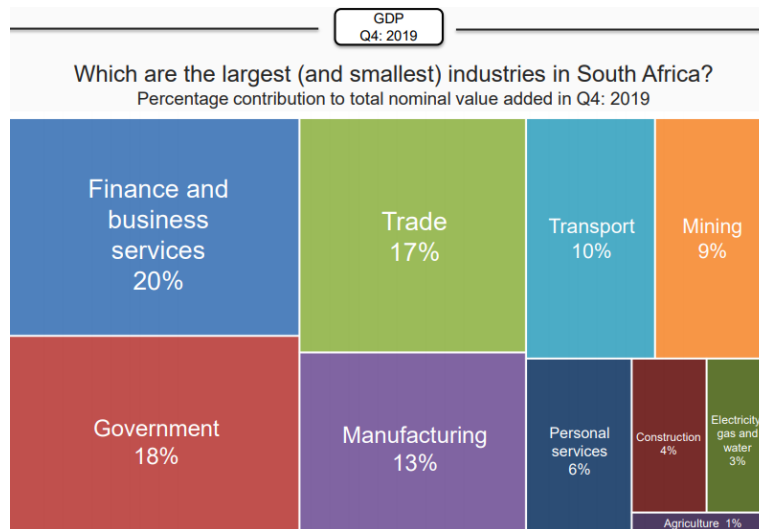
Figure 2.1: South African industries [2]

Various studies on the importance of manufacturing for overall economic development have been reviewed. As a result, the following conclusions were drawn [4] [7] [8] :

➤ Few countries have obtained a high standard of living without a booming manufacturing sector.

➤ Manufacturing growth is directly linked to the overall growth of an economy, especially in developing countries.

➤ Growth in the manufacturing sector has led to employment and growth in other economic sectors, such as services.

➤ New developments in the manufacturing sector accelerate technological progress, which in turn produces skilled labour.

➤ The manufacturing sector accumulates capital more readily and boasts a much higher productivity rate when compared to other sectors, such as agriculture.

2.2 Conventional Manufacturing Processes

Conventional manufacturing processes produce parts through three processing operations: shaping operations, property-enhancing operations, and surface processing operations [9]. Shaping operations change the geometry of the original workpiece to produce the required part. Typical shaping processes include machining, forging, and casting.

Property-enhancing operations are utilised to strengthen or alter a material's material properties without substantially deforming the part. Hardening via a heat treatment process is an example of a property-enhancing operation used to improve the mechanical properties of a part, such as the level of hardness.

Surface processing operations are applied to the surface of the final workpiece to improve its resistance to corrosion and wear. Typical surface processing operations include anodising, shot peening and electroplating [9]. The focus of the research, with respect to conventional manufacturing processes, was steered towards shaping processes, specifically CNC milling and CNC turning.

2.2.1 Computer Numerical Control (CNC) Milling

Parsons et al. [10] developed the first numerical control (NC) system and received a patent for the invention in 1958. Parsons et al. described the invention as: "a means for shaping and modifying work pieces and more particularly to a method of and means for automatically controlling machine tools, such as milling machines." This development sparked significant interest in CNC milling machines globally to accelerate production via autonomous machining in the manufacturing industry.

CAD software is used to model the 3D object to be manufactured through CNC milling. Next, CAM software is utilised to generate the toolpaths required to machine the object. Post-processing software is then used to convert the toolpaths into G-code and M-code, which the machine interprets. G-code refers to the programming language used to control a CNC machine's movement. M-code controls non-geometrical machine functions such as tool changes, switching the coolant on or off and ending the program [10]. The workpiece, generally a solid block, is clamped in place using a machine vice attached to the worktable. A spindle clamps the necessary cutting tools, such as face mills, end mills, ball mills, drills, and taps, to perform the required cutting operations and is capable of reaching high RPM values. When the operator starts the machining cycle, the spindle is raised and lowered along the Z-axis. The worktable, capable of movement in the X and Y axes, feeds the workpiece past the rotating cutting tool.

The G-code governs the X, Y and Z movements of the system. Upon completion of the cutting cycle, the workpiece may be removed from the machine vice, and the necessary post-processing, such as deburring of sharp edges, may commence.

A wide range of cutting tool materials are available, such as high-speed steels (HSS), tungsten carbides, ceramics, and diamonds, to name a few. This extensive range of cutting materials, along with high torque spindles, allows for nearly any material to be machined. Common metallic materials include aluminium, stainless steel, titanium, and carbon steel. Common non-metallic materials include woods, plastics, and foams.

CNC milling is capable of repeatedly producing complex geometries with high levels of dimensional accuracy. Process parameters such as spindle speed, feed, and cut depth determine the produced part's surface finish. Mirror-like surface finishes are achievable if the parameters mentioned above are optimised. Since the machines are capable of autonomous operation, many machines may be run by a single operator, saving time and money. Possible drawbacks of CNC milling include the large amount of material wastage involved in the subtractive process, the machine's high initial cost, and the necessary software. A schematic diagram of a CNC milling machine is shown in Figure 2.2 [12].
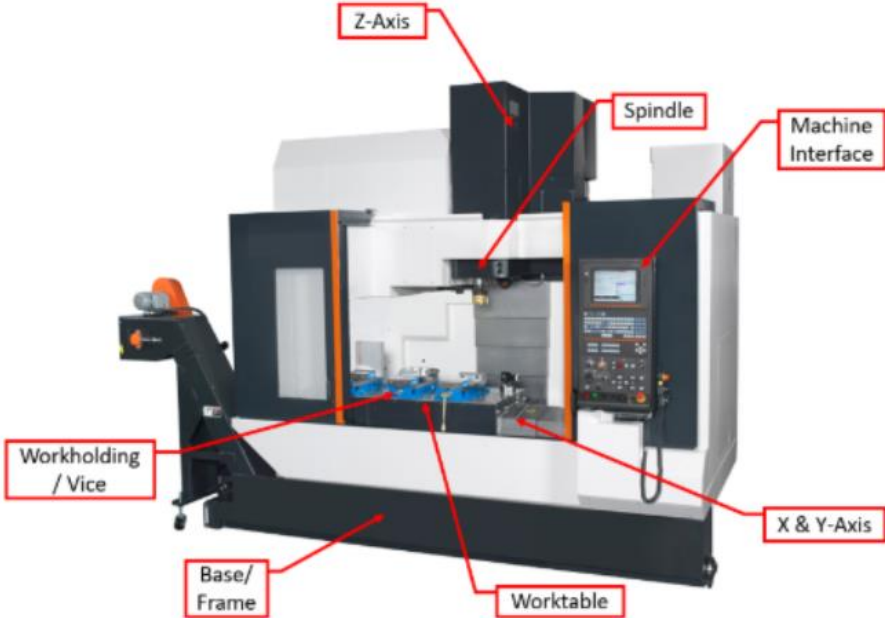
Figure 2.2: Schematic diagram of a CNC milling machine [11]

2.2.2 Computer Numerical Control (CNC) Turning

Turning is a subtractive machining process used to produce cylindrical parts by feeding a single-point cutting tool into the rotating workpiece to produce the required surface. A machine called a lathe is typically used to perform turning operations. CNC lathes automate turning operations and are suitable for high-volume production.

Similar to CNC milling, a 3D object is modelled, and toolpaths are generated using CAD and CAM software, respectively. A self-centring chuck uses jaws, commonly three-jaw or four-jaw, to clamp the rotating workpiece and is mounted to the lathe's headstock. Once the operator starts the machine cycle, the chuck rotates at the programmed RPM. A tool turret serves as an indexing tool holder for the cutting tools required to perform the machining operations. According to the generated M-code, the tool turret calls up the appropriate tool for the cutting operation. Afterwards, the cutting tool is fed into the rotating workpiece to remove material according to the G-code commands. Coolant is used for swarf removal and prevents the workpiece and the cutting tool from overheating. Once the machine cycle is complete, the operator may remove the workpiece from the chuck and load the next piece of material to be turned.

Various lathe cutting tools exist; these include facing tools, OD tools (roughing & finishing), boring bars, parting tools, threading tools, knurling tools, drills (standard & U-drills) and grooving tools. The various tools are used in conjunction to produce complex parts via numerous turning operations accurately. An example of a part produced by multiple turning operations and various lathe cutting tools is shown in Figure 2.3 [12].
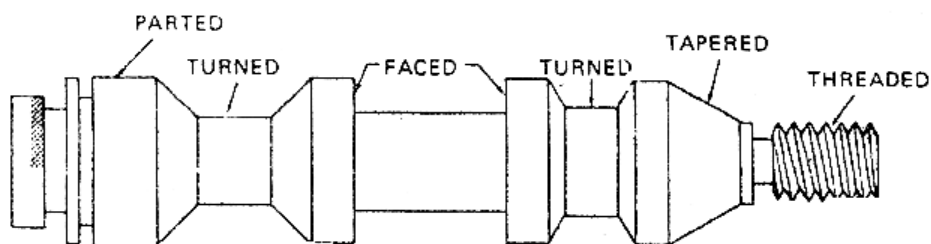
Figure 2.3: Complex part produced using various lathe cutting tools [12]

CNC turning, like milling, may be applied to a wide range of metallic and non-metallic materials. A bar feeder may be attached to a CNC lathe which automatically loads a new piece of material upon completion of a machining cycle. The addition of a bar feeder greatly accelerates production as the machine can run entirely autonomously, and the operator need only inspect the tool wear after long production runs. CNC turning is particularly beneficial to the aerospace, automotive and medical industries [13]. A schematic diagram of a CNC lathe is shown in Figure 2.4 [11].
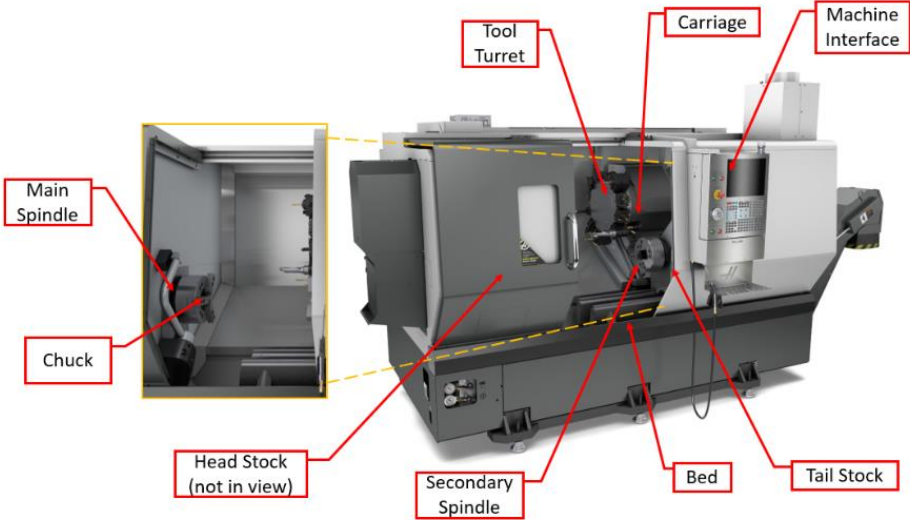
Figure 2.4: Schematic diagram of a CNC lathe [11]

2.3 Rapid Prototyping (RP)

Rapid prototyping has become increasingly popular over the last 30 years in manufacturing. It can be described as the process in which products are produced quickly and with a reduced material wastage to evaluate a design or concept [14]. The definition of RP is ever-changing as the various technologies continue to develop. Developed initially to produce prototype parts for design verification, RP has evolved into a technique capable of fabricating functional parts for real-world implementation. Whilst most conventional manufacturing methods involve the removal of material through subtractive machining processes such as milling or turning to produce parts, RP techniques commonly utilise additive manufacturing to produce parts.

Figure 2.5 illustrates the four critical aspects of rapid prototyping: input, material, applications, and method. The main applications are split up into either design, engineering and analysis or manufacturing and tools [15]. Many industries have experienced the benefits of RP, such as automotive, aerospace, and medical, to name a few [15] [16]. Campbell et al. [17] provided a more in-depth breakdown of the primary applications of RP and can be seen in Figure 2.6 [17].
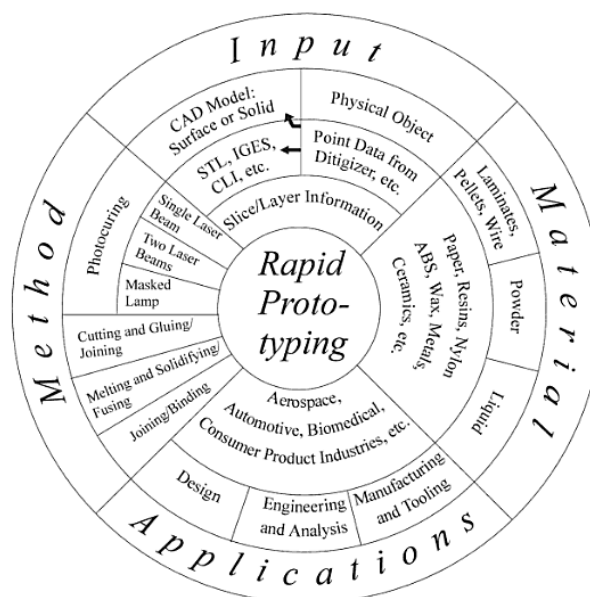
Figure 2.5: The key aspects of RP [15]
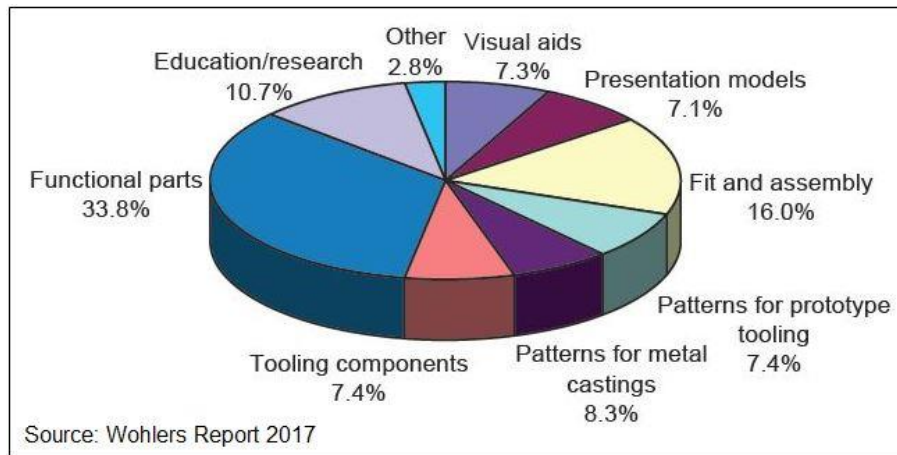
Figure 2.6: Primary applications of RP [17]

From Figure 2.6, it was observed that the primary applications of rapid prototyping were developing functional parts, fitting and assembly, and creating patterns for prototype tooling or metal castings [17]. However, further research and development into RP are expected to widen the range of applications through continuous modifications and improvements to existing technologies [16].

The benefits of RP can be grouped into direct and indirect benefits. The direct benefits of RP include [15] [18]:

➢ Geometric freedom. RP techniques can produce complex geometries that may not have been previously possible through conventional manufacturing methods. This geometric freedom permits designers to apply topology optimisation methods to their designs, which decreases the mass of parts and reduces material costs while supporting the applied loads.

➢ Cost. Conventional manufacturing processes are frequently used in conjunction with one another to produce a part, i.e., a cylindrical part is initially turned on a lathe and then taken to the milling machine to perform the final machining operations that were not possible on the conventional lathe. RP systems serve as general-purpose machines which reduce initial costs, maintenance expenses and require fewer operators.

➢ Design error detection. Early detection of design errors through prototypes eliminates the costly and time-consuming process of modifying production tooling.

The indirect benefits of RP include [15] [18]:

➢ Marketing. Prototypes produced via RP may be used as concept models for visual representations. As a result, potential future customers can physically interact with the product they intend to purchase. This interaction could increase customer confidence levels who may previously have been unsure about whether the product would suit their needs or not.

➢ Consumer benefits. Consumers have more freedom concerning geometry and material selection when designing parts. This design freedom enables consumers to achieve what they are looking for more closely without accommodating the necessary manufacturing processes.

➢ Innovation. The continuous evolution of RP has led to the creation of new technologies that are faster, cheaper to operate and support a broader range of materials. This innovation is essential if RP technologies are to overcome their existing limitations and compete with conventional manufacturing methods.

Rapid Tooling (RT) and Rapid Manufacturing (RM) are two examples of how RP continuously evolves and serves as a catalyst in bridging the gap between design conceptualisation and production.

Rapid Tooling utilises AM technologies such as Stereolithography to produce functional tools, moulds or dies with a decrease in cost and lead time and is achieved by either direct or indirect methods. In the case of direct tooling, the end product is produced directly utilising an RP process without the need for a pattern. Indirect tooling utilises pattern-based methods to produce a mould or die through appropriate RP techniques, which are then used to construct the tooling. Indirect tooling is the more commonly used method of RT, and typical processes include investment casting, vacuum casting, and injection moulding [16]. RT serves as a tool for bridge manufacturing which describes the stage in the process chain between the completion of a prototype and full-scale production. Poor surface finish and visible layer marks resulting from the staircase effect are common limitations encountered by the RT technology [18].

Rapid Manufacturing, otherwise known as Rapid Production, produces end-use parts directly without the need for additional manufacturing processes such as moulding, casting, forming, bending, or machining. The elimination of tooling in the RM process results in a decrease in overall cost and lead time. As a result, RM is suited for low-volume production runs, custom parts as per customer request, and complex geometries such as cavities or intricate surfaces [16]. However, the current absence of industrial-grade materials available for RM, coupled with an inferior dimensional accuracy compared to conventional manufacturing methods, are possible drawbacks of the technology.

A plug is an exact, positive representation of a finished model. First, an oversized block of stock material is cut to size using a saw or a hot wire cutter to create an original plug. Typical plug materials include MDF, clay and various foams [19]. Next, the stock material is loaded onto a CNC milling machine, producing the necessary shapes and features through subtractive manufacturing. Once the shape of the plug has been produced, layers of fibreglass and resin are added to reinforce the plug and produce a rigid shell. The plug is then sanded to produce a rough finish, after which the plug is coated with layers of putty. Then, the plug is re-machined to the final dimensions to produce an accurate, smooth model replica. Next, a layer of surfacing primer is sprayed onto the plug to fix any imperfections that may be present. Finally, the surfacing primer is sanded, and the plug is created [19]. The plug may then be used to create accurate fibreglass moulds for end products [20].

There are numerous categories of AM, which include the following [21]:

- Stereolithography
- Fused Deposition Modelling
- Selective Laser Sintering
- 3D Printing
- Laminated Object Manufacturing
- Direct Metal Laser Sintering

Each method of AM serves a different purpose and has different advantages and disadvantages that need to be considered when determining which method is best suited for the required application. The aforementioned methods of AM were discussed later in this chapter.

2.3.1 Stereolithography (SLA)

On March 11, 1986, Stereolithography was first introduced when Charles Hull obtained a patent for his developed system. Hull defined Stereolithography as "a method and apparatus for making solid objects by successively "printing" thin layers of a curable material, e.g., a UV curable material, one on top of the other."[22]

The stereolithography process begins with the conversion of a CAD generated solid model into a .STL file format which approximates the geometry of the part to be manufactured through a triangular mesh. An ultraviolet (UV) laser beam shines on a layer or surface of UV-curable resin, and the first layer of the .STL file is produced. The elevator lowers the build platform, covering the previously cured layer with a fresh layer of resin, and the next layer is formed and bonded to the layer below. A sweeper is used to level the resin between layers. The process is repeated until the part has been formed. The part is removed from the platform, and any support structures used to generate the part are removed. Finally, the part is placed into a UV curing oven to harden [22][21]. The schematic diagram of the SLA process can be seen in Figure 2.7 [23].
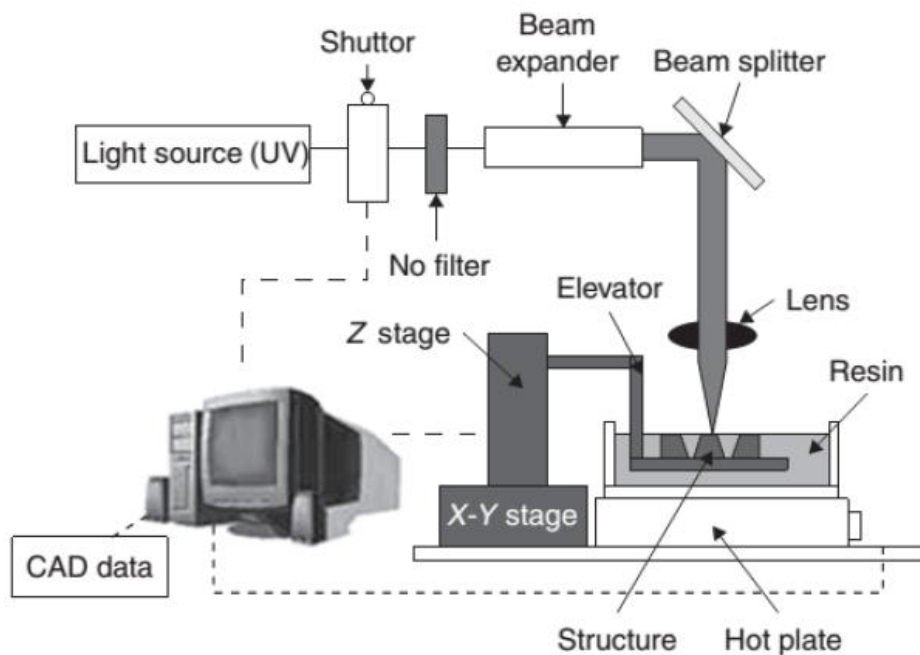
Figure 2.7: Schematic diagram of the SLA process [23]

2.3.1.1 Applications of SLA

Typical applications of SLA include:

➢ SLA may be used for concept models and form-fit testing [24].

➢ Medical models, such as dental implants, may be manufactured to assist surgeons in planning their procedures or to visualise the outcomes of operations [25].

➢ Injection moulding inserts, investment casting patterns and master patterns for low-volume production tooling may be manufactured using SLA [26].

2.3.1.2 Advantages of SLA

Advantages of SLA include:

➢ Produced parts have a smooth surface finish, and the cured layers are nearly invisible compared to the FDM process [27].

➢ SLA systems can produce functional parts at an accuracy of 20 μm [28].

➢ A wide range of materials are available.

➢ Large parts can be produced by splitting the entire part into smaller sections and then joining these sections together.

2.3.1.3 Disadvantages of SLA

Disadvantages of SLA include:

➢ Although many materials are available, photopolymer materials must be used.

➢ Toxic liquid resins may lead to skin irritation and respiratory problems.

➢ Support structures are required to generate the part.

➢ Parts produced by SLA require post-processing by removing support structures and placing the part into a UV curing oven to harden [21].

2.3.2 Fused Deposition Modelling (FDM)

Scott Crump invented Fused Deposition Modelling in 1989, and he received a patent for his invention on June 9, 1992 [29]. Since the expiration of the aforementioned patent in 2009, FDM has become the most widely used method of 3D printing, as stated by Palermo [30].

Like the SLA process, the FDM process begins with the conversion of a CAD generated solid model into a .STL file format. FDM slicing software is used to read the converted file and tweak parameters such as layer height, infill pattern and add support material to the necessary locations. Filament material, usually a thermoplastic, such as Polylactic Acid (PLA), Acrylonitrile Butadiene Styrene (ABS) or Polyethylene Terephthalate (PET), among others, enters the extruder where it is melted and pushed out through the extrusion nozzle [27]. The extrusion nozzle moves along the X and Y axes as it deposits the first layer of the part. Once the first layer has been formed, the build platform lowers itself by the user-defined layer height value, and the process is repeated layer-by-layer until the entire part has been created. A smaller extrusion nozzle diameter may be used to improve the level of detail of the produced part, whilst a larger extrusion nozzle may be used to increase printing speed on parts where precision or quality is not crucial [31]. The schematic diagram of the FDM process can be seen in Figure 2.8 [32].
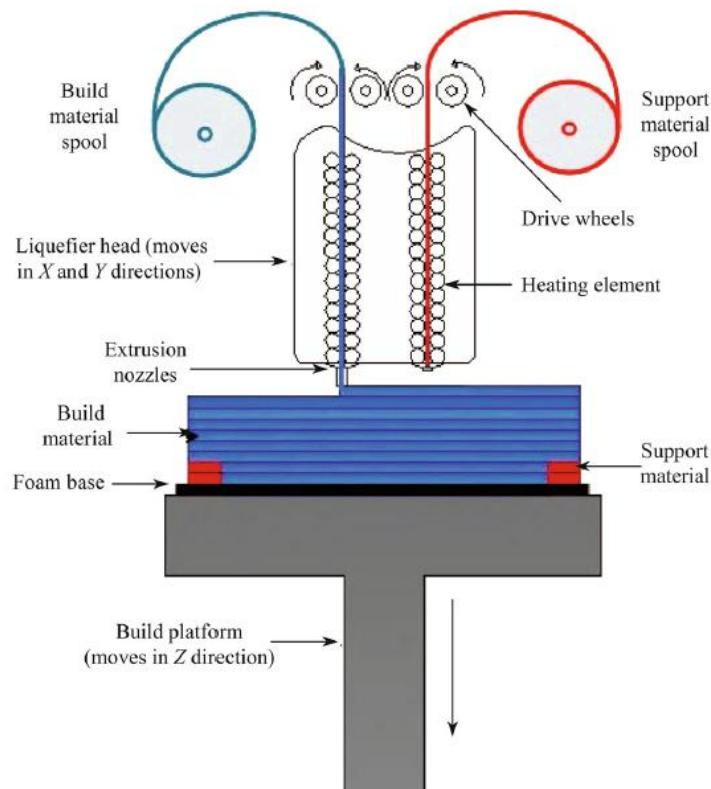
Figure 2.8: Schematic diagram of the FDM process [32]

2.3.2.1 Applications of FDM

Typical applications of FDM include:

➢ Concept models used in the early stages of the design conceptualisation process.

➢ Functional prototypes allow for testing in real-world environments [16].

➢ Jigs, fixtures and production tooling may be produced without any expensive tooling [16].

2.3.2.2 Advantages of FDM

Advantages of FDM include:

➢ A simple, low-cost method of rapidly producing parts.

➢ Numerous thermoplastic materials may be used, e.g., PLA, ABS, PET.

➢ The FDM process is comparatively safer than the other methods of AM as the operator is not exposed to toxic liquid resins or lasers.

➢ Dual head FDM printers allow for multicolour and multi-material parts to be produced.

➢ The filament spools can be changed quickly if the filament snaps or runs out.

➢ Designs may easily be scaled up or down to accommodate different size build platforms without losing accuracy.

2.3.2.3 Disadvantages of FDM

Disadvantages of FDM include:

➢ Dimensional accuracy is restricted by the type and diameter of the filament used.

➢ The extruded layers are visible with a much lower resolution than other AM processes.

➢ The FDM process involves heating the filament material to the point of melting and then allowing it to cool and set, leading to unpredictable shrinkage and distortion of the part [15].

➢ Support structures need to be included in the slicing software and removed upon completion of the print to produce complex geometries.

2.3.3 Selective Laser Sintering (SLS)

This section focused on Selective Laser Sintering of Polymer. SLS was invented by Deckard et al. [33] as a means of creating solid parts through a layer-by-layer additive manufacturing technique and is based on the principle of sintering. Deckard et al. [33] described sintering as: "a process by which particulates are made to form a solid mass through the application of external energy." A CO_2 laser is commonly utilised as this source of external energy.

The SLS additive manufacturing process (for polymers) begins by depositing a thin layer of powdered material onto the bed's surface. The surface is heated up to just below the material's melting point and then an external energy source, such as a CO_2 laser, sinters the powder. The unsintered powder supports the following layer and may be reused in later prints [34][27]. The CO_2 laser is directed to a reflective mirror that controls the laser's motion in the X-Y plane [18]. Upon completion of each layer, pistons are used to lower the build chamber whilst raising the powder supply chamber. A roller distributes the next layer of powder across the bed of the build chamber. The layer-by-layer process is repeated until the entire part has been produced. Czelusniak et al. [35] suggest that Polyamide 12, more commonly known as Nylon 12, is the most commonly used material for the SLS process. The schematic diagram of the SLS process can be seen in Figure 2.9 [27].

1 Laser
2 Scanning system
3 Powder container
4 Cylinder
5 Powder loading mechanism
6 Powder bed
7 Printed object
8 Motorized platform

Figure 2.9: Schematic diagram of the SLS process [27]

2.3.3.1 Applications of SLS

Typical applications of SLS include:

➢ Functional prototypes and form-fit testing.

➢ Investment casting patterns for short production runs [15].

➢ Visual representations for customers or items to display in a showroom.

➢ AM of metal tooling [15].

2.3.3.2 Advantages of SLS

Advantages of SLS include:

➢ Numerous materials may be used in the SLS process, including thermoplastics, metals and ceramics, which allows for countless design capabilities [15].

➢ As stated previously, unsintered powder serves as support material during the SLS (of polymer) process, which removes the need for additional support structures. As a result, the time required to produce the part decreases, and the process's post-processing phase is accelerated.

➢ Minimal material wastage as the unsintered powder may be reused.

➢ Since SLS (of polymer) does not depend on support material, complex geometries are easily produced.

2.3.3.3 Disadvantages of SLS

Disadvantages of SLS include:

➢ The CO_2 laser consumes a large amount of power during operation and requires a preheat and cool down cycle, increasing operation time.

➢ SLS is comparatively more expensive than other AM technologies like FDM and SLA [36].

➢ Awad et al. [37] suggested that unsintered powder may only be reused a limited number of times before the loss of chemical stability and physical changes are induced.

➢ The particle size of the powder substantially affects the surface finish and roughness of the part [15].

2.3.4 Three-Dimensional Printing (3DP)

Three-Dimensional Printing was developed and patented by Sachs et al. [38] at the Massachusetts Institute of Technology (MIT) in 1989. Z Corporation would obtain the license for the developed 3DP technology and produce their first 3D printer in 1996 [39]. Unlike the other AM processes mentioned thus far, Z Corporation chose not to assign a unique name to their technology. For this reason, the Three-Dimensional Printing process is often referred to as Binder Jetting (BJ) to avoid confusion with the other AM technologies [18].

The 3DP process is similar to the SLS process, except that an inkjet printhead replaces the CO_2 laser utilised in SLS. A powder roller spreads a layer across the powder bed by raising the powder supply chamber and lowering the build platform by one layer thickness. The inkjet printhead, controlled by the X-Y positioning mechanism, deposits liquid binder according to the commands provided by the 3DP software package to produce the desired part. The introduction of the liquid binder to the powder bonds the particles together and a single layer of the part is manufactured [34]. The process is repeated until the final layer is produced, upon which the completed part is left in the powder bed to allow the binder to set and the excess powder is removed [18][36]. Like SLS (of polymer), 3DP does not require additional support structures as the loose powder supports the part. The schematic diagram of the 3DP process can be seen in Figure 2.10 [40].
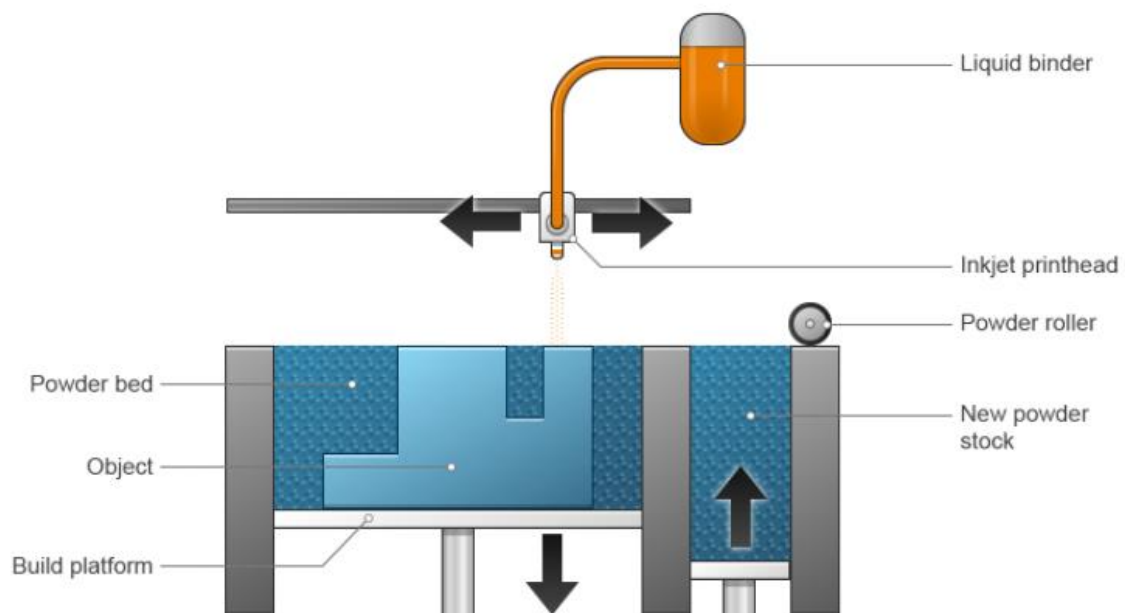
Figure 2.10: Schematic diagram of the 3DP process [40]

2.3.4.1 Applications of 3DP

Typical applications of 3DP include:

➢ Full-colour 3D models for visualisation purposes.

➢ Casting patterns to create moulds and cores for casting [36].

➢ Form-fit testing.

2.3.4.2 Advantages of 3DP

Advantages of 3DP include:

➢ Like SLS (of polymer), loose powder supports the part, and additional support structures are not required. This support-free technology allows for increased freedom when designing parts to be produced by 3DP.

➢ Various parts can be arranged within the slicing software and produced simultaneously.

➢ The 3DP process is fast, and additional printer nozzles may be added to augment the process. 3DP is therefore capable of producing large-scale prototypes as well [41].

➢ Coloured dyes allow for full-colour 3D models to be produced.

➢ Many materials are available, including metals, ceramics, glass and sand [42].

2.3.4.3 Disadvantages of 3DP

Disadvantages of 3DP include:

➢ Like SLS, the large size powder particles used produce a rough surface finish.

➢ Post-processing through infiltration is required to strengthen the mechanical properties of the manufactured part [36].

➢ Powder removal from complex parts with cavities may prove challenging [43].

➢ The layer-by-layer process creates a staircase effect on the produced part. This effect may be removed by polishing or sanding the affected surfaces; however, it should be noted that the dimensions and features will have been altered [43].

2.3.5 Laminated Object Manufacturing (LOM)

Michael Feygin invented Laminated Object Manufacturing in 1987, and he received a patent for his invention on June 21, 1988. Feygin defined LOM as: "a method for forming an integral three-dimensional object from laminations of the same or gradually varying shape."[44] Helisys would go on to commercialise LOM in 1991 [39].

A CAD generated solid model is sliced into thin 2D cross-sections by additive manufacturing software. The thickness of each cross-section is equivalent to the thickness of the material sheets used in the LOM process. A heated roller lays a sheet of adhesive-backed material across the build platform. The heat produced by the roller melts the adhesive, which serves as the bonding agent between layers. Next, a laser, controlled by an X-Y positioning mechanism, cuts the outline of the part according to the slicing software. Upon completion of each layer, the build platform is lowered, and the process is repeated until the final layer of the part has been produced [36]. Unused material is cut into rectangles called "tiles", which act as support material during the manufacturing process [43]. These "tiles" are removed during the post-processing operation, and the excess sheet material may be recycled [34]. This method of AM is particularly popular with model makers as the appearance of the final product resembles that of wood [45]. The schematic diagram of the bond-then-form LOM process can be seen in Figure 2.11 [36].
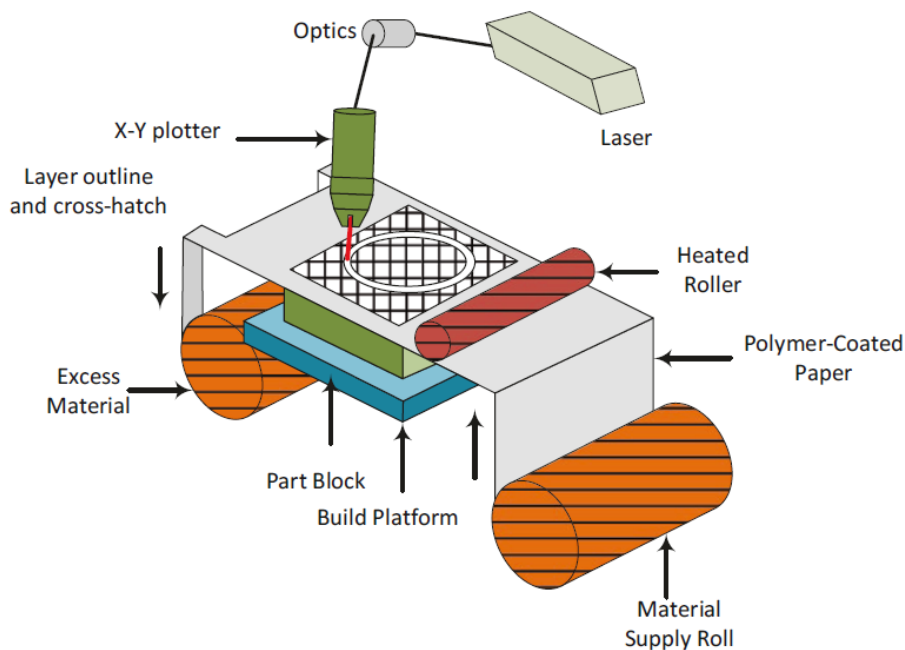
Figure 2.11: Schematic diagram of the bond-then-form LOM process [36]

2.3.5.1 Applications of LOM

Typical applications of LOM include:

➤ As stated previously, the final product in the LOM process resembles that of wood and can be painted to create a replica for visualisation [45].

➤ Patterns for investment and sand casting.

➤ Form-fit testing.

➤ Rapid tooling [15].

2.3.5.2 Advantages of LOM

Advantages of LOM include:

➤ A comprehensive selection of organic and inorganic materials are available, including paper, metals, ceramic-filled tapes and composites [36].

➤ The LOM process produces parts quickly as the laser only cuts the outline of the part.

➤ LOM does not require additional support structures as "tiles" support the material during the manufacturing process.

➤ The sheet material does not undergo a physical or chemical change during operation, which means that LOM parts do not experience considerable deformation or warpage [15].

2.3.5.3 Disadvantages LOM

Disadvantages of LOM include:

➤ The removal of support structures is both labour intensive and time-consuming.

➤ LOM is not suited for complex geometries as removing support material from these areas may prove to be a challenge, if not impossible.

➤ The mechanical strength of produced parts is limited to the strength of the adhesive-backed material, which bonds the layers together.

➤ Cutting combustible materials may lead to a potential fire hazard [36].

➤ A large amount of material wastage.

2.3.6 Direct Metal Laser Sintering (DMLS)

Although the focus of this research was on Polymer AM, DMLS was discussed to convey the differences between metal AM systems and polymer AM systems. DMLS is a variant of the Powder Bed Fusion (PBF) manufacturing process that was first introduced in 1994 and was capable of producing metal parts utilising a single process [46].

The DMLS process begins by filling the hopper with the desired metal powder (the various available metal powders were detailed later). Like the SLS additive manufacturing process, the DMLS process deposits a thin layer of powdered metal material over the build plate. The support structures which fixture the part to the build plate are created initially, followed by the part itself. Once the desired cross-section has been selectively sintered, the build platform is lowered, and a fresh layer of powdered metal material is deposited within the inert build chamber. The layer-by-layer process is repeated until the build is complete [47]. Unlike the SLS (of Polymer) process, where the unsintered powder supports the following layers of the build, DMLS requires support structures that need to be removed upon completion of the build. The produced parts require numerous post-processing operations, which were discussed later in Section 2.3.6.3. The schematic diagram of the DMLS process can be seen in Figure 2.12 [47].
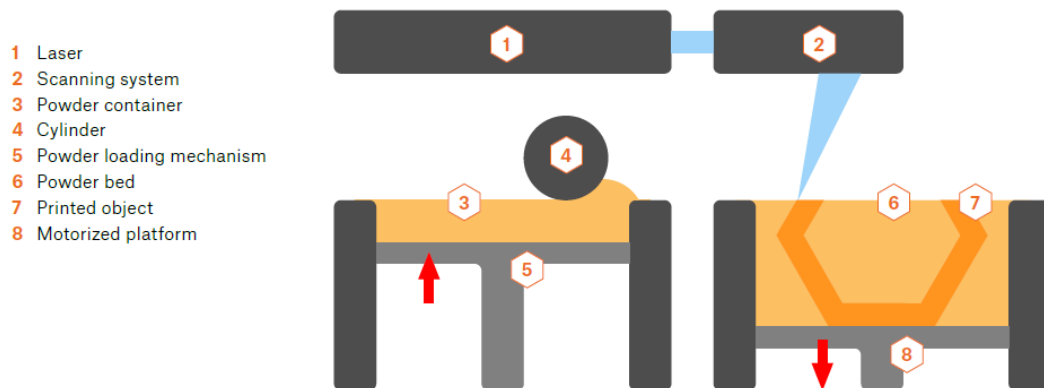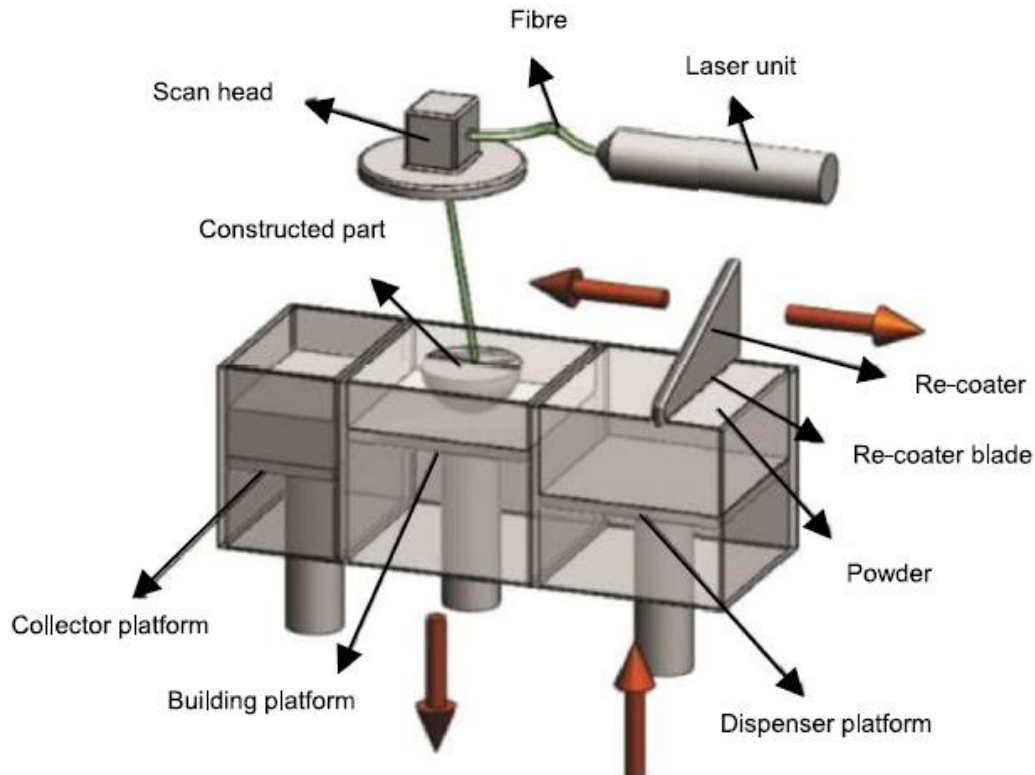

Figure 2.12: Schematic diagram of the DMLS process [47]

2.3.6.1 Applications of DMLS

Typical applications of DMLS include:

- ➢ Functional prototypes [48].
- ➢ Functionally graded metallic implants [47].
- ➢ Die and mould inserts.
- ➢ Rapid tooling.
- ➢ Aerospace parts such as rocket engines and heat exchangers.

2.3.6.2 Advantages of DMLS

Advantages of DMLS include:

- ➢ DMLS can produce parts with up to 95% density [46].
- ➢ DMLS can accurately produce highly complex, functional metal parts [47].
- ➢ An extensive range of metal and metal alloy powders are available, including bronze, steel, stainless steel, aluminium, and titanium [46].
- ➢ High levels of resolution are obtained with good mechanical properties.
- ➢ Streamlined production since a single DMLS machine can produce metal parts utilising a single process. In contrast, conventional manufacturing methods require numerous operations and assembly steps to produce the same part.

2.3.6.3 Disadvantages DMLS

Disadvantages of DMLS include:

- ➢ Support structures are necessary.
- ➢ Produced parts may possess rough surfaces [49].
- ➢ DMLS machines and materials are comparatively more expensive than other AM technologies.
- ➢ Parts produced using DMLS require numerous post-processing operations before a fully functional part is obtained. These processes include heat treatment, support removal, and excess powder removal. Additionally, machining or polishing may be required to improve the surface finish of the parts [46].

A summary table of the discussed AM technologies can be seen in Appendix A1.

2.3.7 Hybrid Manufacturing

Hybrid manufacturing (HM) is another example of rapid prototyping and describes the combination of additive and subtractive manufacturing in a single platform. Additive manufacturing methods, such as FDM, build up the model layer-by-layer. Subtractive manufacturing methods, such as a CNC milling machine, may then machine the model to its final dimensions. Hybrid manufacturing combines the flexibility of additive manufacturing with the precision of conventional subtractive processes. Where conventional manufacturing methods prove costly and time-consuming, hybrid systems are a quick and cost-effective method of rapidly producing prototypes that design engineers may use to evaluate their designs and present to their clients. In addition, the hybrid method of manufacturing uses less energy and is less harmful to the environment since the material is only deposited where needed. The applications, advantages and disadvantages of AM and conventional manufacturing processes are transferred over to HM. A diagram of existing hybrid AM processes is shown in Figure 2.13, with the focus of this research project steered towards hybrid AM by machining [36].
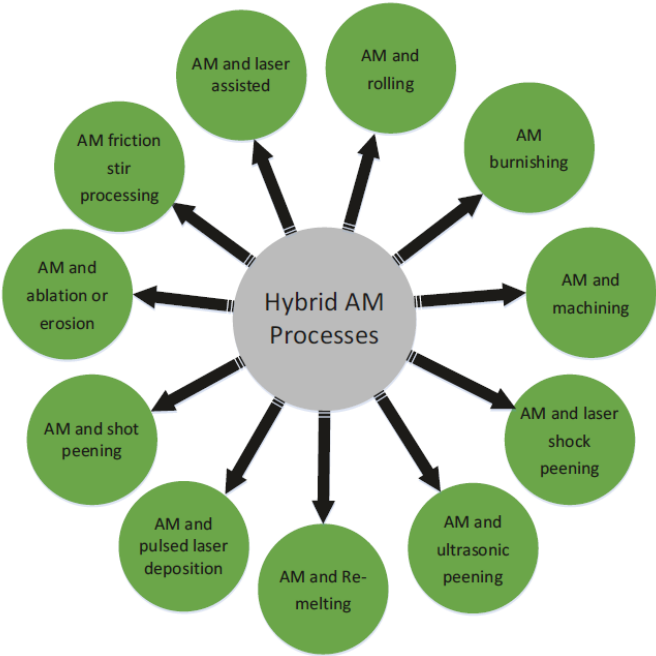
Figure 2.13: Diagram of existing hybrid AM processes [36]

2.3.7.1 Hybrid AM by Machining

Hybrid AM by machining combines additive manufacturing with conventional machining processes, such as milling or turning. Alternating between additive and subtractive techniques between layers allows for complex geometries and internal features to be produced. Milling is commonly coupled with AM to machine both the sidewalls and top surface upon deposition of each successive layer. Sidewall machining seeks to improve the surface finish and correct the dimensional errors produced by the additive process. Face milling of the top surface provides a smooth, level surface for the subsequent layers [50].

Figure 2.14 indicates the characteristics of both rapid prototyping and CNC machining technologies. Whilst rapid prototyping on its own offers speed, ease of fabrication and process automation, it lacks the precision and overall accuracy provided by CNC machining. An amalgamation of the two manufacturing techniques would provide the one-setup capability of rapid prototyping with the precision of CNC machining [51]. The various additive and subtractive manufacturing processes were discussed earlier, and academic studies concerning AM and HM were discussed in Section 2.4.1.
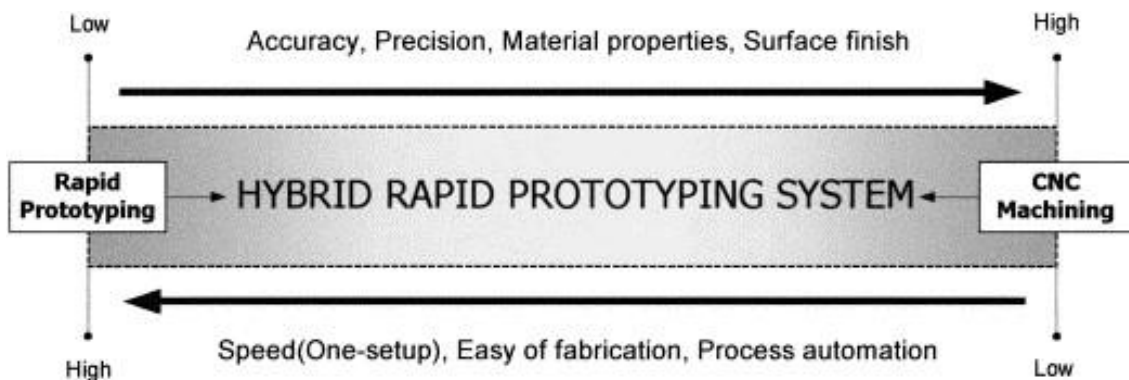
Figure 2.14: Hybrid-RP system characteristics [51]

2.4 Related Research

A study into the available literature on existing research within the field of RP, with the focus on AM, was undertaken to provide insight into the available systems for the intended application of this research project and to highlight possible limitations within these systems.

2.4.1 Academic Studies

Hur et al. [51] developed a combined additive and subtractive manufacturing platform for rapid prototyping. As shown in Figure 2.15, the proposed hybrid-RP system differed from that of other existing systems. In the proposed hybrid-RP approach, the machining process was considered early in the process planning phase, rather than only finishing the deposited additive material. The flexibility offered by the alternating deposition and machining processes during operation allowed for the material to be added or removed at any time. The experimental analysis of the hybrid manufacturing system revealed that the research was successful as a highly competitive dimensional accuracy of 0.05 mm was obtained and a 79.5% reduction in build time compared to an FDM-alone process. This study proved to be a valuable source to draw from as this rapid prototyping method provided a cost-effective method for producing finished quality parts quickly.
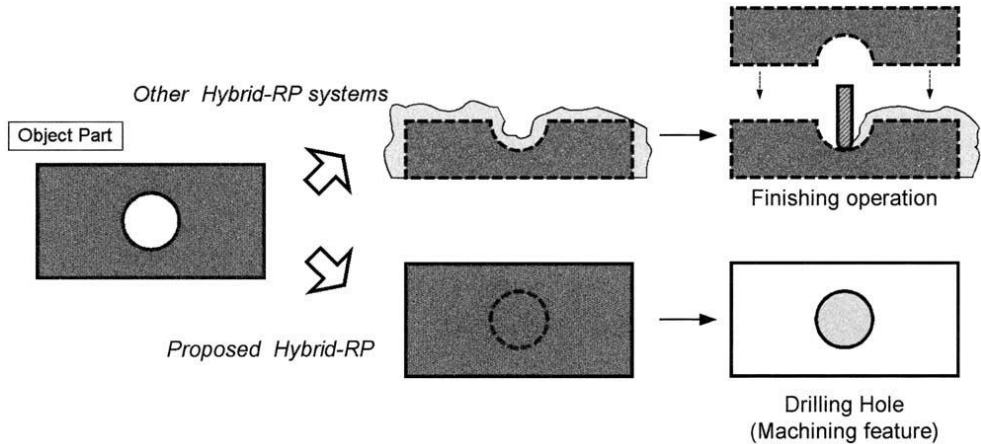
Figure 2.15: Proposed Hybrid-RP system versus existing Hybrid-RP systems [51]

Lee et al. [52] developed a hybrid rapid prototyping system using FDM and five-axis machining. The FDM extruder and cutter spindle were mounted on a rotary axis, offset at 180° from each other. This configuration meant that no additional actuation mechanism was required to alternate between the two methods. Five case studies were conducted to test the capabilities of the integrated manufacturing platform. The maximum dimensional error obtained by the hybrid machine was less than 0.3 mm. In addition, the hybrid system produced a 44% reduction in build time compared to a mid-priced commercial FDM machine. The five-axis system allowed for parts with embedded material to be produced, which increased the stiffness of the FDM part and decreased the cycle time [52].

Akula et al. [53] developed a system for producing metallic dies and moulds by integrating a Metal Inert Gas (MIG) welding process with CNC milling. The MIG-CNC hybrid process, which could be used as a stand-alone system or fitted to an existing CNC milling machine, followed three stages [53]:

i. The near-net-shape of the die or mould was deposited via the controlled MIG welding process.
ii. Residual stresses might have been present due to thermal variations within the part. Therefore, a heat treatment process was performed to relieve stresses induced during the welding process.
iii. The deposited near-net-shape was CNC machined to the final dimensions. The post-processing via machining improved both the surface quality and dimensional accuracy of the die or mould.

This method of depositing the near-net-shape and then machining the final dimensions yielded a much lower cycle time when compared to other stand-alone AM methods, such as SLS and 3DP. In addition, the accuracy of the MIG-CNC hybrid process was equivalent to that of CNC machining, and no post-processing was necessary to improve the density of the produced parts [53].

Shah et al. [54] developed a large-scale 3D printer for additive manufacturing of full-scale products. Fused filament fabrication (FFF), an equivalent to FDM, was the chosen material extrusion method due to its simplicity and robustness when scaled up. As stated previously, in FDM, the model is built up layer-by-layer. The research was evaluated, and the following conclusions were made [54]:

➢ Precise environmental control was needed for large-scale 3D printers due to the temperature effects on the produced products.
➢ Long print times were experienced due to the small nozzle diameter used. However, simply using a larger nozzle size was not an option as the effective melting of the material was deemed a challenge.

The conclusions drawn from this study contributed towards the refinement of the system for the proposed research project.

Big Area Additive Manufacturing (BAAM) is an industrial-sized additive manufacturing machine designed for production manufacturing [55]. Roschli et al. [56] used the BAAM machine to establish design guidelines for large-scale additive manufacturing, and the following conclusions were drawn from the research [56]:

➢ Support material should be avoided as significant defects are formed.
➢ Overhang angles must be considered to avoid sagging, drooping, or part failure during printing.
➢ The use of topology optimisation software is encouraged to save print time, material wastage and overall cost.
➢ A short layer time would cause the layers of a part to sag, and a long layer time could cause delamination.

These design recommendations for large-scale 3D printers were used as guidelines when developing and implementing the additive manufacturing component of the research project.

2.4.2 Commercial Systems

2.4.2.1 Hyrel 3D Hydra 16A

Hyrel 3D, an American-based manufacturer of professional desktop 3D printers, developed the Hydra 16A model. The Hydra 16A supports numerous materials, including, but not limited to, two- and three-part mixtures, UV-curable materials, clays, and standard thermoplastic filaments. In addition, the platform is compatible with several interchangeable head options, such as filament heads, laser heads, milling heads, and syringe heads [57]. This interchangeability allows for countless design possibilities through a single system. Finally, the one-setup capability of the system lowers the initial capital cost and provides an accurate method of combining multiple rapid prototyping processes into a single platform.

2.4.2.2 BLB Industries

BLB Industries is a machining manufacturer in Värnamo, Sweden. Their flagship product is The Box Large which has a build area of 2000 x 2000 x 1500 mm high. All BLB large-format 3D printers use the Fused Granular Fabrication (FGD) method of additive material deposition. In FGD, molten plastic granules build the product up in successive stages, and this method reduces material costs and allows for a broader selection of materials. The system is suited for both large-scale prototyping and full-scale mass production [58]. BLB Industries promotes the following features for their large-scale 3D printers [58]:

- High-quality linear modules from Rexroth.
- Interchangeable extruder heads for varying resolution.
- Patented heated vacuum build plate.
- 15-inch touch screen.
- Software: IndraWorks Operation and Simplify 3D.

2.4.2.3 Zmorph

Zmorph is a Polish 3D printer manufacturer based in Wrocław, Lower Silesia. Founded in 2012, Zmorph manufactures platforms for rapid prototyping, home crafting and low-volume production by integrating 3D printing, CNC milling, and laser engraving into a single machine. The Zmorph i500 is a high-performance industrial 3D printer that maximises productivity through a large build volume and simultaneous production of parts in various materials. The Zmorph Fab is an all-in-one 3D printer developed based on customer feedback for learning and prototyping.

The i500 and the Fab come equipped with Voxelizer, the all-inclusive software platform for 3D printing, CNC milling and laser engraving. An intuitive and user-friendly interface allows users with limited experience to effortlessly navigate through the menu prompts and prepare the system for manufacturing. The various tool heads available for the Zmorph machines seamlessly integrate into the platform without the need for any disassembly. In addition, the machines are equipped with tool head detection sensors that automatically detect and calibrate the newly inserted tool head. The Zmorph Fab is available as an all-in-one set or as a stand-alone 3D printer for users solely interested in 3D printing [59]. The Zmorph Fab can be seen in Figure 2.16 [59].
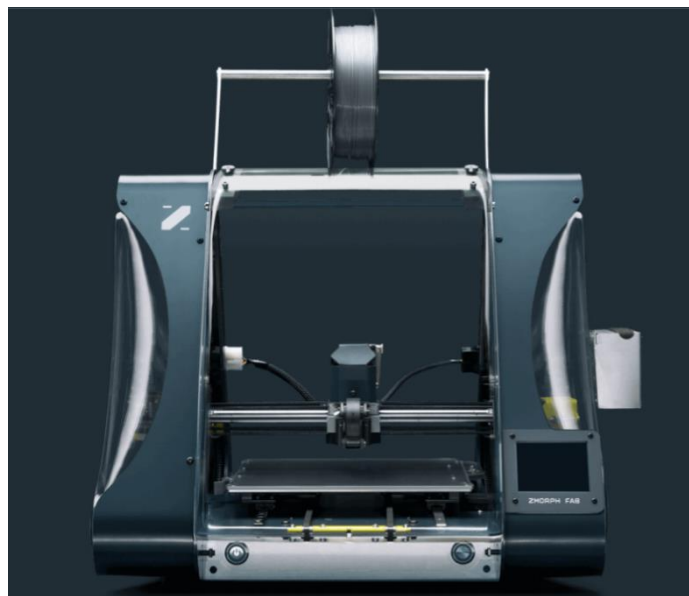
Figure 2.16: Zmorph Fab 3D printer [59]

2.5 Chapter Conclusion

This chapter reviewed and compared the currently available methods of rapid prototyping. Academic studies, as well as commercial systems regarding AM and HM, were analysed. The academic research conducted noted that a reduction in build time - compared to stand-alone manufacturing techniques - was frequently obtained by implementing hybrid manufacturing systems. In addition, Hur et al. and Lee et al. obtained competitive dimensional accuracies, and both studies proved to be valuable sources of information. A trend in using the layer-by-layer additive manufacturing technique could be seen from the commercially available systems. Chapter 3 discussed the design and development process of this research project's hardware and software architecture.

Chapter 3

System Architecture

This chapter discussed the developed combined additive manufacturing and machining platform utilised for large-scale AM. The hardware and software architecture utilised in this research project were discussed.

3.1 Hardware Architecture

3.1.1 CNC Milling Spindle Motor

The EYS8043-18/3.0 model from Changzhou Huajiang Electrical Appliances Co., Ltd was selected as the CNC milling spindle motor for the proposed platform. The high-speed electro spindle, along with its technical specifications, can be seen in Figure 3.1 and Table 3.1, respectively [60].

Figure 3.1: EYS8043-18/3.0 CNC milling spindle motor [60]

Table 3.1: EYS8043-18/3.0 CNC milling spindle motor technical specifications

Parameter	Value	Unit
Power	3	kW
Electric Current	8.6	A
Voltage	220	V
Frequency	300	Hz
Maximum Spindle Speed	18000	RPM
Shaft End Connection	ER20	-

As stated previously, the spindle speed significantly affects the surface finish of the produced part. The maximum spindle speed of 18000 RPM provided by the CNC milling spindle motor allowed for smooth surface finishes to be produced by adjusting the spindle speed during milling operations. The ER20 shaft end connection provided a tool clamping range from 1 mm to 13 mm in diameter. Larger diameter end mills were used to perform facing and contour operations where a high material removal rate (R_{MR}) was required. Smaller cutting tools produced detailed features and surfaces. Cutting tool manufacturers, such as ISCAR, provide cutting speed recommendations based on the material designation, material condition and hardness. Figure 3.2 illustrates an example of cutting speed recommendations for various steels [61].

Cutting Speed for: 16ERM 2.50 ISO IC908 - 5901564

ISO	Material	Material Designation	Material Condition	Hardness	Cutting Speed Recommendations (Vc)
P	1	Non-alloy steel and cast steel, free cutting steel <0.25% C	Annealed	125 HB	85-165 m/min
P	2	Non-alloy steel and cast steel, free cutting steel >=0.25% C	Annealed	190 HB	85-160 m/min
P	3	Non-alloy steel and cast steel, free cutting steel <0.55% C	Quenched and tempered	250 HB	80-155 m/min
P	4	Non-alloy steel and cast steel, free cutting steel >=0.55% C	Annealed	220 HB	80-150 m/min
P	5	Non-alloy steel and cast steel, free cutting steel >=0.55% C	Quenched and tempered.	300 HB	75-140 m/min
P	6	Low alloy and cast steel (less than 5% of alloying elements)	Annealed	200 HB	90-140 m/min
P	7	Low alloy and cast steel (less than 5% of alloying elements)	Quenched and tempered	275 HB	85-130 m/min
P	8	Low alloy and cast steel (less than 5% of alloying elements)	Quenched and tempered	300 HB	80-125 m/min
P	9	Low alloy and cast steel (less than 5% of alloying elements)	Quenched and tempered	350 HB	75-120 m/min
P	10	High alloyed steel, cast steel and tool steel	Annealed	200 HB	70-125 m/min
P	11	High alloyed steel, cast steel and tool steel	Quenched and tempered	325 HB	60-110 m/min
P	12	Stainless steel and cast steel	Ferritic/martensitic	200 HB	85-130 m/min
P	13	Stainless steel and cast steel	Martensitic	240 HB	85-120 m/min

Figure 3.2: ISCAR cutting speed recommendations [61]

Two parameters were required to determine the spindle speed for the milling operations: the cutting speed recommendation, V_c , taken from the catalogue of a tool manufacturer and the diameter of the cutting tool used. Equation 3.1 described the cutting speed of the cutting tool.

$$V_c = \frac{\pi D N}{60}$$
(3.1)

Where V_c represented the cutting speed, D represented the diameter of the cutting tool, and N represented the spindle speed.

3.1.2 CNC Mill Workholding

Workholding refers to the process in which the workpiece is firmly secured before the milling process is initiated. Accurate and precise workholding is crucial in CNC milling and may lead to failure if approached incorrectly. During milling, the workpiece is subjected to large cutting forces, resulting in unintentional movement of the workpiece. At high spindle speeds and feed rates, this unintentional movement, due to inadequate workholding, could lead to catastrophic failure and endanger the operator. There are numerous methods for clamping workpieces, including machine vices, fixture plates, step clamps and even double-sided tape for specific materials. Commercial methods of workholding were analysed, and concepts were generated to determine the best possible solution for the required application.

3.1.2.1 Aluminium Extrusions

Aluminium extrusions are lightweight, corrosion-resistant, and readily available in numerous square, rectangular, and round profiles. They possess a high strength-to-weight ratio, and any necessary modifications to the extrusions, such as the drilling of mounting holes, may easily be carried out. Aluminium extrusions are commonly used for cutting beds due to their wide clamping range and increased mounting flexibility. The entire length of the slotted aluminium extrusion may be used to secure the workpiece using T-nuts. A standard clamping kit is used to secure the workpiece. The increased level of mounting flexibility stems from the capability of simply moving the extrusions closer together or further apart to accommodate parts of different shapes and sizes. The aluminium extrusions that form the cutting bed workspace are attached to the machine's main frame using a connector plate. The connector plates are fastened to the frame using socket head cap screws and T-nuts. A drawback, however, for the application of the proposed project is the cost due to the considerably long extrusions that would be required. An illustration of the aluminium extrusions workholding concept can be seen in Figure 3.3.
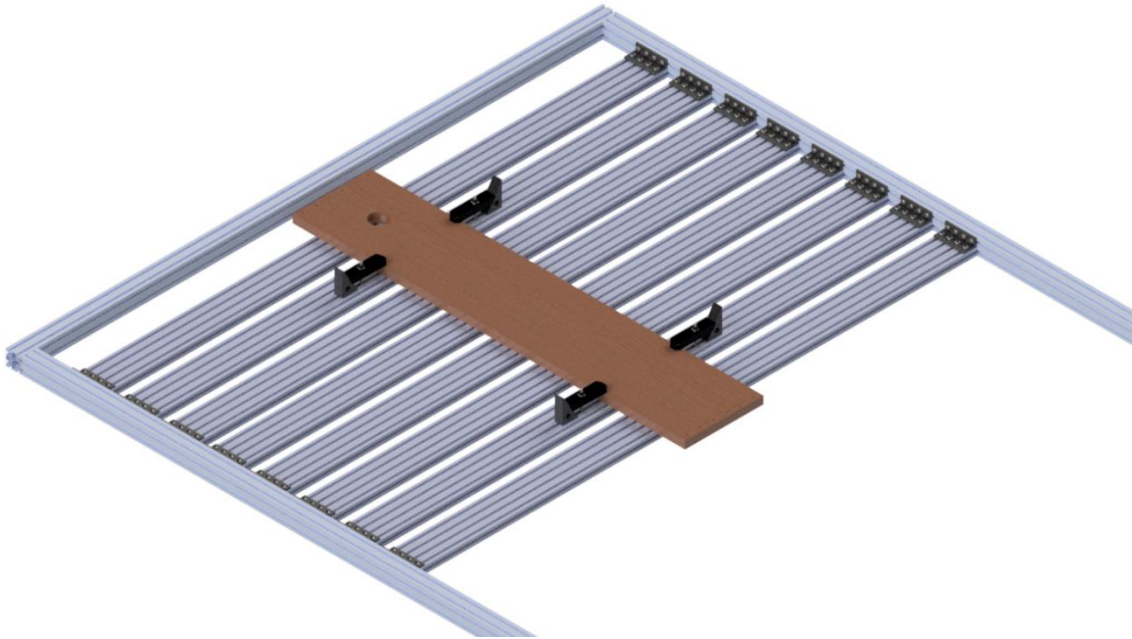
Figure 3.3: Aluminium extrusions concept CAD model

3.1.2.2 Fixture Plate and Sacrificial Bed

For the second concept, a laser-cut plate is welded to the base frame, which is formed by joining sections of square tubing together. The plate has a rectangular hole pattern, and hex nuts are welded to the bottom of the plate according to this pattern. With the fixture plate and hex nuts securely attached, the base frame is fastened to the V-slot aluminium extrusions using mounting plates. A sacrificial machine bed, made out of a soft material such as medium-density fibreboard (MDF), is installed on top of the plate. The same hole pattern as the laser-cut plate is produced for the sacrificial bed. A facing toolpath is generated to ensure that the sacrificial bed is level with reference to the fixture plate. The holes used to secure the sacrificial bed to the fixture plate are counterbored to ensure that the socket head cap screws would not interfere with the cutting tool during the bed levelling operation. Like the initial concept, the workpiece is held in place using a standard milling machine clamp kit. This method of workholding is comparatively cheaper when compared to aluminium extrusions, but the additional weight needs to be taken into consideration. This concept possesses a reasonable level of mounting flexibility but is far inferior to the initial aluminium extrusions concept. Isometric and bottom views of the fixture plate with a sacrificial bed mounted on top can be seen in Figure 3.4 and Figure 3.5, respectively.
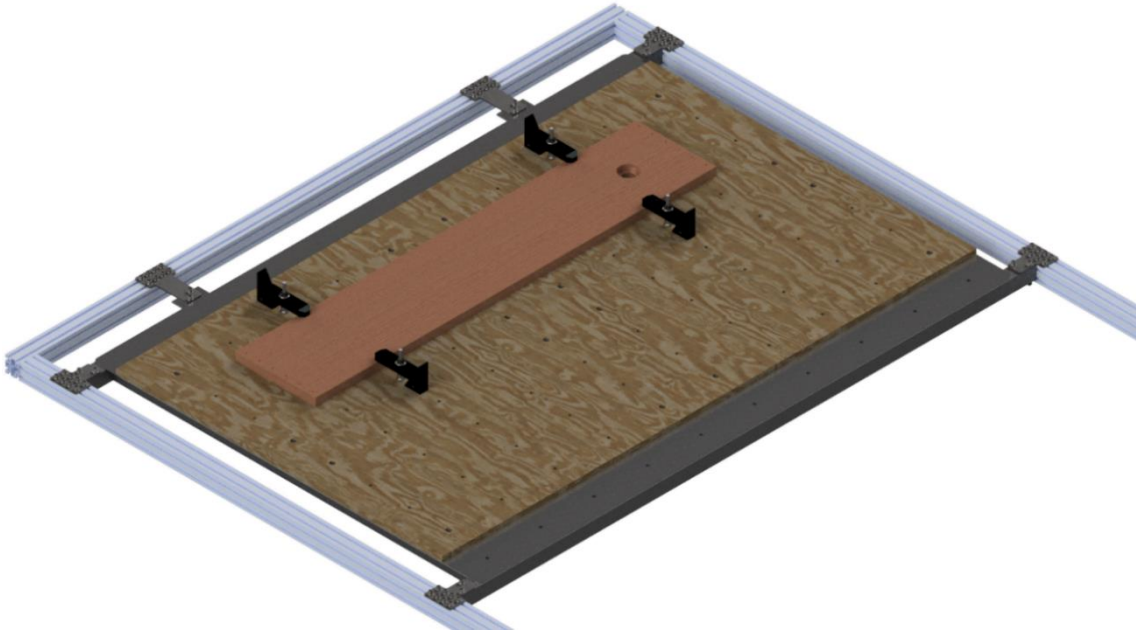
Figure 3.4: Isometric view of fixture plate & sacrificial bed concept CAD model
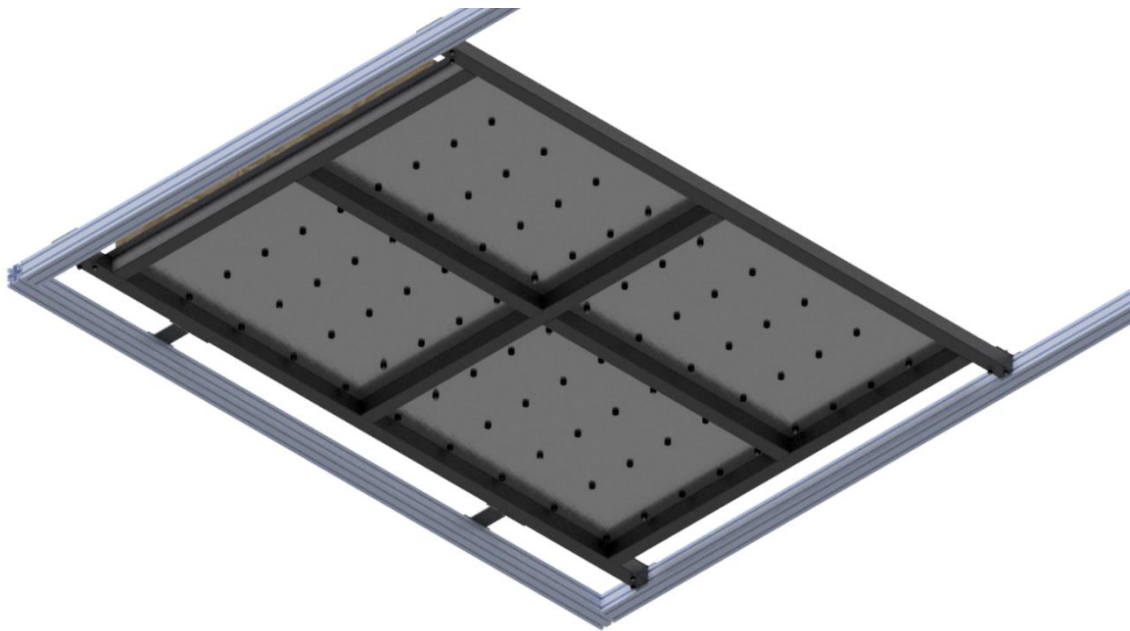
Figure 3.5: Bottom view of fixture plate & sacrificial bed concept CAD model

3.1.2.3 Fixture Plate and Machine Vice

The third concept followed the fixture plate workholding technique; however, machine vices were used to clamp the workpiece. A machine vice is a mechanical clamping device used to hold a workpiece during material removal operations. A machine vice provides excellent workpiece stability owing to the flanged-bottom design. Parallels are metal blocks that have been ground and lapped to a specific size and thickness and are used to evenly raise the workpiece within the machine vice, which allows for through-hole machining without damaging the vice. The fixture plate is attached to the main frame in the same manner as the second concept, and the machine vices are directly secured to the fixture plate using hex head cap screws. Machine vices are commonly made of cast iron which significantly increases the overall weight of this workholding concept. As with the aluminium extrusions, this concept yields increased mounting flexibility since the machine vices can be readily relocated on the fixture plate to accommodate various workpieces. However, the clamping range of this concept is limited by the range of motion of the machine vice's moveable jaw. An illustration of the fixture plate with two machine vices mounted on top can be seen in Figure 3.6.
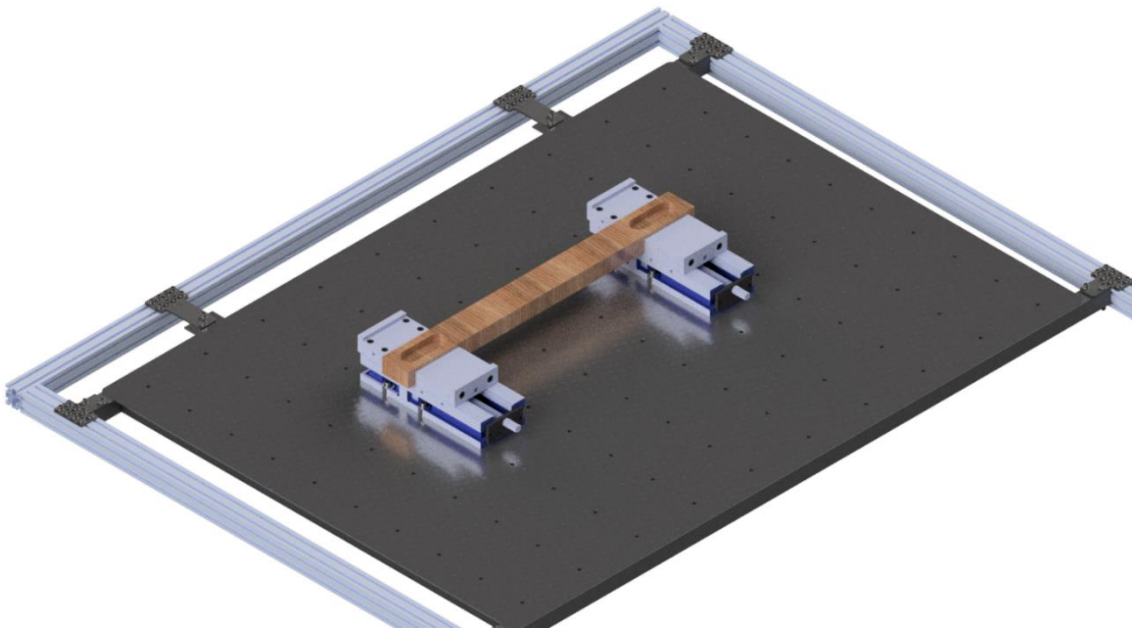
Figure 3.6: Fixture plate & machine vice concept CAD model

The proposed concepts were previously expanded on, and a comparison of the workholding methods can be seen in Table 3.2 and Figure 3.7. The cost, weight, clamping range and mounting flexibility of the final three proposed concepts were used as the evaluation criteria.

Table 3.2: CNC mill workholding evaluation matrix

Rating (/10)		_Aluminium Extrusions_		_Fixture Plate & Sacrificial Bed_		_Fixture Plate & Machine Vice_	
Criteria	_Weight (%)_	_Rating_	_Weighted_	_Rating_	_Weighted_	_Rating_	_Weighted_
Cost	40	3	1.2	8	3.2	5	2
Weight	30	7	2.1	4	1.2	3	0.9
Clamping Range	15	6	0.9	8	1.2	4	0.6
Mounting Flexibility	15	8	1.2	5	0.75	6	0.9
Total Score	**100**		**5.4**		**6.35**		**4.4**
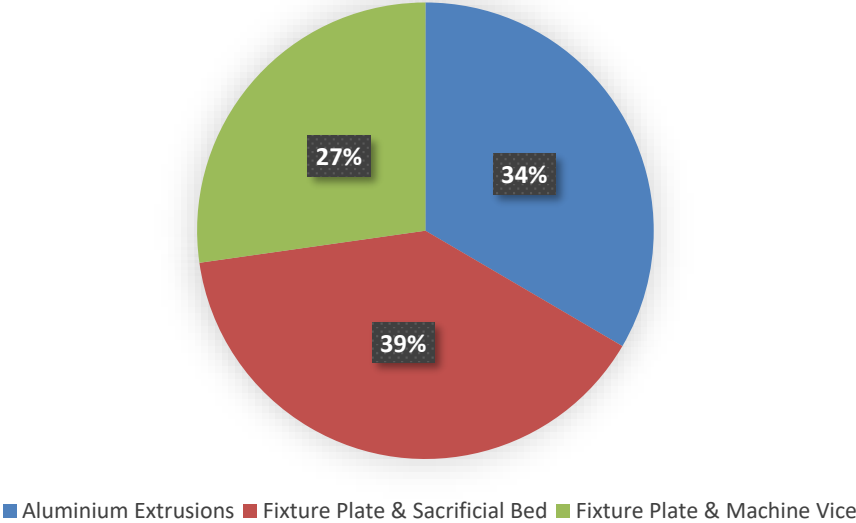
Figure 3.7: CNC mill workholding evaluation chart

Referring to Table 3.2 and Figure 3.7, the fixture plate and sacrificial bed concept was selected as the workholding method. The selected workholding concept can be seen in Figure 3.8. In addition, the sacrificial bed was face milled to produce a level workholding surface, as seen in Figure 3.9.
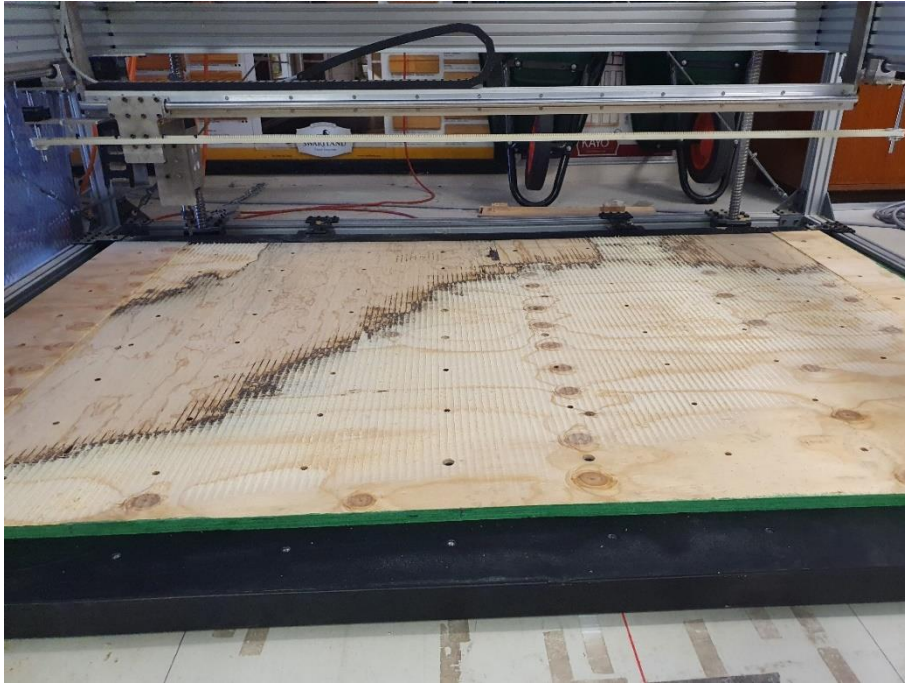
Figure 3.8: Selected workholding technique installed on the CNC milling machine

Figure 3.9: Face milled sacrificial bed

3.1.3 Dosing System

The design and development of a system for depositing the additive material was necessary for this research project. The developed system was required to accurately mix and deposit the polyurethane foam according to the formulation provided by the PU foam technical data sheets, as seen in Appendix B1.

A peristaltic pump was proposed as a possible solution to meet the research requirements. A peristaltic pump is a positive displacement pump whereby the fluid does not come into contact with any mechanical components. This separation prevents cross-contamination and provides a clean pumping solution. The peristaltic pump operation principle can be seen in Figure 3.10 [62].
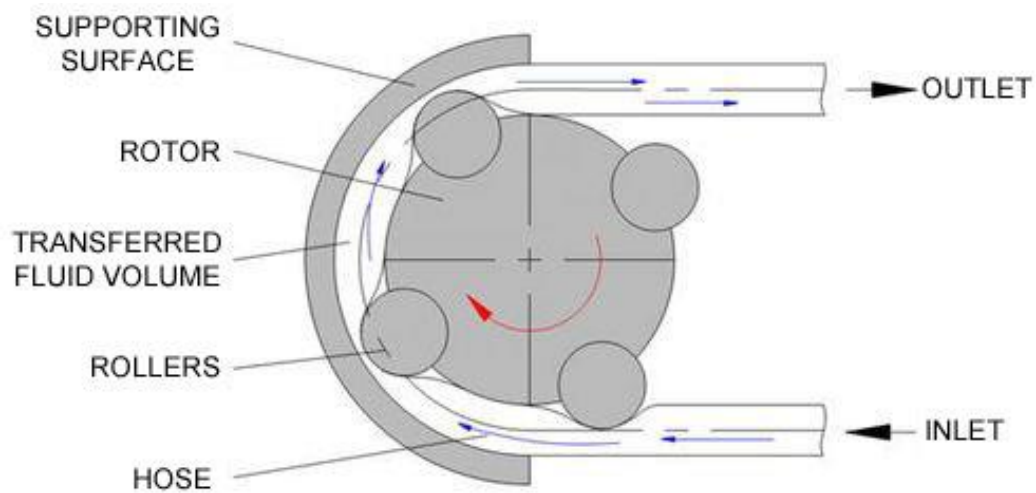
Figure 3.10: Peristaltic pump operation principle [62]

In a peristaltic pump, the motor's output shaft is connected to a rotor with a series of rollers attached. Hose or flexible tubing passes through these rollers within the pump housing and transports the liquid from the inlet to the outlet position. As the motor drives the rotor, the rollers compress the flexible tubing and force the fluid towards the pump outlet. Once the roller has compressed a section of the tubing, a vacuum is created, drawing in additional fluid from the pump inlet. The number of rollers used affects both the flow rate and the pulsation of the pump. The entrapment of the fluid between rollers is referred to as a "pillow". The formed "pillow" is proceeded by a "void", a momentary pocket absent of fluid. The continuous alternation between these "pillows" and "voids" causes pulsation to occur [63]. A high level of pulsation produces turbulent and intermittent flow.

Peristaltic pumps can accurately and repeatedly transfer fluid from the pump inlet to the outlet. Typical advantages of peristaltic pumps include [64]:

➢ Clean pumping solution owing to the separation of the fluid and the mechanical pumping components.
➢ Self-priming and capable of running dry without the presence of the fluid that is to be pumped.
➢ The flow direction of the pump may be reversed in the event of a blockage.
➢ Repeatable and accurate dispensing by preventing backflow.
➢ Low maintenance cost.
➢ The pump's flow rate can be altered by changing the diameter, or the material, of the flexible tubing.

Typical applications of peristaltic pumps include [64]:

➢ Medical applications where cross-contamination is prohibited.
➢ Chemical metering.
➢ The manufacturing of circuit boards.
➢ Pumping of aggressive and volatile fluids.
➢ Water treatment.

Despite the numerous advantages provided by a peristaltic pumping system, the continuous compression of the flexible tubing will eventually lead to rupture. Therefore, frequent maintenance may be necessary if the pumps are to be operated for extended periods.

3.1.3.1 Grothen G728-2 Peristaltic Dosing System

The Grothen G728-2 peristaltic liquid dosing system was used to conduct initial flow tests of the polyurethane foam. The G728-2 pump, along with its specifications, can be seen in Figure 3.11 and Table 3.3, respectively [65].

Figure 3.11: Grothen G728-2 peristaltic liquid dosing system [65]

Table 3.3: Grothen G728-2 specifications

Specifications	*Grothen G728-2*
Input Voltage	100-240 V AC
Output Voltage	24V/1A
DC Motor	12V
Peristaltic Pump Heads	2
Speed Control	Stepless Speed Control
Flow Rate	10-160 ml/min
Pulsation	3 Planetary Gears
Item Weight	266 g

A static mixer, used for continuous mixing of the PU foam, was connected to the dosing system via the supplied food-grade silicone tubing. Parts A and B of the polyurethane foam containers were connected to the two separate pump heads. The flow rate knobs were set to the same positions, and the pumps were switched on. The pumps were allowed to run until sufficient product had cured within the bucket. The initial flow testing using the G728-2 dosing system can be seen in Figure 3.12.
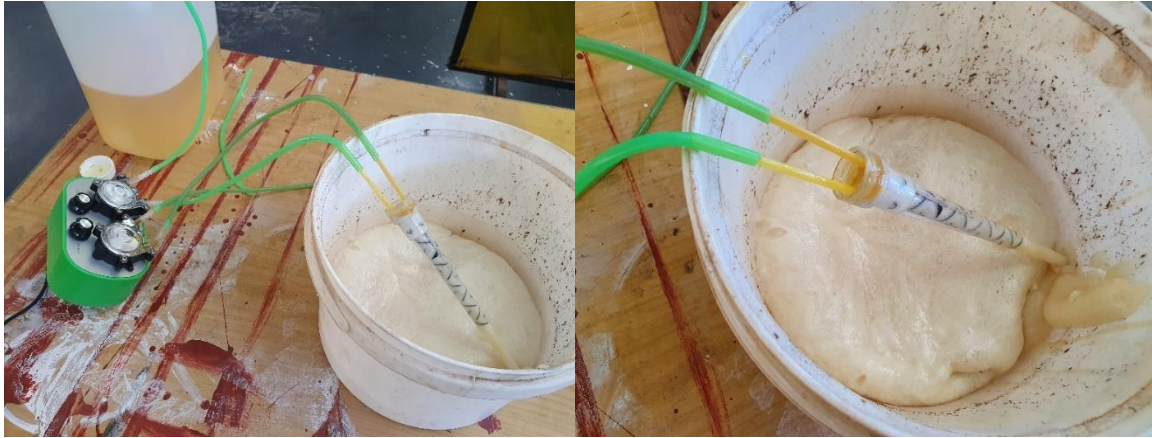
Figure 3.12: Initial flow testing using the G728-2 dosing system

3.1.3.2 Grothen G728-2 Splined Modification Peristaltic Dosing System

The second concept sought to improve the flow control of the initial G728-2 dosing system solution by replacing the two 12V DC motors with two stepper motors. The output shafts of the stepper motors were splined to accommodate the planetary gear arrangement of the G728-2 pump utilising an electrical discharge machining (EDM) process. A housing unit was designed and manufactured to mount the rotor housing and the splined stepper motors. The splined stepper motor shafts and the assembled splined stepper motor dosing system can be seen in Figure 3.13 and Figure 3.14, respectively.
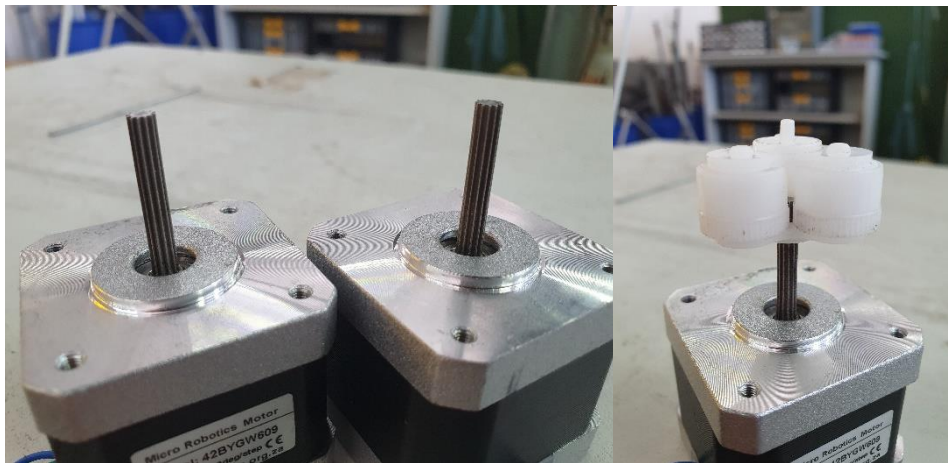
Figure 3.13: Splined stepper motor shafts to accommodate G728-2 gearing arrangement

Figure 3.14: Assembled splined stepper motor dosing system

3.1.3.3 Direct-Drive Peristaltic Dosing System

The final concept sought to improve the flow rate of the second concept by removing the gearing arrangement and utilising a direct-drive system. The rotor consisted of six 624 deep groove ball bearings. The ball bearings were attached to the rotor hubs, and washers were used to prevent contact between the inner races of the bearings and the rotor hubs. A flat section was CNC milled onto the stepper motor output shafts to locate the rotor assembly firmly. A new housing was required to accommodate the stepper motors and the newly manufactured rotor assembly. The pump housing was directly attached to the NEMA stepper motor using four socket head cap screws. A housing unit was 3D printed and can be seen in Figure 3.15.
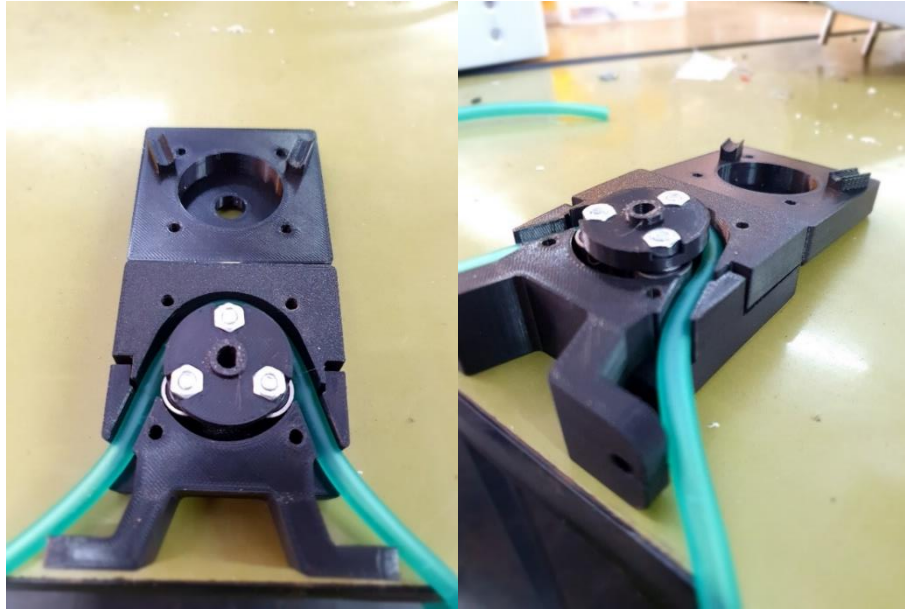
Figure 3.15: 3D printed peristaltic pump housing unit

A comparison of the possible dosing system options can be seen in Table 3.4 and Figure 3.16. The flow control, flow rate, cost, and interchangeability of the final three proposed peristaltic pump concepts were used as the evaluation criteria.

Table 3.4: Peristaltic dosing system evaluation matrix

Rating (/10)		_Grothen G728-2_		_Grothen G728-2 Splined Modification_		_Direct-Drive_	
Criteria	_Weight (%)_	_Rating_	_Weighted_	_Rating_	_Weighted_	_Rating_	_Weighted_
Flow Control	40	2	0.8	8	3.2	8	3.2
Flow Rate	30	5	1.5	6	1.8	8	2.4
Cost	20	7	1.4	5	1	6	1.2
Interchange-ability	10	4	0.4	5	0.5	8	0.8
Total Score	**100**		**4.1**		**6.5**		**7.6**
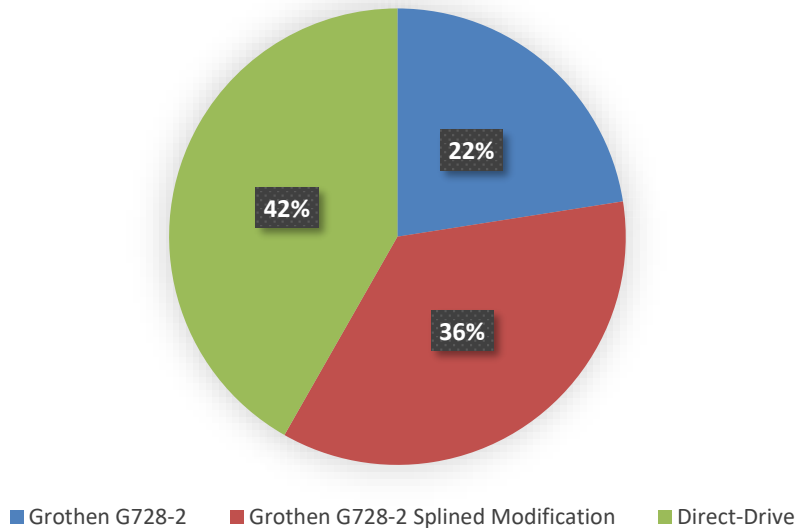
Figure 3.16: Peristaltic dosing system evaluation chart

Referring to Table 3.4 and Figure 3.16, the direct-drive arrangement was selected as the desired dosing system. As seen in Table 3.4, the highest weighting was given to the flow control and the flow rate of the dosing system. Although both the Grothen G728-2 splined modification and the direct-drive arrangements utilised stepper motors to enhance the flow control, the planetary gearing arrangement of the former impaired the maximum achievable flow rate of the system. Both the splined modification and the direct-drive concepts used NEMA stepper motors and stepper motor drivers, which significantly increased the cost of both systems when compared to the 12V DC motors of the initial Grothen G728-2 concept. In addition, the direct-drive solution possessed an increased level of interchangeability since the majority of the pump housing was manufactured via 3D printing, and any necessary design alterations could be made to improve the performance of the dosing system.

3.1.3.4 Stepper Motor

Aranjo et al. [66] defined a stepper motor as: "a digital electromechanical system wherein each electrical pulse input moves the rotor by a discrete angle called the step angle." For example, a stepper motor with a step angle of 1.8° would require 200 steps to perform one revolution. Since the rotors of stepper motors move in fixed increments when pulses are applied, they provide precise positioning and speed control capabilities. As stated previously, the dosing system's flow control and flow rate were critical elements, which made using stepper motors ideal for the proposed solution. Equation 3.2 was used to convert the pulses per second (PPS) applied to the stepper motors to RPM.

$$RPM = \frac{steps}{pulse} \times \frac{pulses}{second} \times \frac{degrees}{step} \times \frac{1\ revolution}{360\ degrees} \times \frac{60\ seconds}{minute} \qquad (3.2)$$

Suitable stepper motors for the dosing system can be seen in Table 3.5 [67].

Table 3.5: Suitable stepper motors

Stepper Motor Specifications	NEMA 17 (0.4 A, 0.28 Nm)	NEMA 17 (1.7 A, 0.4 Nm)	NEMA 17 (1.7 A, 0.42 Nm)
Step Angle (°)	1.8	1.8	0.9
Motor Length (mm)	34	38	48
Rated Voltage (V)	12	3.4	2.8
Rated Current (A)	0.4	1.7	1.7
Phase Resistance (Ω)	30	2	1.65
Phase Inductance (mH)	37	3	4
Holding Torque (N.m)	0.28	0.4	0.42
Detent Torque (N.m)	0.02	0.022	0.022
Rotor Inertia (g.cm^2)	34	54	68
Motor Weight (kg)	0.2	0.24	0.34
Price (ZAR)	249.95	279.95	329.95

The NEMA 17 (1.7 A, 0.4 Nm) was selected as the desired stepper motor for the dosing system. Since the output torque of a stepper motor is directly proportional to the current, the 1.7 A provided by the NEMA17 (1.7 A, 0.4 Nm) meant that increased motor speeds could be obtained before stalling the motor when compared to the significantly lower 0.4 A provided by the 0.28 Nm NEMA 17 motor. Aside from being the cheaper option, the 1.8° step angle of the selected motor provided faster rotations at lower pulse frequencies. Had the 0.9° step angle motor been utilised, it would have required double the number of pulses to obtain the same speed as the selected motor. Dimensions of the selected stepper motor can be seen in Appendix C1 [68].

3.1.3.5 Stepper Motor Driver

A stepper motor driver was required to drive each stepper motor utilised in the dosing system. The primary reasons for adding stepper motor drivers onto the printed circuit board (PCB) included [67][69]:

➢ Flexible current control by either stepping up or stepping down the supply voltage.
➢ Microstepping capability. Microstepping provides smoother motion than full-stepping and reduces resonance generated by the inertia of the moving rotor. Microstep resolutions can range from 1/2 of a step to 1/256 of a step.
➢ Overcurrent, undervoltage and elevated temperature protection features.
➢ Built-in translators provide movement control of the stepper motor using the Step and Direction pins.

Suitable stepper motor drivers for the dosing system can be seen in Table 3.6 [68].

Table 3.6: Suitable stepper motor drivers

Specifications	*Pololu DRV8825*	*Pololu STSPIN820*	*Pololu AMIS-30543*
Minimum operating voltage (V)	8.2	7	6
Maximum operating voltage (V)	45	45	30
Continuous current per phase (A)	1.5	0.9	1.8
Maximum current per phase (A)	2.2	1.5	3
Minimum logic voltage (V)	2.5	2	2.5
Maximum logic voltage (V)	5.25	5.5	5.5
Microstep resolutions (Step)	Full, 1/2, 1/4, 1/8, 1/16, 1/32	Full, 1/2, 1/4, 1/8, 1/16, 1/32, 1/128, 1/256	Full, 1/2, 1/4, 1/8, 1/16, 1/32, 1/64, 1/128
Reverse voltage protection (Yes/No)	No	No	Yes
Price (ZAR)	135.7	112.7	217.35

The Pololu DRV8825 was selected as the desired stepper motor driver to drive the two NEMA 17 stepper motors due to its high amperage, low cost, and small form factor compared to the other suitable stepper motor drivers that were considered. The Pololu DRV8825 was also more readily available at several electronic stores if the driver needed to be replaced. The wiring diagram of the selected stepper motor driver can be seen in Appendix C2 [68].

3.1.3.6 Microcontroller Board

A microprocessor fetches, decodes and executes instructions obtained from the system's memory. A microcontroller is a microprocessor with additional components such as digital-to-analogue (DAC) and analogue-to-digital converters (ADC) [70]. The microcontrollers are programmed using the Arduino IDE. Suitable microcontroller boards can be seen in Table 3.7 [68][71][72].

Table 3.7: Suitable microcontroller boards

Specifications	Arduino Nano	ESP32 Dev Board	Teensy 4.0 Dev Board
Operating Voltage (V)	5	2.2-3.6	5
Flash Memory (KB)	32	4000	1984
SRAM (KB)	2	520	1024
Clock Speed (MHz)	16	240	600
Analog IN Pins	8	18	14
EEPROM (KB)	1	0.512	1.08
Input Voltage (V)	7-12	3.3	3.3
Digital I/O Pins	22	36	40
PWM Output	6	16	31
Power Consumption (mA)	19	80	100
Width x Length (mm)	18 x 45	28.33 x 51.45	18 x 36.8
Weight (g)	7	10	2.8
Price (ZAR)	189.95	147.2	565.80

The ESP32 development board was selected as the desired microcontroller board for the system due to its cost-effectiveness compared to the Teensy, and its significantly greater clock speed compared to the Nano. The 240 MHz clock speed of the ESP32 allowed for swift processing and execution of the instructions provided by the Arduino IDE. The pin-out schematic of the selected microcontroller can be seen in Appendix C3 [68].

A morphological chart and cost analysis of the peristaltic dosing system can be seen in Table 3.8 and Table 3.9, respectively. The morphological chart was used to identify possible combinations of sub-solutions and was then used to conclude the final concept. The highlighted entities in Table 3.8 represented the chosen combination of the possible means for all the features considered. The peristaltic pump enclosure, which housed the two peristaltic pumping units, can be seen in Figure 3.17. The peristaltic pump control box, which contained all of the electrical components required to operate the pump, can be seen in Figure 3.18.

Table 3.8: Morphological chart

Feature	Means		
Dosing System	Grothen G728-2 Peristaltic Dosing System	Grothen G728-2 Splined Modification Peristaltic Dosing System	**Direct-Drive Peristaltic Dosing System**
Stepper Motor	NEMA 17 (0.4 A, 0.28 Nm)	**NEMA 17 (1.7 A, 0.4 Nm)**	NEMA 17 (1.7 A, 0.42 Nm)
Stepper Motor Driver	**Pololu DRV8825**	Pololu STSPIN820	Pololu AMIS-30543
Microcontroller	Arduino Nano	**ESP32 Development Board**	Teensy Board 4.0 Dev Board

Table 3.9: Peristaltic dosing system cost analysis

Item	Quantity	Price per Item (ZAR)	Vendor
24V Power Supply	1	850.95	RS Components
NEMA 17 (1.7A, 0.4 Nm) Stepper Motor	2	279.95	DIYElectronics
ESP32 Development Board	1	147.2	Micro Robotics
Pololu DRV8825 Stepper Motor Driver	2	135.7	Micro Robotics
Enclosure Grey Lid 190 x 140 x 70	2	135.7	ACDC Express
OLED 1.3 Inch I2C Display - White on Black	1	125.35	Micro Robotics
6x4 mm Silicone Tubing (per 15m length)	1	362.25	Clure Projects CC
Ultra-Small DC-DC Step Down Power Supply Module (Adjustable Buck Converter)	1	34.95	Leobot Electronics
624 2RS BTC Deep Groove Ball Bearing	12	21.1	BMG
Panel Mount Linear Taper Potentiometer	2	20	Micro Robotics
Panel Mount Toggle Switch	1	10.35	Micro Robotics
TOTAL COST (ZAR)		**2926.95**	
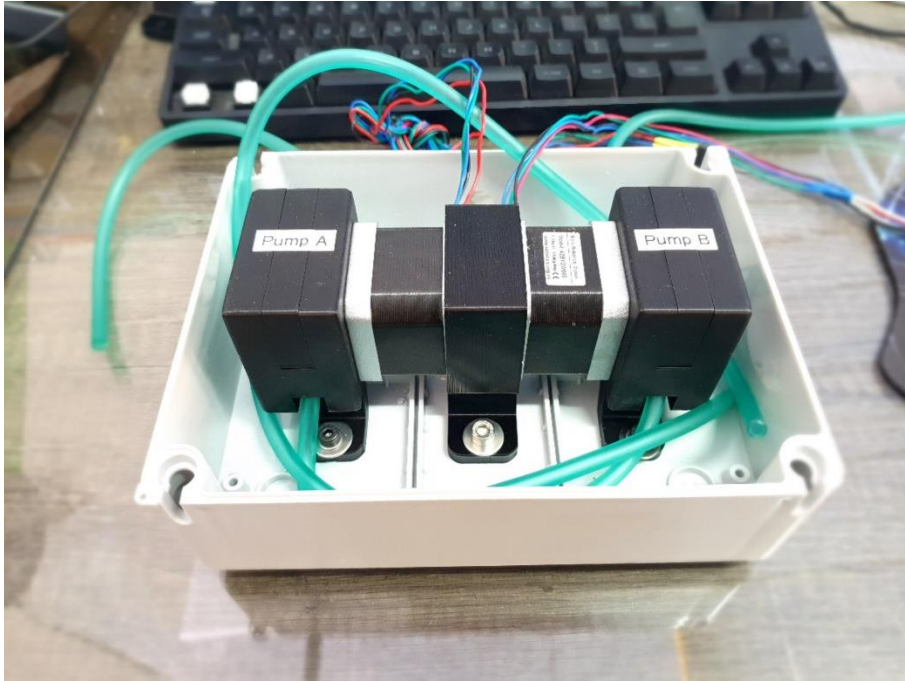
Figure 3.17: Peristaltic pump enclosure
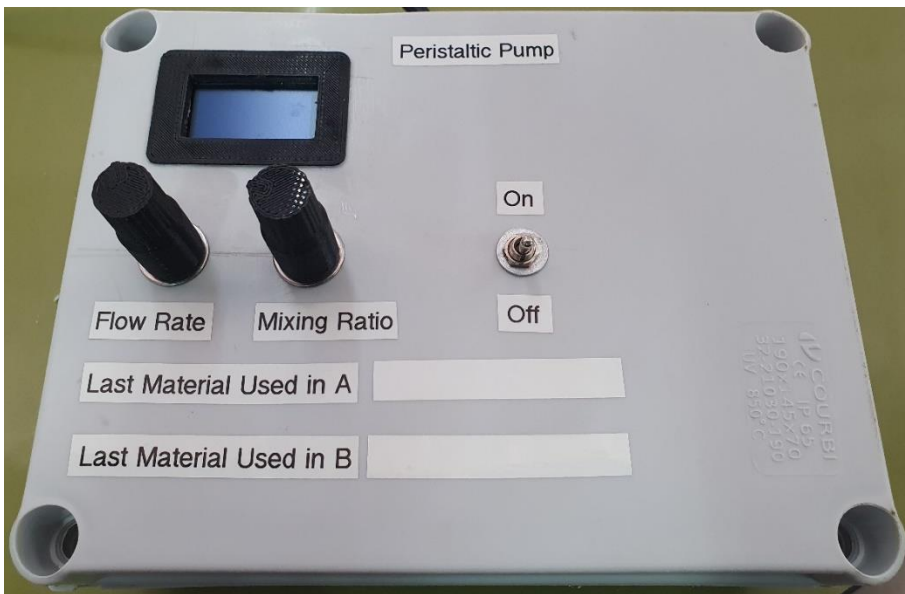
Figure 3.18: Peristaltic pump control box

3.2 Software Architecture

3.2.1 Modelling Software

Autodesk Inventor was used to design parts to be manufactured utilising the developed hybrid manufacturing platform. The traditional method to produce the fuselage for a vertical take-off and landing aircraft (VTOL), similar to the one shown in Figure 3.19, would be by starting with a large block of stock material and then producing the complex shape by milling away the material according to the generated G-code and M-code. This manufacturing method is wasteful and time-consuming as a considerable portion of the machining cycle is spent removing large amounts of excess stock material. A more suited method of producing the model shown in Figure 3.19 would be to deposit the additive material such that the stock material is just larger than the required dimensions. This method would significantly reduce the machining time and material wastage.
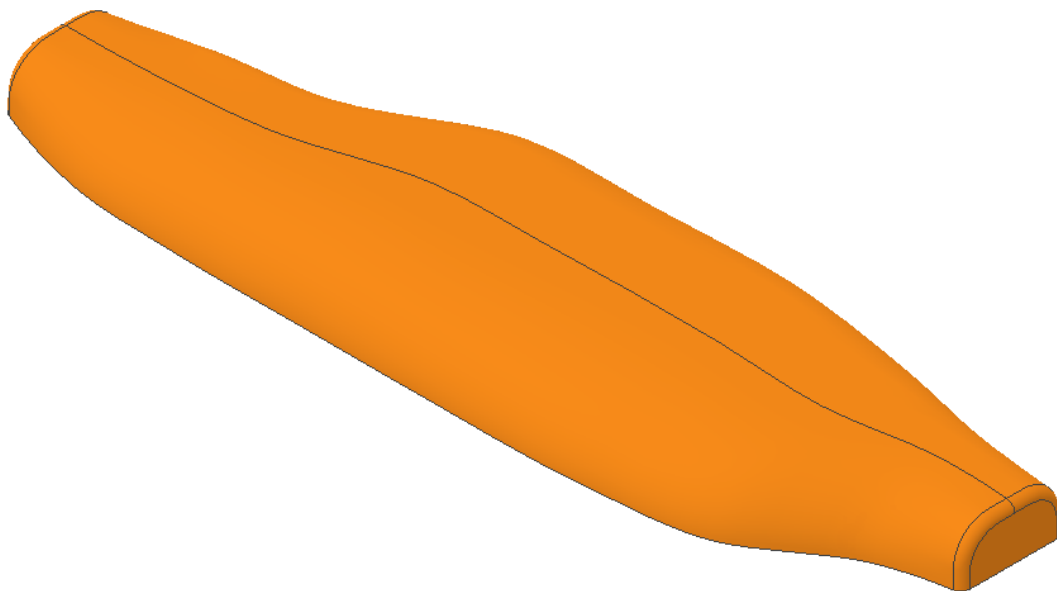
Figure 3.19: VTOL half fuselage modelled using Autodesk Inventor

Mastercam is a CAD/CAM software package used for designing parts, fixtures, and assemblies. The application range of Mastercam includes aerospace, education, medical, and energy – to name a few [73]. Mastercam was utilised for this research to program toolpaths for the hybrid system and to generate G-code to control the CNC machine. The creation of the toolpaths required to produce half of the scaled-down version of the VTOL's fuselage shown in Figure 3.19 was elaborated on in later chapters. In addition, Mastercam was used to create toolpaths for both the additive and subtractive aspects of this research.

3.2.2 Dosing System Software

Arduino Integrated Development Environment (IDE) is an open-source platform used to create and upload programs to compatible microcontroller boards such as the ESP32 development board. The IDE was used to develop and implement code to operate the dosing system. A calibration sequence used for initial testing of the dosing system was also created using the IDE platform. The developed code allowed the dosing system's flow rate and mixing ratio to be altered via two separate potentiometers. Additionally, the panel mount toggle switch was coded to enable or disable the two stepper motors, thus starting or stopping the flow of the additive material. The flow rate, measured in pulses per second, and the mixing ratio are displayed using the OLED I2C display. The dosing system code and the calibration sequence can be found in Appendix D1 and Appendix D2, respectively.

3.2.3 Beckhoff HMI

The Beckhoff Human-Machine Interface (HMI) was added and connected to the TwinCAT project that operated the CNC machine. The HMI was a user-friendly interface that allowed the operator to set the zero points for the X, Y and Z axes. This setting was done by jogging the machine to the desired position using the "Manual" mode and then pressing the "Set G54 Z Origin" and "Set G54 XY Origin" buttons once at the desired position. An override function allowed the operator to reduce the feed rate set in the G-code if the feed rate was too high. The operator could start, pause, stop and reset the machine cycle within a single screen. The HMI can be seen in Figure 3.20.
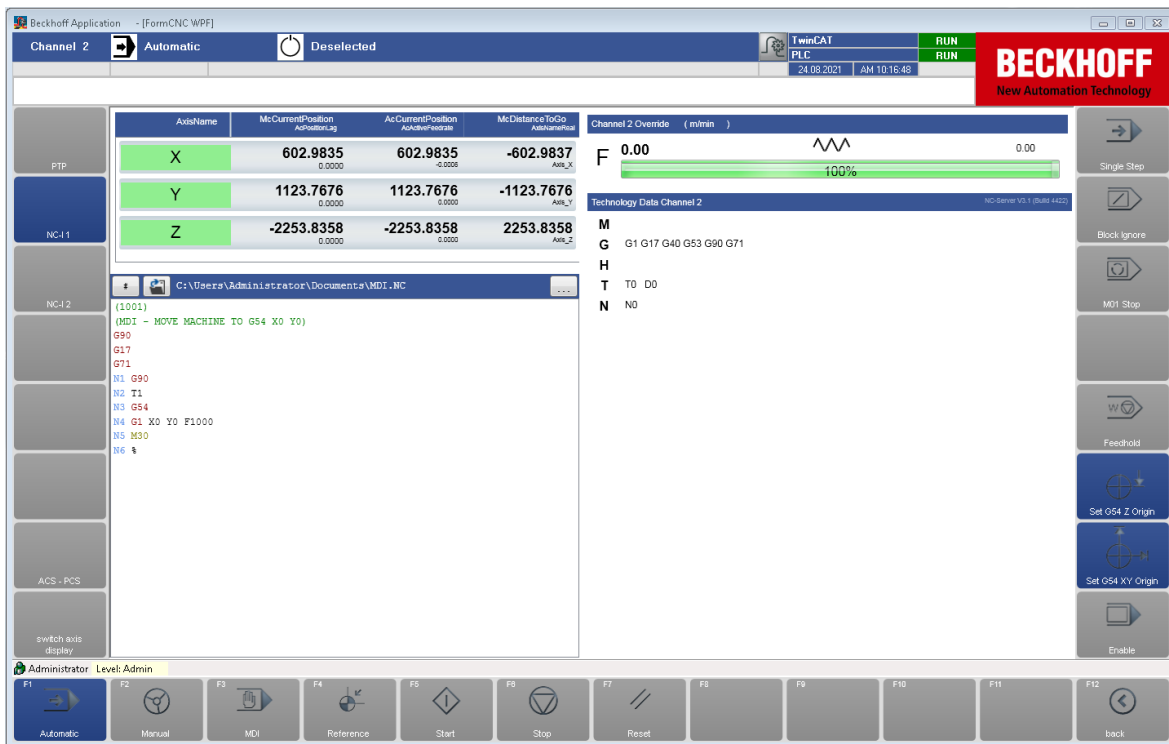
Figure 3.20: Beckhoff HMI illustrating the provided features

3.3 Chapter Conclusion

This chapter discussed the hardware and software architecture that was utilised in this research project. Elements such as the CNC mill workholding, the development of a dosing system, and the software utilised for both the additive and subtractive portions of this research were discussed. A design conceptualisation process using evaluation matrices was undergone, and the final proposed design was illustrated by the morphological chart shown in Table 3.8. Finally, a cost analysis for the proposed peristaltic dosing system to be utilised for this research project was undergone and can be seen in Table 3.9.

Chapter 4

Methodology

This chapter detailed the experimental procedure established to achieve the research objective as stated in Chapter 1. This experimental procedure was followed to produce data to evaluate and quantify the performance of the developed hybrid manufacturing system.

4.1 Experimental Procedure

The established experimental procedure to produce a working prototype from a 3D CAD model is detailed in Figure 4.1. This section expanded on the individual processes shown in Figure 4.1 that formed the experimental procedure for this research. The reverse arrows shown in Figure 4.1 indicated that it was possible to alternate between those processes if necessary.
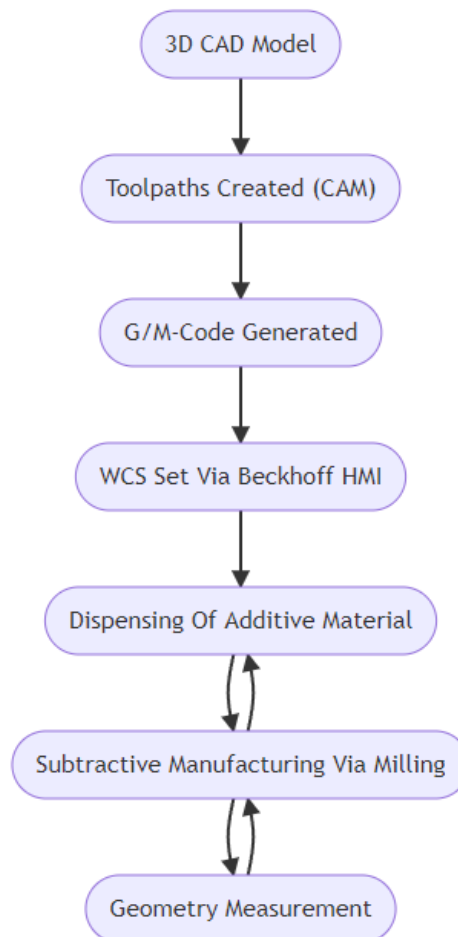
Figure 4.1: Flowchart describing the experimental procedure

4.1.1 3D CAD Model

As shown previously in Figure 3.19, a scaled-down version of half of the VTOL's fuselage was modelled using Autodesk Inventor. This model was used to describe the experimental procedure as illustrated in Figure 4.1. The VTOL's fuselage was merely utilised as an example, and the experimental procedure could be applied to countless other designs. The CAD model was exported to a STEP file format to be opened by a CAM software package, namely Mastercam for this research.

4.1.2 Toolpaths Created (CAM)

4.1.2.1 Subtractive Toolpaths

Once the CAD model had been imported into Mastercam, subtractive toolpaths – for roughing and finishing - were created to mill the geometry as shown in Figure 4.2 and Figure 4.3, respectively. First, a surface rough pocket toolpath was created to remove the majority of the stock material and produce the general shape of the fuselage whilst leaving a small amount of stock material on the drive surfaces to be cleaned up via a subsequent surface finish parallel toolpath. Next, various parameters needed to be set, including defining the cutting tool that was to be used for the operation, specifying the spindle speed, the feed rate, and the plunge rate, defining the surface parameters, which included the clearance height, retract height, feed plane, the stock to leave on the drive and check surfaces, and the tool containment. Finally, the finish parallel parameters needed to be defined, which included the cutting method, maximum stepover, and the machining angle, to name a few.
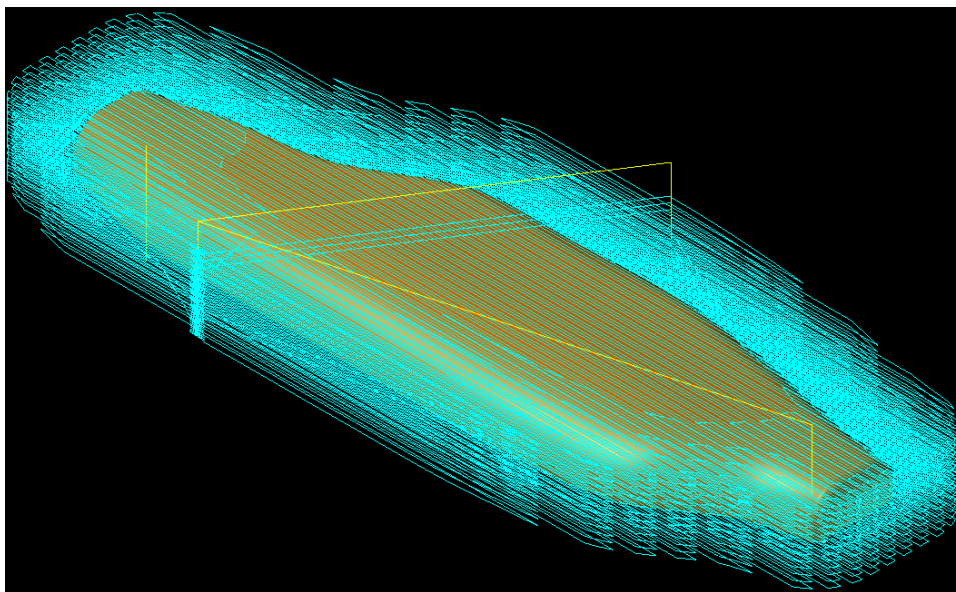
Figure 4.2: Surface rough pocket toolpath
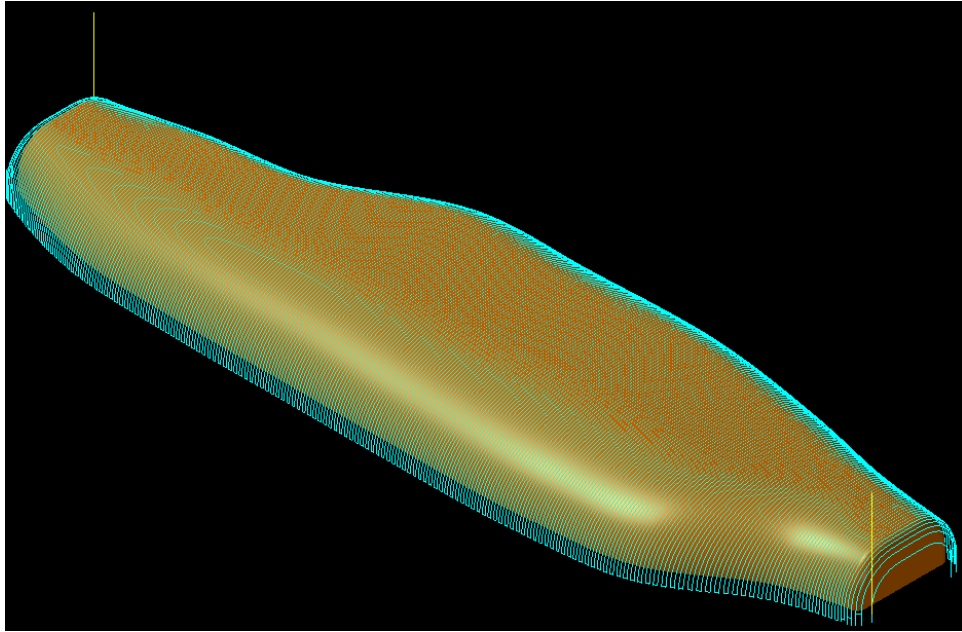
Figure 4.3: Subsequent surface finish parallel toolpath

The initial surface rough pocket toolpath was used to elaborate on the process of creating the required toolpaths. A 12 mm ball nose end mill was selected as the desired cutting tool to perform the roughing and finishing operations. When milling soft materials, such as the PU foam utilised in this research, a significantly high spindle speed and feed rate may cause the material to tear or burn rather than cut. Therefore, a spindle speed of 12000 RPM and a feed rate of 3000 mm/min was selected and programmed, as shown in Figure 4.4. Since a VFD controlled the spindle speed and the Beckhoff HMI provided a feed override function as shown in Figure 3.20, the speed and feed could be adjusted during the milling operations and were not fixed at these predetermined values.
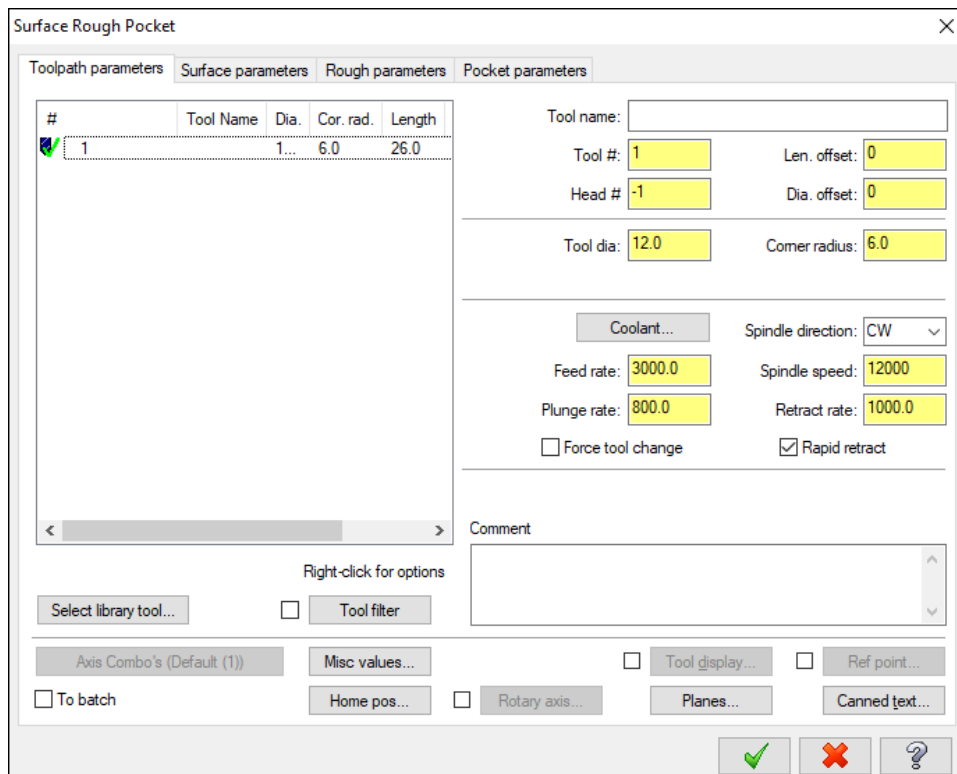
Figure 4.4: Defined toolpath parameters within Mastercam

The next step in the process was to define the surface parameters, as shown in Figure 4.5. The clearance and retract heights were set to an absolute value of 80 mm. These heights ensured that the tool would not collide with the material when moving between cutting passes. Incremental meant that the displayed value was relative to the chained geometry when creating the toolpath, whilst absolute was relative to the defined WCS of the model. The feed plane was set as incremental so that the cutting tool would rapid to exactly 5 mm above the previous cutting depth. Had absolute been selected for the feed plane, the cutting tool would rapid to 5 mm above the initial top of stock upon completion of each successive cutting depth, significantly increasing the cycle time. The stock to leave on the drive surfaces was set to 0.4 mm. This 0.4 mm would be cleaned up afterwards utilising a subsequent surface finish parallel toolpath, producing a smoother surface finish.
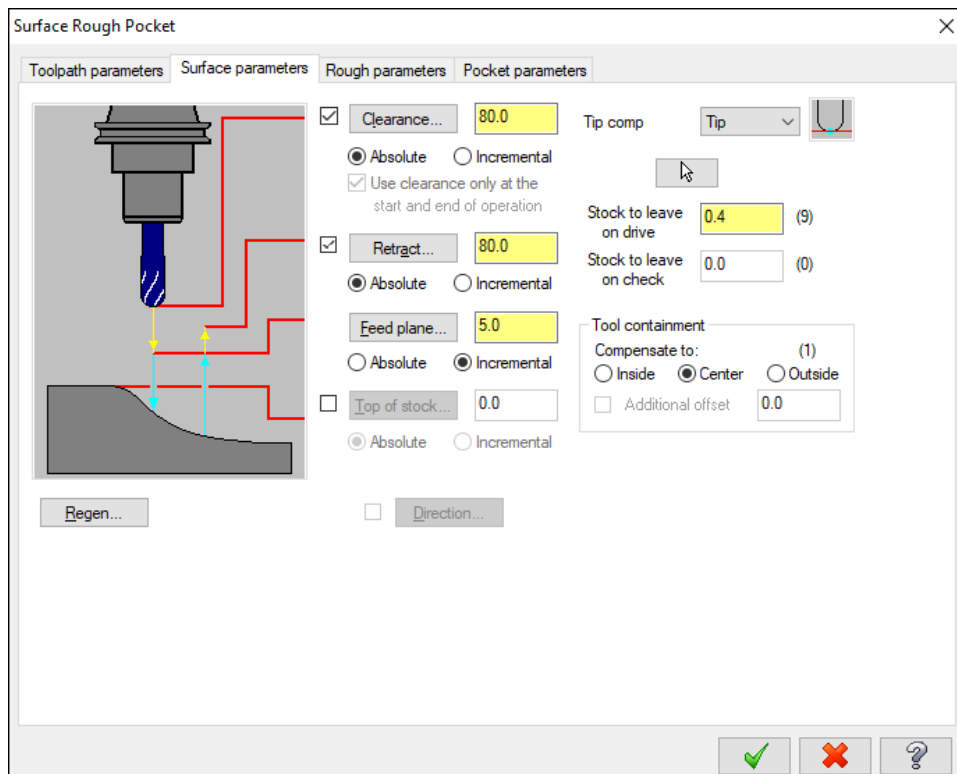
Figure 4.5: Defined surface parameters

Figure 4.6 detailed the defined rough parameters. In conventional milling, the direction of motion of the cutting tool is opposite to that of the feed direction. In climb milling, the direction of motion of the cutter is in the same direction as the feed direction [74]. As a result, climb milling produces a smoother surface finish and improves tool life as the forces experienced at the tool's cutting edge are reduced. Climb milling was therefore selected as the preferred machining direction for the surface rough pocket toolpath. Since the cutting material was PU foam, a highly machinable material, the maximum stepdown was set to 5 mm, just less than half the diameter of the ball nose end mill utilised. The maximum stepdown represented the maximum depth that the tool would descend before completing a single cutting pass. The cut depths shown in Figure 4.7 ensured that the cutting tool machined past the base of the drive surfaces by setting the maximum depth 6 mm below the Z zero position, relative to the centre of the ball nose end mill. The gap settings defined in Figure 4.8 ensured that the cutting tool stayed engaged with the material as much as possible and prevented any unnecessary retracts that would have increased the cycle time.
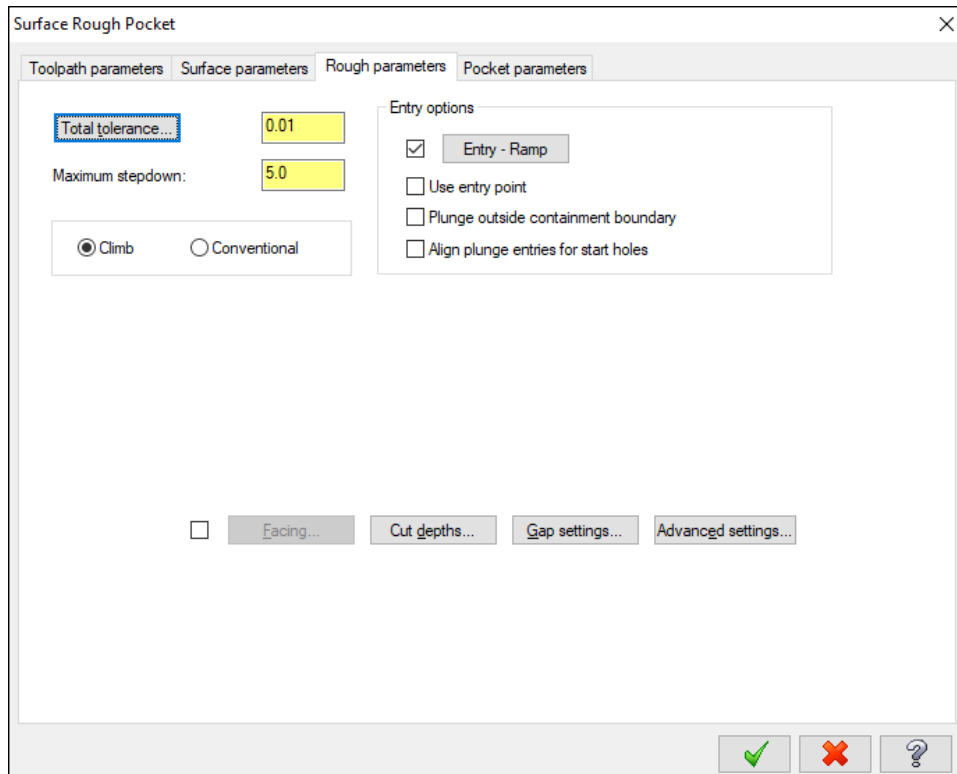
Figure 4.6: Defined rough parameters
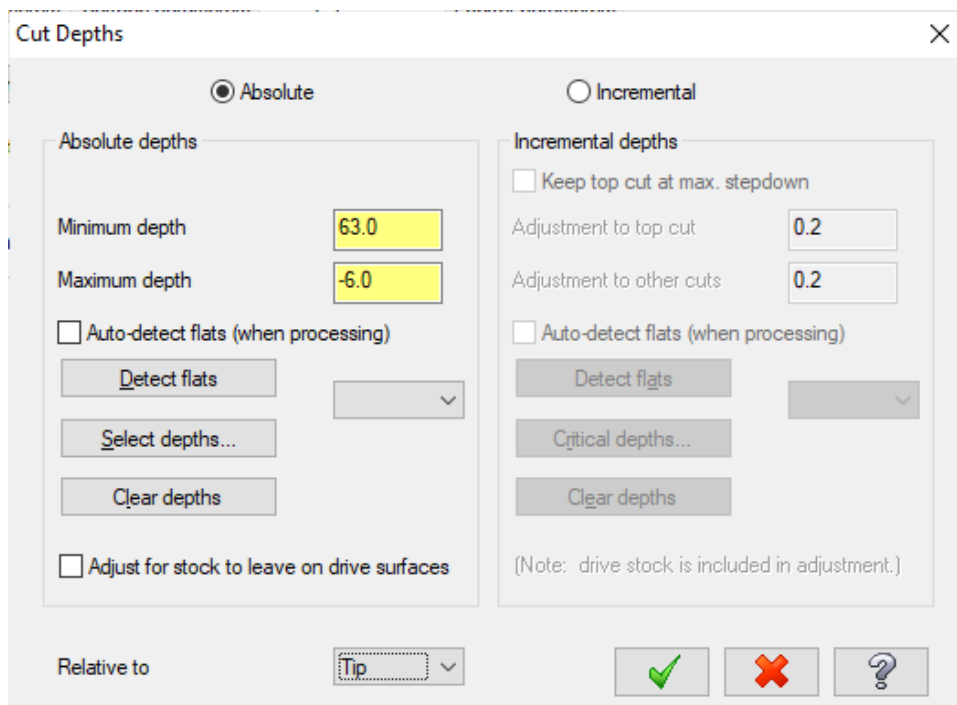
Figure 4.7: Defined cut depths
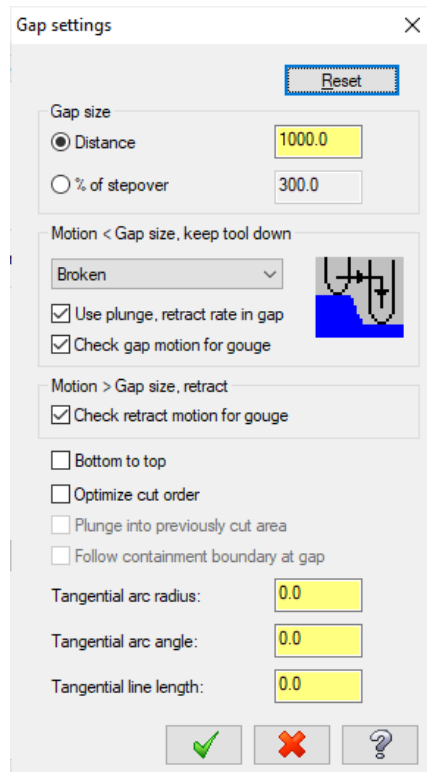
Figure 4.8: Defined gap settings

A ramping entry motion was defined to avoid plunging the cutting tool into the material, as shown in Figure 4.9. The plunge zig and zag angles were both set to 3° to speed up the ramping motion.
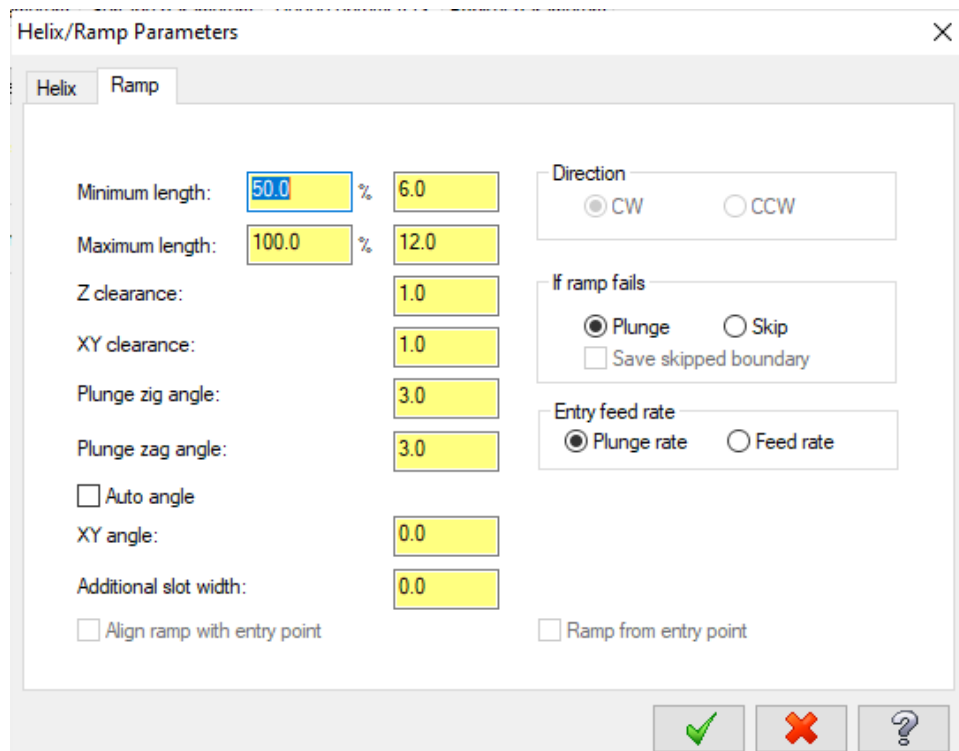
Figure 4.9: Defined ramp parameters

Figure 4.10 depicts the pocket parameters. A zigzag cutting method with a stepover percentage of 60 percent of the tool's diameter was selected to perform the pocket operation.
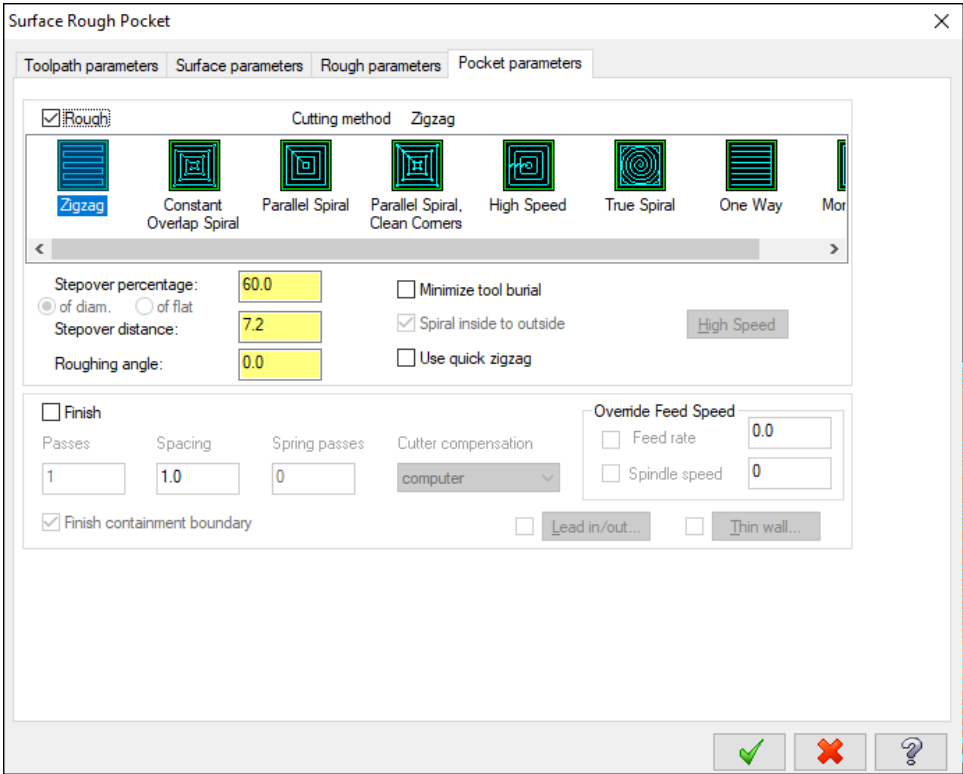
Figure 4.10: Defined pocket parameters

Finally, to completely define the surface rough pocket toolpath, a containment boundary needed to be defined. The containment boundary restricted the cutting tool to the interior of the boundary. The containment boundary depicted in Figure 4.11 was created using an offset contour transform of the VTOL fuselage.
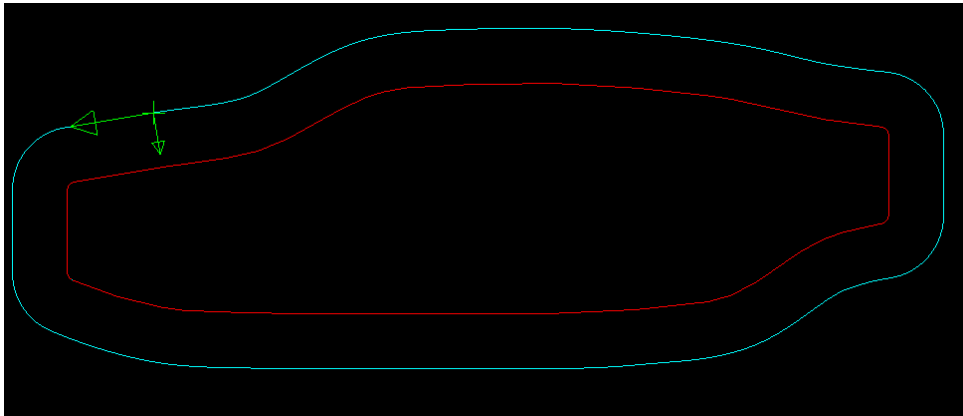
Figure 4.11: Containment boundary

4.1.2.2 Additive Toolpaths

Standard slicer software for 3D printing utilises many G and M-codes that would not be recognised by the proposed hybrid system for this research. For example, "E" in slicer G-code refers to the length of the filament that is to be extruded during a move. Therefore, it was decided that creating a facing toolpath that was contained within the perimeter of the shape to be produced, whilst inverting the Z values so that the nozzle of the dosing system moved upwards instead of downwards, was the optimal solution. The additive toolpath would be loaded onto the Beckhoff HMI and executed before finishing the hybrid process with the subtractive toolpaths. An example of an additive facing toolpath is shown in Figure 4.12, whereby the general shape of the model would be produced by additively depositing the PU foam.
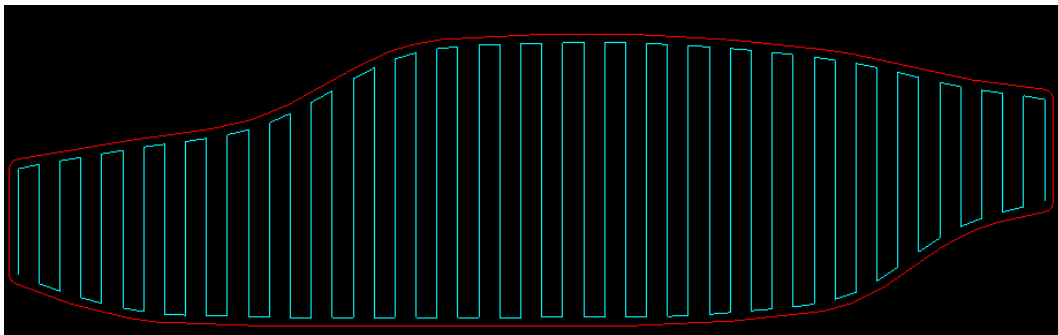
Figure 4.12: Additive facing toolpath

4.1.3 G/M-code Generated

Once the additive and subtractive toolpaths had been generated and verified using the Mastercam verify function, the toolpaths were posted, and a .NC file was generated. Figure 4.13 displayed the initial verified surface rough pocket toolpath, and Figure 4.14 displayed the verified combination of the initial surface rough pocket toolpath and the subsequent surface finish parallel toolpath. Mastercam automatically detected the stock material by creating a rectangular bounding box around the CAD model.
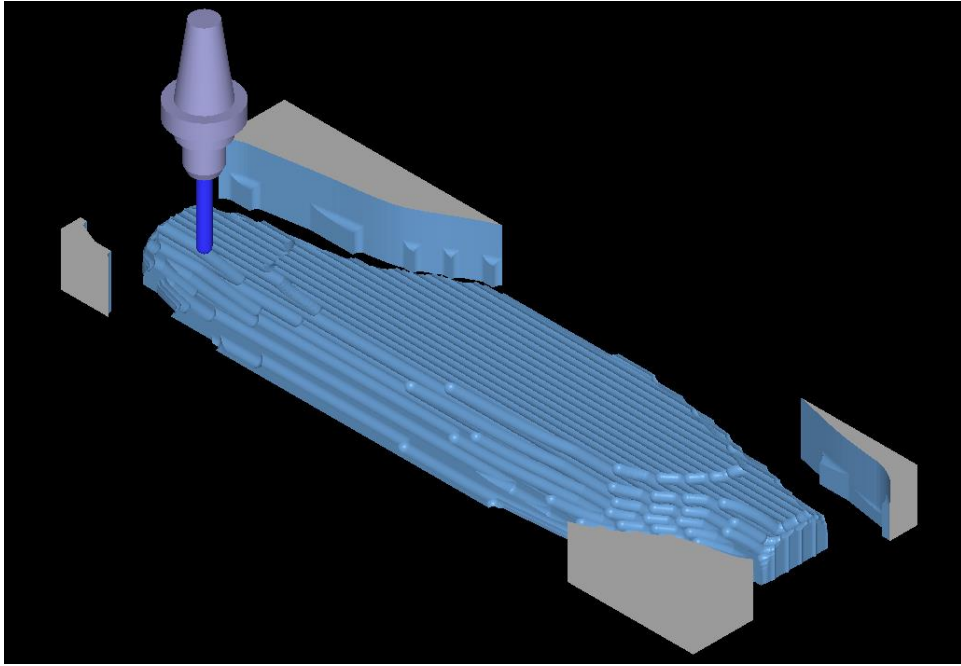
Figure 4.13: Initial surface rough pocket toolpath verified
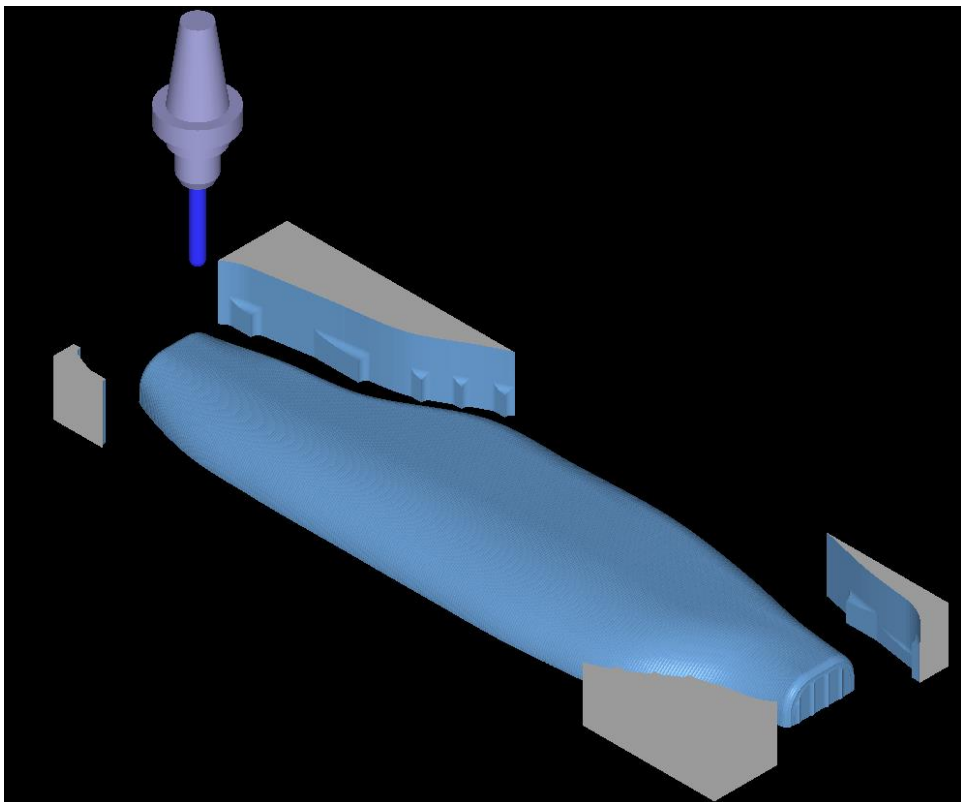
Figure 4.14: Combined rough and finish toolpaths verified

A .NC file contains the numerical control instructions that control the motion of the CNC machine. CIMCO Edit is a CNC program editor capable of interpreting and editing .NC files. CIMCO Edit was utilised for this research project to edit the produced G/M-code so that the Beckhoff software could recognise it. An example of where CIMCO Edit was frequently needed was for radius programming. According to the Beckhoff Information System, "for Radius Programming the centre point is derived from the radius that is given by the U parameter." [75] The R parameter represented radii produced using Mastercam, a parameter not recognised by the Beckhoff software, and CIMCO Edit was thus required to replace all R parameters with U parameters. An extract of the additive facing G/M-code generated can be seen in Figure 4.15, whereby the rough shape of the model was deposited. An extract of the subtractive G/M-code generated to rough and finish the VTOL fuselage can be seen in Figure 4.16. An example of how CIMCO was used to replace all R parameters with U parameters is depicted in Figure 4.17.

```
 1  (1001)
 2  (ADDITIVE_TOOLPATH)
 3  G90
 4  G17
 5  G71
 6  G90
 7  (TOOL - PU FOAM NOZZLE)
 8  N10T2
 9  G54
10  N20G0X-298.998Y-64.057S0M5
11  N30Z20.
12  N40G1Z3.F2000.M8
13  N50Y14.028
14  N60X-293.018Y16.177
15  N70Y-63.859
16  N80X-287.038Y-66.27
17  N90Y17.174
```

Figure 4.15: CIMCO used to display the additive facing G/M-code generated

Figure 4.16: Combined roughing and finishing G and M-codes

Figure 4.17: CIMCO used to replace R parameters with U parameters

Previously defined parameters such as the spindle speed, plunge rate, and feed rate could be altered within the editor before being sent to the CNC machine. Figure 4.18 displays the list of cycles and macros assigned to the G and M codes used in the program. Once all the necessary changes to the .NC files had been made, the files were loaded onto the CNC machine via the Beckhoff HMI.
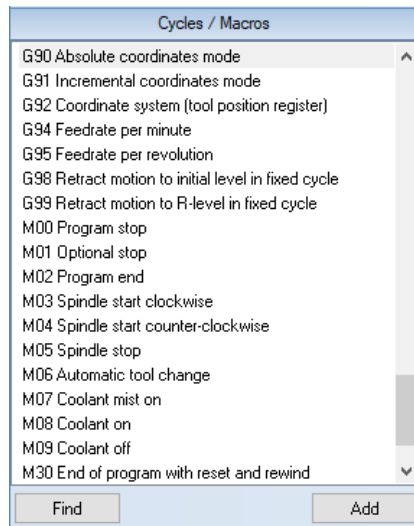
Figure 4.18: List of cycles/macros assigned to the G/M-codes

4.1.4 WCS Set via Beckhoff HMI

With the necessary .NC files loaded onto the Beckhoff HMI and ready to run; the next stage of the experimental procedure was to define the WCS by setting the X, Y, and Z zero points of the part to be manufactured. As shown in Figure 4.19, the X and Y zero points were located in the middle, and the bottom of the fuselage was the Z zero location. Next, the CNC milling machine was set to manual mode within the Beckhoff HMI and moved to the location that matched the defined WCS within Mastercam. Once at the desired location, the "Set G54 Z Origin" and "Set G54 XY Origin" buttons shown in Figure 3.20 were pressed. The same zero position was utilised for the additive and subtractive processes to execute the two operations within a single setup.
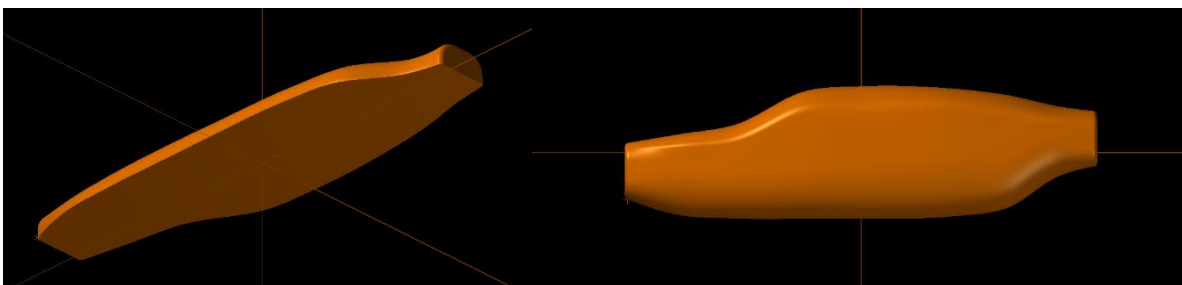
Figure 4.19: Axes lines indicating the active WCS within Mastercam

4.1.5 Dispensing of Additive Material

With the WCS of the milling machine defined, the additive facing toolpath that was previously created and shown in Figure 4.12 could be executed. The PU foam would expand over the perimeter of the desired part, thus creating the stock material to be milled away. The foam was allowed to expand and cure until it was rigid enough to be milled.

4.1.6 Subtractive Manufacturing via Milling

Since the same WCS was utilised in programming both the additive and subtractive toolpaths, the zero position, relating to the X, Y and Z coordinates of the part, had already been set. Thus, alternating between the additive and subtractive processes was achieved by loading and executing the appropriate G-code file required to perform the operation via the Beckhoff HMI. This interchangeability between additive and subtractive manufacturing allowed for complex geometries, such as internal features and undercuts, to be produced.

4.1.7 Geometry Measurement

Upon measurement of the produced parts, additional material could be added or removed if the produced part did not fall within the permissible tolerance range as governed by the ISO 2768 standard. This standard was detailed later on in this dissertation.

4.2 Chapter Conclusion

This chapter detailed the methodology of this research project and described the established experimental procedure that was executed to produce working prototypes. The experimental procedure shown in Figure 4.1 served as a guideline to be followed to manufacture a working prototype through the use of HM by material deposition and machining. As stated previously, the experimental procedure described in this chapter would apply to any other CAD model, and the scaled-down version of the VTOL fuselage was merely used to describe the processes followed. Additionally, had the surface finish of the produced part been inadequate, a layer of additive material could be deposited and re-machined until an acceptable surface finish was obtained.

Chapter 5

Results and Discussion

This chapter discussed the results of testing the developed system by utilising the experimental procedure described in Chapter 4. First, theoretical analysis in the form of locational accuracy for the CNC gantry was undertaken. Second, statistical analysis was performed on the experimentally produced parts, which included dimensional accuracy, repeatability, and stability after a certain period had elapsed. Third, the effects of altering the process parameters such as the spindle speed, feed rate, and depth of cut were considered and analysed. Fourth, the theoretical and experimental material wastage was computed and compared. Fifth, the cycle time of the developed system was compared against a commercially available AM system. Finally, the findings and trends deduced were discussed.

5.1 Theoretical Analysis

A theoretical analysis was conducted to evaluate the locational performance of the CNC gantry. The results obtained gave a broad indication of the dimensional accuracy expected once the experimental analysis had begun. Fine tolerance grades would not have been possible had the locational evaluation of the CNC gantry yielded unsatisfactory results.

5.1.1 CNC Gantry Locational Accuracy

Two Beckhoff AM8131-0F20 servomotors were used to drive the X and Y axes, and the Beckhoff AM8131-0F21 servomotor drove the Z-axis. As shown in Figure 5.1, the system accuracy for the AM813x series was approximately 0.17° [76].

Feedback system	Resolution	System accuracy		Comment
OCT, single-turn OCT, multi-turn	18-bit	± 120 angular sec.	approx. 0.03°	Standard
OCT, single-turn OCT, multi-turn	24-bit	± 25 angular sec.	approx. 0.0069	SIL 2
Resolver	14-bit	± 600 angular sec.	approx. 0.17°	**Option:** AM812x, AM813x and AM814x

Figure 5.1: Beckhoff feedback system specifications [76]

Equation 5.1 defined the linear travel of the belt per complete revolution of the servomotor.

$$C = 2\pi r \tag{5.1}$$

Where C represented the pulley's circumference, and r represented the outside radius of the pulley.

Using Equation 5.1 and an outside pulley diameter of 37 mm, the linear travel of the belt per complete revolution for both the X and Y axes was calculated to be:

$$C = 2\pi \left(\frac{37}{2}\right)$$

$$= 116.239 \, mm$$

Equation 5.2 defined the relationship between the linear travel of belt the and the degrees of rotation of the servomotor. The linear travel of the belt per degree of rotation was defined by k.

$$C = k\theta \tag{5.2}$$

Where

$$k = \frac{116.239}{360}$$

$$= 0.323 \, mm/°$$

No gearbox, or any other form of speed reduction, was implemented between the output shaft of the servomotor and the linear carriage that controlled the X and Y movements of the CNC machine. Therefore, for a 0.17° rotation of the servomotor, the minimum theoretical movement of the carriage along the X and Y axes was calculated as:

$$d = 0.323 \times 0.17$$

$$= 0.055 \, mm$$

This 0.055 mm (represented by d) was computed by neglecting the elasticity and wear of the timing belts. Misalignment, a poorly-tensioned belt, and swarf build up on the timing belt or pulley may affect the motion of the linear carriage.

The ball screws used to raise and lower the gantry had a pitch of 10 mm. Equation 5.3 defined the linear travel per complete revolution of the ball screw.

$$L = np \tag{5.3}$$

Where L represented the lead - the linear travel per complete revolution of the ball screw, n represented the number of starts and p represented the pitch of the ball screw.

The lead for the single-start ball screw was calculated to be:

$$L = 1 \times 10$$

$$= 10 \ mm$$

The linear travel per degree of rotation of the ball screw was found to be as follows:

$$k = \frac{10}{360} = 0.0278 \ mm$$

Therefore, for a 0.17° rotation of the servomotor, the minimum theoretical movement of the carriage along the Z-axis was calculated as:

$$d = 0.0278 \times 0.17$$

$$= 0.0047 \ mm$$

Similar to the minimum theoretical movement of the linear carriage about the X and Y axes, this 0.0047 mm was computed by neglecting the elasticity and wear of the timing belts used to drive the ball screws along the Z-axis of the CNC machine.

The minimum theoretical movements of 0.055 mm in X and Y, and 0.0047 mm in Z, were calculated as reference values, and the actual minimum movements of the carriage would not be as accurate.

5.2 Experimental Analysis

An experimental analysis was conducted to evaluate the performance of the developed system. The experimental analysis was divided into various system tests. Each system test consisted of a description of how the test was carried out, the observations made during the testing, and a discussion section that detailed the findings of the individual system tests.

5.2.1 System Test 1

The first system test aimed to isolate and evaluate the performance of the developed dosing system. Had the dosing system not produced accurate, repeatable results, the hybrid system would not have yielded desirable results.

5.2.1.1 Description of Test 1

An experimental procedure was established to measure the experimentally obtained discharge, and the measurements were taken at STP conditions using water as the pumping fluid. The two peristaltic pumps were primed with water from the supply container, and both outlet lines were placed within the 500ml Glassco measuring cylinder, as shown in Figure 5.2. The test platform to conduct the initial dosing system testing can be seen in Figure 5.2. The calibration sequence was loaded onto the ESP32 via the Arduino IDE so that the pumps could be set to run for a fixed duration. Once the calibration sequence had been loaded, the Arduino IDE prompted the user to begin the calibration sequence via the serial monitor. The serial monitor within the IDE and the command required to begin the calibration sequence can be seen in Figure 5.3. Once the calibration sequence had finished, the outputs were disabled, and the serial monitor prompted the user, as shown in Figure 5.4.
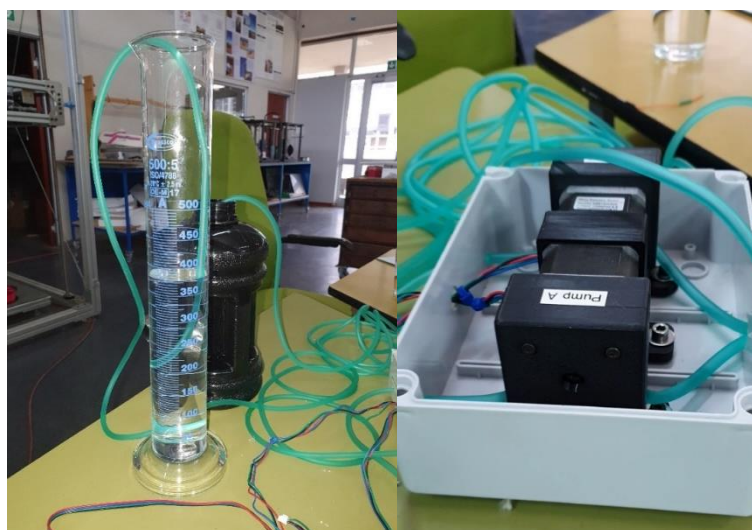
Figure 5.2: Test platform for initial dosing system testing
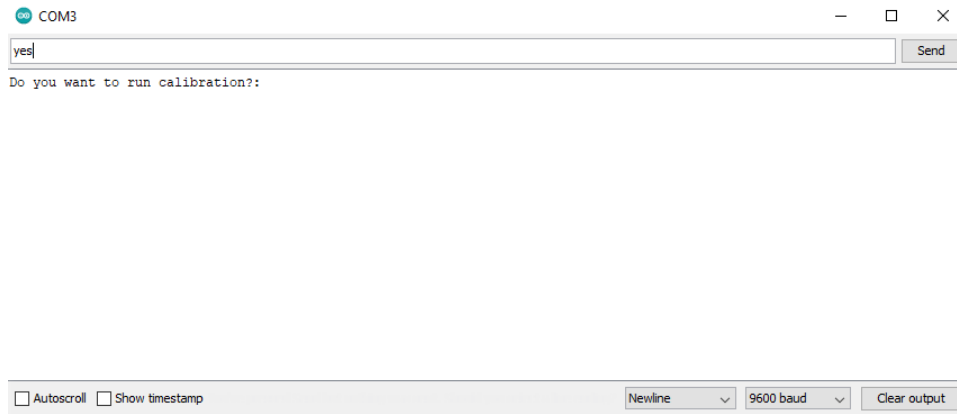
Figure 5.3: Initiation of the calibration sequence utilising the IDE serial monitor
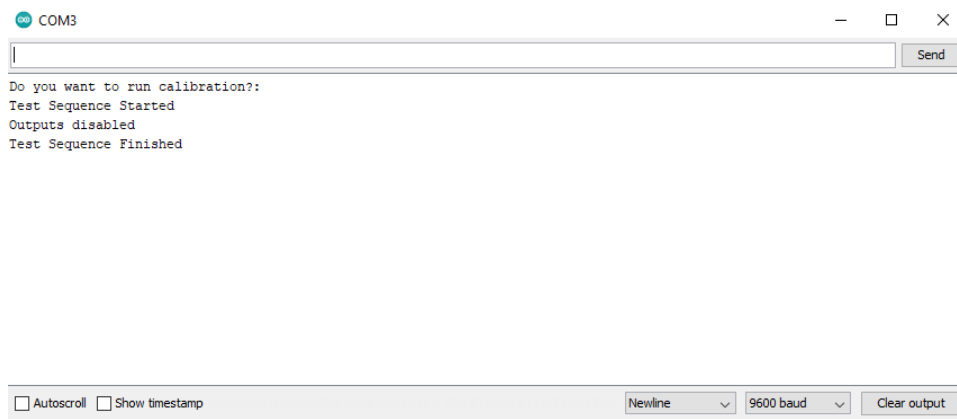
Figure 5.4: Serial monitor displaying the end of the test sequence

5.2.1.2 Observations of Test 1

The experimental discharge for a 64-second cycle can be seen in Table 5.1. The cycle consisted of a four-second ramp to 2000 PPS at a constant acceleration of 500 pulses/s^2, followed by 60 seconds of steady-state flow at 2000 PPS.

Table 5.1: Experimental discharge measured during a 64s cycle

Test Number	Pulses per Second (PPS)	Duration (s)	Experimental Discharge (ml)
1	2000	64	375
2	2000	64	375
3	2000	64	375
4	2000	64	385
5	2000	64	385
6	2000	64	385
7	2000	64	385
8	2000	64	390
9	2000	64	385
10	2000	64	390

The ramping experimental discharge was defined by how many ml of water was discharged during the ramping cycle alone. The acceleration of the ramp was set to a constant 500 pulses/s^2 throughout the experimental procedure, which resulted in a four-second ramp to reach the required 2000 pulses/s. The ramping experimental discharge for the four-second ramping cycle can be seen in Table 5.2.

Table 5.2: Experimental discharge measured during the 4s ramping cycle to 2000 PPS

Test Number	Pulses per Second (PPS)	Duration (s)	Ramping Experimental Discharge (ml)
1	2000	4	12.9
2	2000	4	12.7
3	2000	4	12.8
4	2000	4	12.7
5	2000	4	12.8
6	2000	4	12.7
7	2000	4	12.7
8	2000	4	12.6
9	2000	4	12.5
10	2000	4	12.7

The resultant experimental discharge was defined by how many ml of water was discharged by the pump per minute of steady-state flow. Therefore, the resultant experimental discharge for 60 seconds of steady-state flow at 2000 PPS was determined by subtracting the experimental discharge for the four-second ramping cycle shown in Table 5.2 from the 64-second cycle shown in Table 5.1. The resultant experimental discharge can be seen in Table 5.3.

Table 5.3: Resultant experimental discharge for 60 seconds of steady-state at 2000 PPS

Test Number	Pulses per Second (PPS)	Resultant Experimental Discharge (ml/min)
1	2000	362.1
2	2000	362.3
3	2000	362.2
4	2000	372.3
5	2000	372.2
6	2000	372.3
7	2000	372.3
8	2000	377.4
9	2000	372.5
10	2000	377.3

The described experimental procedure was repeated at various motor speeds, and the obtained results can be seen in Table 5.4. The minimum, maximum, and average discharge (measured in ml/min) for a set motor speed was obtained using the resultant discharge values shown in Table 5.3. The accuracy range was calculated by subtracting the minimum discharge from the maximum discharge and was used to estimate the expected accuracy of the system for a desired motor speed. Finally, Figure 5.5 was generated to illustrate the minimum, maximum, and average experimental discharge measured at various motor speeds.

Table 5.4: Minimum, maximum, and average experimental discharge values at various motor speeds

PPS	*Motor Speed (RPM)*	*Min Discharge (ml/min)*	*Max Discharge (ml/min)*	*Average Discharge (ml/min)*	*Accuracy Range (Max-Min) (ml/min)*
400	120	69.3	74.6	72.5	5.3
800	240	142.7	152.9	147.31	10.2
1200	360	220.3	230.5	223.91	10.2
1600	480	287	297.2	293.14	10.2
2000	600	362.1	377.4	370.29	15.3
2400	720	442.1	452.2	446.17	10.1
2800	840	503.6	523.8	512.68	20.2
3200	960	550.6	570.4	561.42	19.8
3600	1080	624.2	634.6	628.38	10.4
4000	1200	683.2	703.2	697.02	20
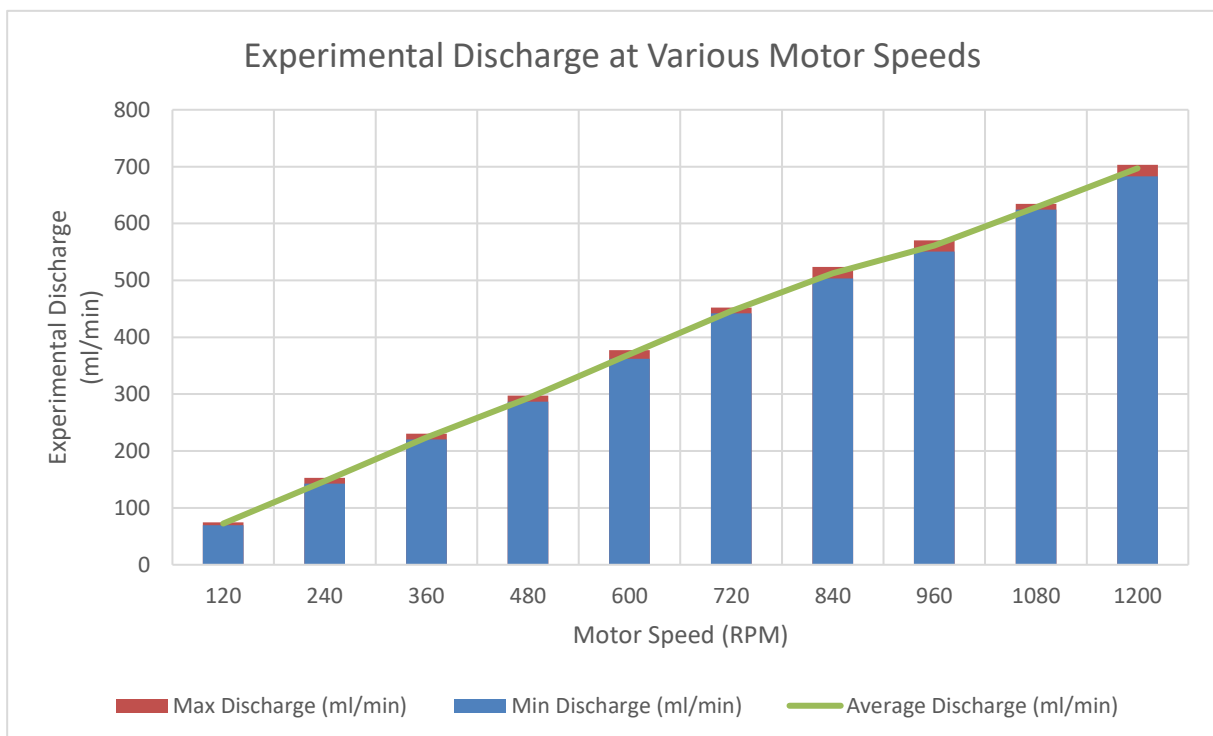
Figure 5.5: Minimum, maximum, and average experimental discharge values at various motor speeds

Figure 5.6 illustrated the accuracy range that was recorded at various motor speeds. An exponential trendline was plotted to visualise the effect on the accuracy range with an increase in motor speed.
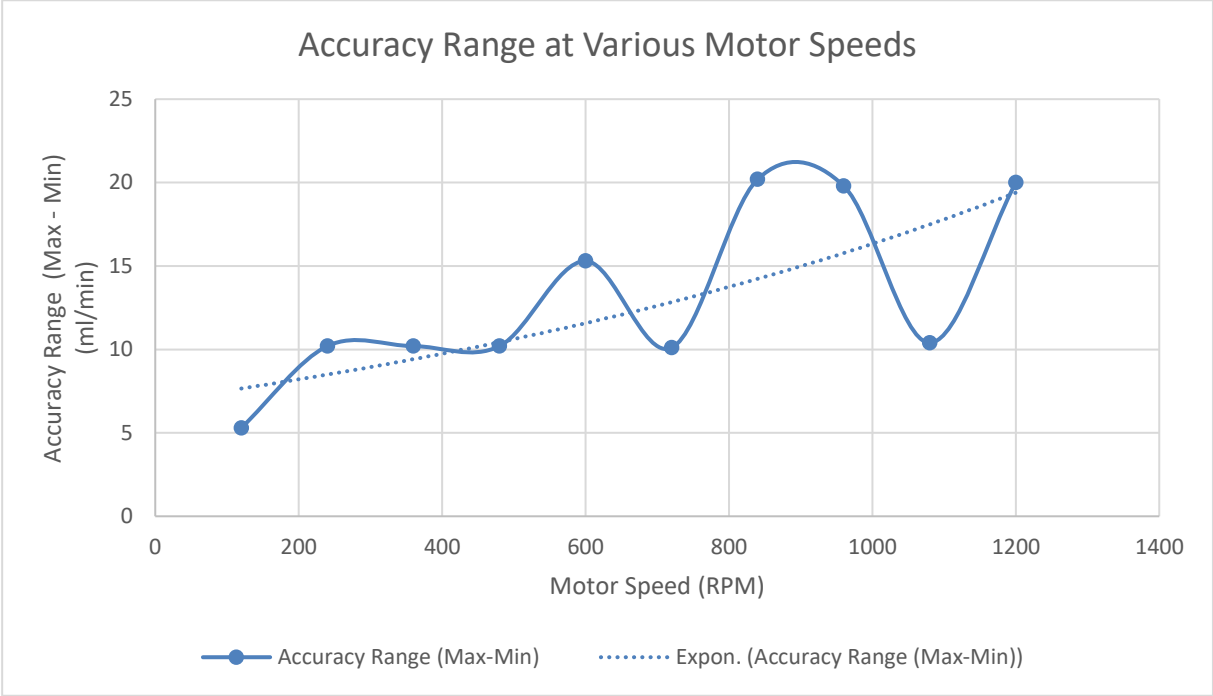
Figure 5.6: Accuracy range at various motor speeds

5.2.1.3 Discussion of Test 1

Table 5.4 and Figure 5.5 displayed the minimum, maximum, and average experimental discharge recorded at various motor speeds. From Figure 5.5, it was found that the experimental discharge was directly proportional to the speed of the motor. The largest accuracy range value of 20.2 ml/min occurred at a motor speed of 840 RPM. The accuracy errors that were obtained may have been a result of the following influencing factors:

➢ Pipe losses caused by friction.
➢ Deterioration of the silicone tubing with each rotation as the tubing was compressed by the rollers.
➢ Human error – inaccurate reading of the fluid in the measuring cylinder (i.e., parallax error), inaccurate weighing of the measuring cylinder.

5.2.2 System Test 2

The second system test aimed to determine the flow ratio required to produce the appropriate mixing ratio for the Ecospray RS3030 PU foam.

5.2.2.1 Description of Test 2

The PU foam technical data sheets shown in Appendix B1 indicated that the volume concentration of the two-part formulation was to be 100:100. The Resinate 200 had a density of 1.15 g/ml, while the Ecospray RS3030 had a density of 1.22 – 1.23 g/ml. The difference in densities between the two parts meant that the mass ratio of Ecospray RS3030 to Resinate 200 was 100:107 pbm. Two separate containers were placed onto a scale, and equal parts by mass of Ecospray RS3030 and Resinate 200 were poured into these containers. Two holes were drilled into the top of both containers to accommodate the silicone tubing utilised by the dosing system. The inlet and outlet lines of pump A and pump B were connected to the Ecospray RS3030 (Part A) container and the Resinate 200 (Part B) container, respectively. The pumps were primed to fill the lines with the two separate parts and to remove any air that may have been present. With the lines primed, two empty containers, identical to the containers used to hold part A and part B, were placed onto a scale, and the mass of each was measured. The calibration sequence utilised previously was loaded onto the ESP32 and was set to run for 15 seconds. Upon completion of the calibration sequence, the mass of part A and part B collected in the empty containers were recorded.

Figure 5.7 illustrates the described procedure utilised to determine the mass flow rate of the two different PU foam products. The process was repeated, and the results obtained can be seen in Table 5.5 and Table 5.6. In addition, a thermocouple was used to measure the temperature of the product, as shown in Figure 5.8.

Figure 5.7: Experimental procedure to determine the mass flow rate of both products

Figure 5.8: Thermocouple used to measure the temperature of the product

5.2.2.2 Observations of Test 2

Upon investigation of the flow exhibited by both part A and part B, it was noted that part A had a higher level of viscosity, which resulted in a higher resistance to flow when compared to part B. Therefore, the flow ratio of the dosing system needed to be adjusted to produce the desired mass flow ratio. The mass of part A and part B collected during a specified cycle time for a set motor speed was measured and can be seen in Table 5.5 and Table 5.6.

Table 5.5: Product collected during a 15s cycle with a 50:50 flow ratio

Test Number	Ratio (A:B)	A Temperature (°C)	B Temperature (°C)	A PPS	B PPS	A Measured (g)	B Measured (g)
1	50	19	19	1800	1800	3.8	15.4
2	50	19	19	1800	1800	3.6	15.2
3	50	19	19	1800	1800	3.6	15.2

Table 5.6: Product collected during a 15s cycle with a 75:25 flow ratio

Test Number	Ratio (A:B)	A Temperature (°C)	B Temperature (°C)	A PPS	B PPS	A Measured (g)	B Measured (g)
1	75	19	19	3150	450	3.9	14.4
2	75	19	19	3150	450	3.8	14.6
3	75	19	19	3150	450	3.8	14.4

Table 5.5 and Table 5.6 noted that increasing the PPS of motor A by setting a 75:25 flow ratio yielded no significant change in the mass collected during a 15-second cycle. The mass collected in container B had, however, experienced a slight decrease with a decrease in motor speed. To increase the mass flow rate of part A, heat was introduced into the system to decrease the product's viscosity. A 24V heated bed, commonly used in 3D printers to improve part adhesion, was connected to an STC-1000 temperature controller and was used to supplement the system with the necessary heating. The plastic container previously used to hold part A of the mixture was replaced with a stainless steel container. The stainless steel container proved to be more conductive than the plastic container, which allowed the desired temperature to be obtained more rapidly. The stainless steel container could also maintain the desired temperature once it had reached the setpoint.

The programming of the setpoint and the resolution of the STC-1000 can be seen in Figure 5.9. The resolution was set to 0.1 °C, which meant that once the measured temperature had decreased below the set temperature by 0.1 °C, the heating cycle was enabled. The described temperature control system utilised to decrease the viscosity of part A and thus increase its mass flow rate can be seen in Figure 5.10.

Figure 5.9: Programming the temperature setpoint and resolution on the STC-1000 temperature controller

Figure 5.10: Temperature control system utilised to decrease the viscosity of part A

To determine the effect of heat on the mass flow of part A of the PU foam mixture, the temperature control system shown in Figure 5.10 was utilised. First, the setpoint of the STC-1000 temperature controller was programmed. Once the system had reached the specified setpoint, the temperature of the product was recorded by reading the value displayed by the thermocouple placed in the product. Once the system had stabilised around the programmed setpoint, a 15-second cycle at a motor speed of 1800 PPS was executed. The mass collected within the stainless steel container upon completion of the cycle was recorded. This described process was repeated at varying STC-1000 setpoints, and the results can be seen in Table 5.7. Finally, the graph in Figure 5.11 was generated to compare the mass of part A collected within the container at different temperature setpoints.

Table 5.7: The effects of temperature on the mass flow of part A for a 15-second cycle at 1800 PPS motor speed

Test Number	STC-1000 Setpoint (°C)	Container Thermocouple Reading (°C)	A Measured (g)
1	40	32	5.5
2	40	32	5.5
3	40	32	5.6
4	50	41	7
5	50	41	7.1
6	50	41	7.1
7	60	50	10.5
8	60	50	10.5
9	60	50	10.7
10	62	52	14
11	62	52	14.1
12	62	52	14.2
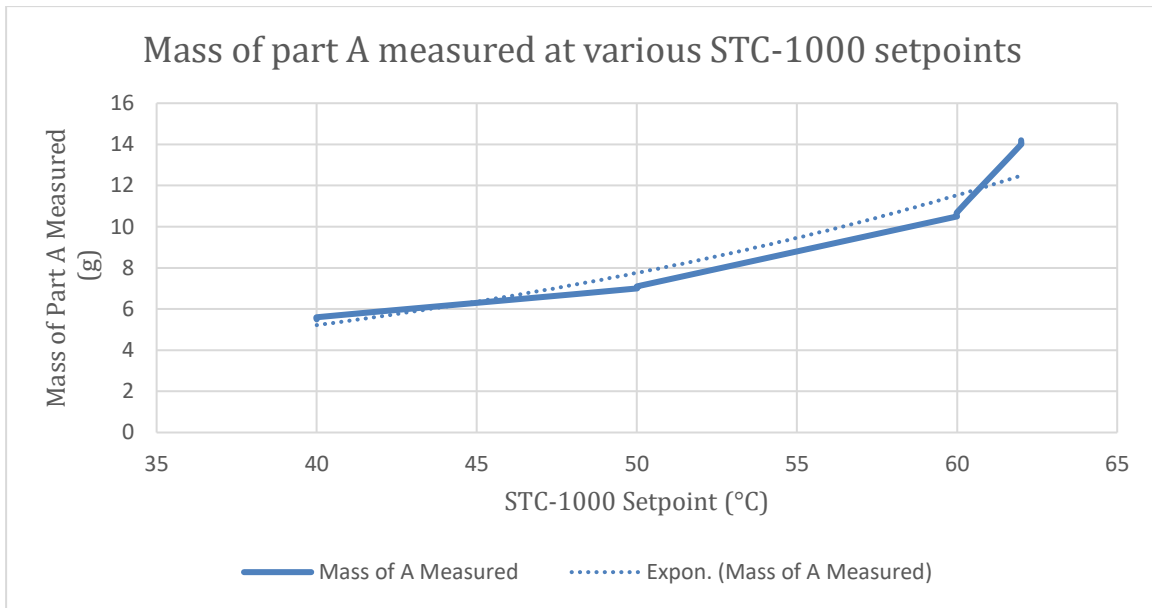
Figure 5.11: Mass of part A measured at various STC-1000 temperature setpoints

5.2.2.3 Discussion of Test 2

From Table 5.7 and Figure 5.11, it was noted that the mass of part A collected during a cycle was directly proportional to the increasing temperature setpoint of the STC-1000. From Table 5.5, the average mass of part B collected during a cycle was 15.27 g. Therefore, 14.27 g of part A was required to produce a mass ratio 100:107 (A: B) pbm. Referring to Table 5.7, an STC-1000 setpoint of 62 °C yielded an average mass flow of 14.1 g for part A, which in turn provided a mass ratio of 100:108 (A: B) pbm. The thermocouple reading of 52 °C was used for the remainder of this research to provide the necessary mass ratio as governed by the product data sheets. Using the thermocouple reading as the reference temperature to produce the necessary mass ratio rather than the STC-1000 setpoint, the container used to produce the results shown in Table 5.7 could be replaced. The testing process would not need to be repeated to determine the required mass flow ratio as the STC-1000 setpoint could be adjusted until the thermocouple produced a reading of 52 °C.

5.2.3 System Test 3

The third system test aimed to determine the machinability of the Ecospray PU foam that was used to perform System Test 2.

5.2.3.1 Description of Test 3

A 150x150x20 mm deep square pocket was milled into a block of polystyrene foam to determine the machinability of the Ecospray PU foam, as shown in Figure 5.12. Part A of the PU foam mixture was heated to the necessary temperature to produce the appropriate mass ratio. Next, the two-component mixture was pumped into the square pocket utilising the static mixing nozzle that can be seen in Figure 5.13. Offset distances between the centres of the cutting tool and the static mixing nozzle were determined so that the same WCS could be utilised for both the initial subtractive pocket toolpath and the subsequent additive process. Finally, an additive toolpath, similar to the toolpath displayed in Figure 4.12, was utilised to deposit the PU foam.
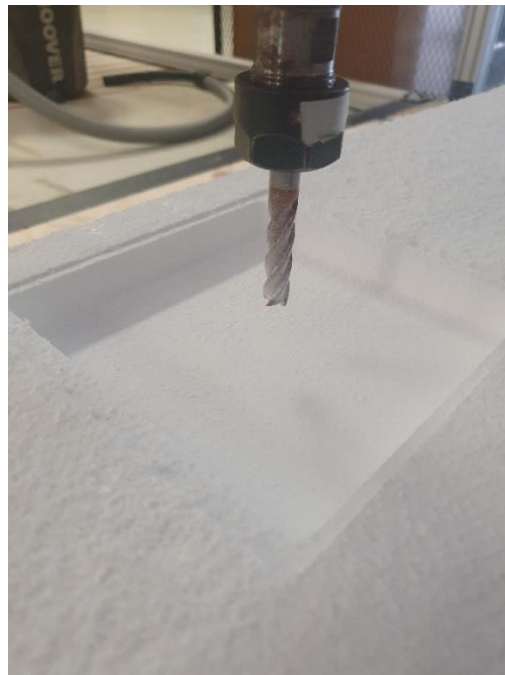
Figure 5.12: 150x150x20 mm deep pocket milled into polystyrene foam
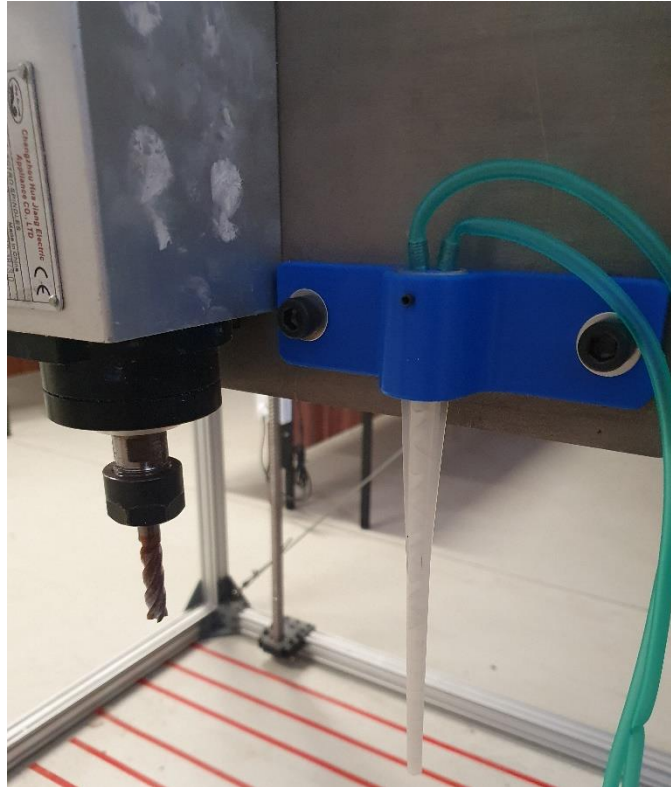
Figure 5.13: Static mixing nozzle mounted next to CNC milling spindle motor

5.2.3.2 Observations of Test 3

The PU foam deposited into the milled pocket expanded and cured, as shown in Figure 5.14. A subtractive toolpath was created to mill three features into the PU foam: a slot, a circle, and a rectangle. These three features varied in size and depth. Although the sizes of the milled features were accurate, the surface finish was rough and highly porous. The milling of the deposited Ecospray RS3030 PU foam can be seen in Figure 5.15.

Figure 5.14: Deposited Ecospray RS3030 PU foam
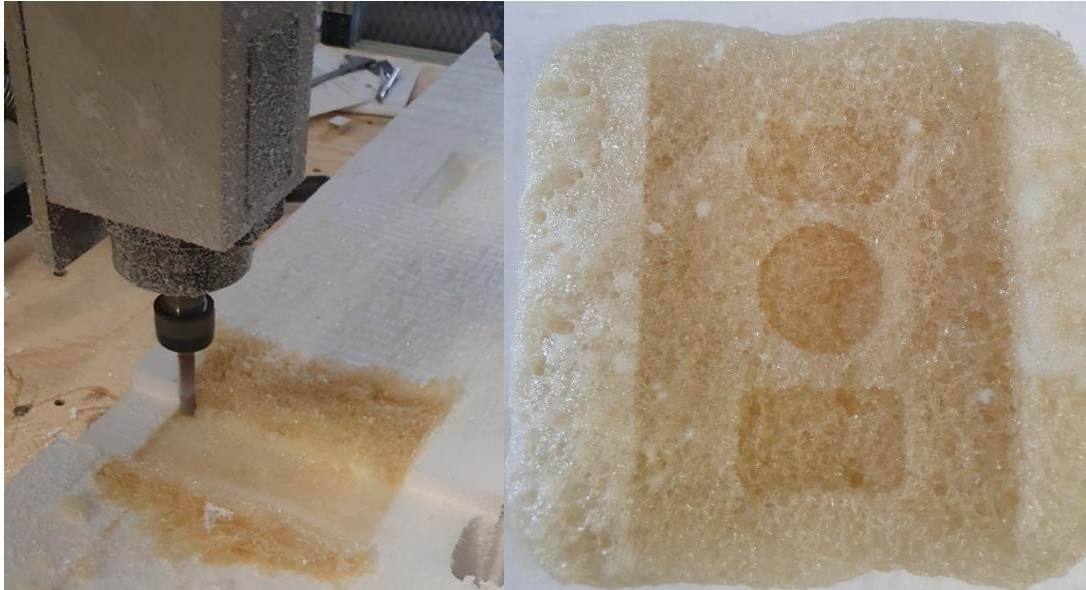
Figure 5.15: Milling of Ecospray RS3030 PU foam

5.2.3.3 Discussion of Test 3

As shown in Figure 5.14, the Ecospray RS3030 PU foam expanded and covered the entire surface area of the milled pocket. The cured foam was stable; however, it possessed a high porosity level and seemed to break rather than cut upon attempting to mill it. The developed dosing system may not have been the suitable method for depositing this particular type of PU foam, and a high-pressure airless spray dispensing system may have provided improved results in processing the PU material. Although this system test could not yield optimal machining results, the processes involved provided a rapid method of additively depositing the PU foam utilising the developed dosing system and a static mixing nozzle, followed by subsequent machining with minimised material wastage.

5.2.4 System Test 4

The fourth system test utilised an alternative method for depositing the additive material. This system test was evaluated by producing half of the scaled-down version of the VTOL's fuselage, as shown in Figure 3.19. The expansion and machinability of the deposited foam were the two focal points of this system test.

5.2.4.1 Description of Test 4

Due to the poor surface finish and high porosity level obtained in System Test 3, it was decided that an alternative deposition method would be developed and tested in an attempt to obtain improved results. This deposition method mounted a can of one-part moisture curing expanding PU foam to the milling machine to deposit the additive material. The PU foam can was mounted next to the CNC milling spindle motor, as shown in Figure 5.16. It was possible to load a new can of PU foam by loosening the lower mounting bracket and dropping the empty can out of the upper spigot end cap. Thus, large-scale models could be produced by depositing multiple cans worth of PU foam. In addition, the lower mounting bracket and spigot end cap ensured that the PU foam can was correctly located and supported during the deposition processes.
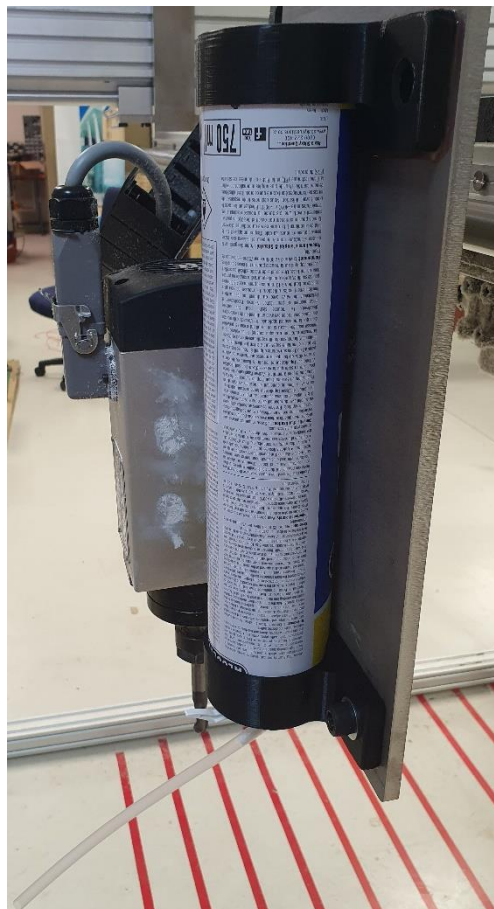
Figure 5.16: PU foam can mounted next to CNC milling spindle motor

Piano wire was used to automate the spraying of the PU expanding foam by connecting a servo arm to the can's adapter lever. Next, the RC servo was attached to the PU foam can, as shown in Figure 5.17. After the RC servo had been mounted to the can of expanding PU foam, the servo was connected to an Arduino Nano microcontroller. The microcontroller was wired to a digital output on the I/O card of the PLC that controlled the CNC machine. An opto-isolator board was used to convert the 24V logic output of the PLC to the 5V CMOS logic of the Nano. The program used to trigger or release the adapter lever and dispense the expanding PU foam accordingly can be seen in Appendix D3. As seen in Appendix D3, if the digital input attached to the PLC I/O card was high, the RC servo arm would turn to a preset angle, corresponding to a predetermined pulse width, to pull the adapter lever and spray the foam. Conversely, if the digital output from the PLC was low, the servo would release the lever and halt the spraying. A circuit diagram of the described setup is illustrated in Figure 5.18.
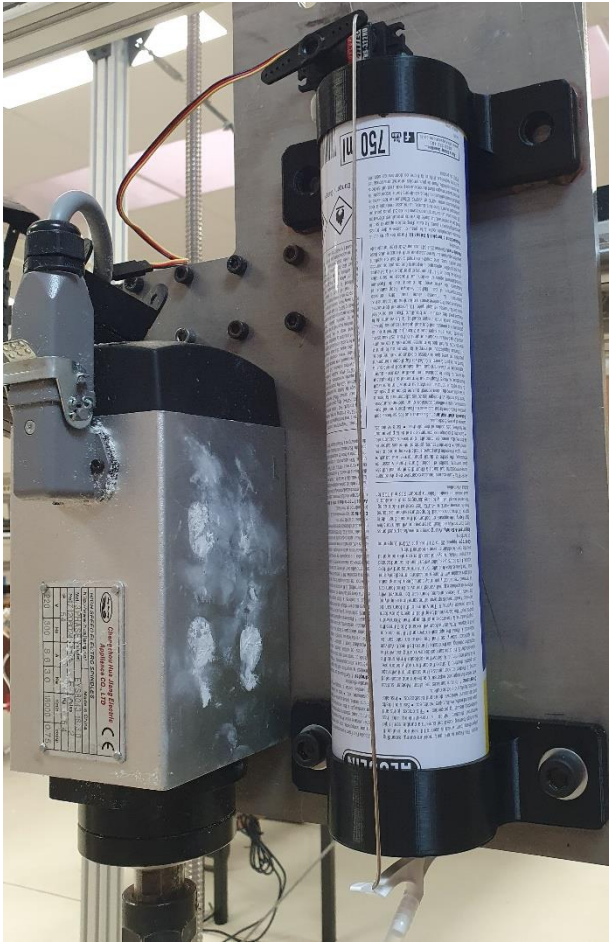
Figure 5.17: RC servo attached to expanding foam can
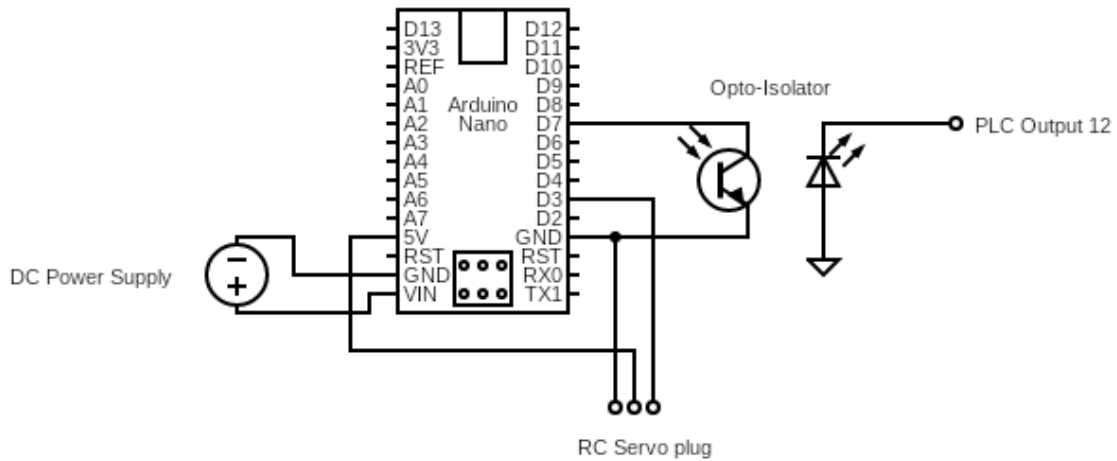
Figure 5.18: Circuit diagram connecting the RC servo to the PLC

Finally, to automate the spraying of the PU foam, the standard M8 and M9 G-codes were utilised. The M8 G-code, typically used to switch the coolant on, was programmed to pull the adapter lever and spray the PU foam. The M9 G-code, typically used to switch the coolant off, was programmed to release the adapter lever and halt the spraying of the foam. When the CNC machine read the M8 command, the digital output would be high, and the servo would initiate the deposition process. Conversely, the digital output would be low when the M9 command was read, thus halting the deposition process. Having programmed the M8 and M9 commands to trigger and release the PU foam's adapter lever allowed the additive material to be deposited where and when necessary. The microcontroller and the opto-isolator can be seen in Figure 5.19. As shown in Figure 5.19, the input and output LEDs of the opto-isolator were enabled when the signal was high, which indicated that the M8 command was being executed. The LEDs would remain enabled until the duration of the dwell command had concluded or until the M9 command was executed.
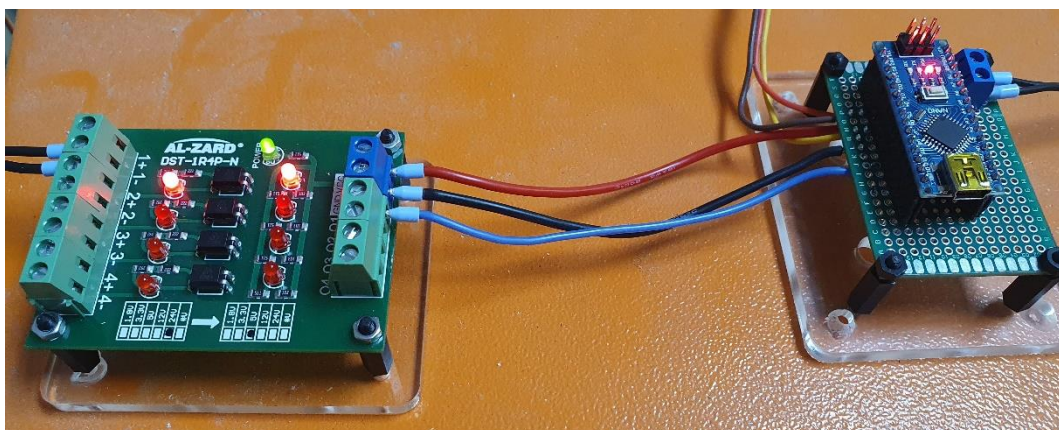
Figure 5.19: Microcontroller and opto-isolator with LEDs enabled

5.2.4.2 Observations of Test 4

The oversized shape of the scaled-down version of the VTOL's fuselage was produced utilising the system described in Section 5.2.4.1, as shown in Figure 5.20. The PU foam expanded and cured to produce the stock material to be milled away. The foam was secured utilising the workholding technique discussed in Section 3.1.2.2.

Figure 5.20: Additively deposited fuselage model

Figure 5.21 illustrates the roughing and finishing milling operations executed to produce the VTOL fuselage. The processes followed to form the additive and subtractive toolpaths to produce the completed model shown in Figure 5.22 were detailed in Section 4.1.2. As stated previously, the focus of this system test was to determine the machinability of the deposited PU foam and to obtain an indication of how much the foam would have expanded once it had cured. By obtaining an indication of the expected expansion, the material wastage aspect of this research project - which was considered later in this chapter - could be optimised. Therefore, the significant material wastage displayed in Figure 5.21 and Figure 5.22 was not an accurate indication of the reduction in material wastage capability of the system developed in this research.
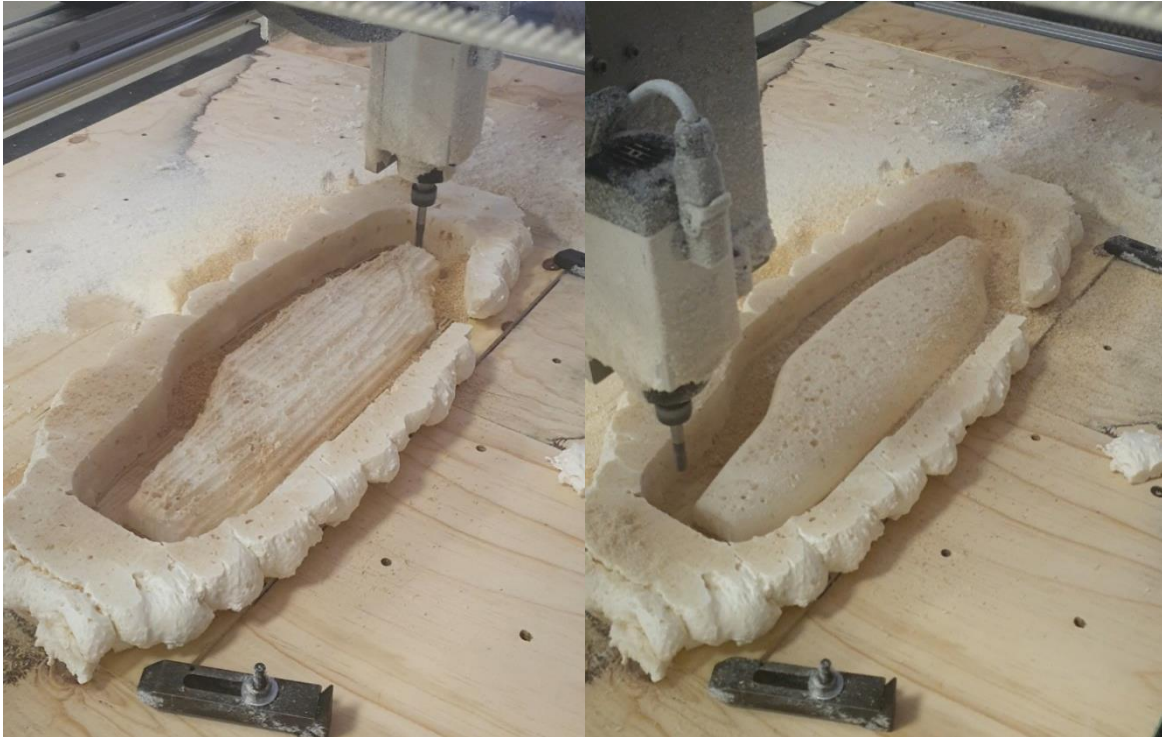
Figure 5.21: Roughing and finishing passes

Figure 5.22: VTOL fuselage produced utilising combined additive and subtractive manufacturing

The surface finish of the model produced in Figure 5.22 utilising the developed HM system was significantly superior to that illustrated in Figure 5.15. Additionally, unlike the Ecospray RS3030 utilised in System Test 3, the expanding PU foam used to conduct this system test was highly machinable and was capable of being milled without tending towards breaking or shattering. Furthermore, a considerable stepover distance of 2 mm was used for the surface finish operation, and the surface finish could therefore be further improved using a smaller stepover distance. Finally, the measurable dimensions of the produced model matched that of the CAD model within the expected tolerance range of the developed platform. This expected tolerance range was discussed later in this chapter. The CAD model measured 800 mm in length and 58.5 mm in height, whilst the model produced in Figure 5.22 measured 800.3 mm in length (X) and 58.7 mm in height (Z).

5.2.4.3   Discussion of Test 4

As seen in Figure 5.22, the developed system could additively deposit the PU foam and then machine the excess material to produce the desired CAD model. The surface finish of the machined PU foam was smooth; however, a considerable number of voids were present. These voids could be sealed by depositing an additional layer of PU foam along the finished surface. Then, the newly deposited layer of foam could be re-machined by running the surface finish parallel toolpath. This deposition-machining process could be repeated until a desirable surface finish was obtained.

With refinement, the developed system could yield minimal material wastage compared to conventional manufacturing techniques of producing the same CAD model. In addition, the indication of the expected expansion obtained in Section 5.2.4.2 meant that the containment boundary for the additive deposition toolpath could be undersized to allow for the expected expansion to commence. Figure 5.23 illustrates the optimisation of the reduction in material wastage. The red contour represented the geometry of the CAD file to be produced, the green contour represented the undersized tool containment boundary, and the blue lines represented the additive toolpath. This undersized tool containment boundary ensured that a significant amount of stock material was not produced during the deposition process, unlike the initial testing displayed in Figure 5.21 and Figure 5.22, where the red contour was used as the containment boundary.
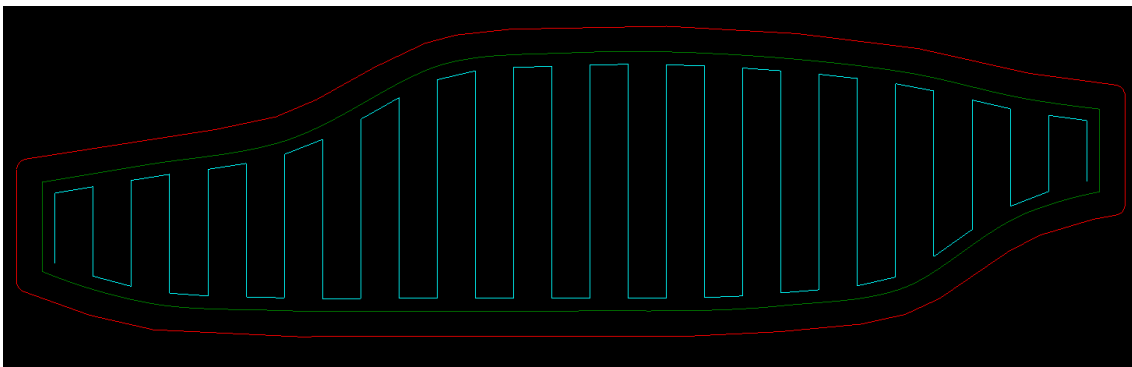
Figure 5.23: Undersized containment boundary to optimise reduction in material wastage

5.2.5 Statistical Analysis

5.2.5.1 Dimensional Accuracy, Repeatability and Stability

The system detailed in Section 5.2.4 was tested for dimensional accuracy and repeatability of the produced parts. The accuracy was based on the system's ability to replicate the 3D CAD model within an acceptable engineering tolerance grade. ISO 2768 was selected since it is predominantly used for parts that have been manufactured via a material removal process such as milling [77]. An extract of the ISO 2768 standard, which governs the permissible deviations in linear dimensions, is shown in Figure 5.24 [77].

Permissible deviations in mm for ranges in nominal lengths	f (fine)	Tolerance class designation (description)		v (very coarse)
		m (medium)	c (coarse)	
0.5 up to 3	±0.05	±0.1	±0.2	–
over 3 up to 6	±0.05	±0.1	±0.3	±0.5
over 6 up to 30	±0.1	±0.2	±0.5	±1.0
over 30 up to 120	±0.15	±0.3	±0.8	±1.5
over 120 up to 400	±0.2	±0.5	±1.2	±2.5
over 400 up to 1000	±0.3	±0.8	±2.0	±4.0
over 1000 up to 2000	±0.5	±1.2	±3.0	±6.0
over 2000 up to 4000	–	±2.0	±4.0	±8.0

Figure 5.24: ISO 2768 permissible deviations in linear dimensions [77]

A 3D plan view of a house was modelled using Autodesk Inventor to perform statistical analysis on the developed system, as shown in Figure 5.25. This tall, thin-walled model showcased the reduction in material wastage of the developed system as the PU foam was deposited along the thin wall sections, and the excess material that expanded and cured over the boundaries of these sections was milled away. In addition, the model was used to quantify the dimensional accuracy, repeatability and stability of the parts produced using the developed system.
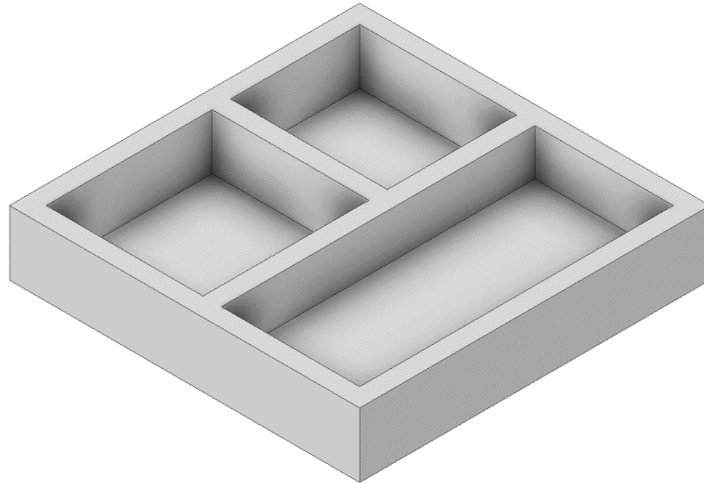
Figure 5.25: 3D plan view of a house CAD model

A dimensional checklist was created for all features to be measured upon completion of the model shown in Figure 5.25. A top view of Figure 5.25 indicating the feature numbers for the dimensional checklist is shown in Figure 5.26. The dimensional checklist is detailed in Table 5.8, whereby the CAD dimensions for the corresponding feature numbers were displayed. For the statistical and repeatability analyses, the spindle speed, feed rate, depth of cut and width of cut were kept constant at 12000 RPM, 3000 mm/min, 5 mm, and 7.5 mm, respectively. For Feature Number 5, the average wall thickness throughout the entire model was used.
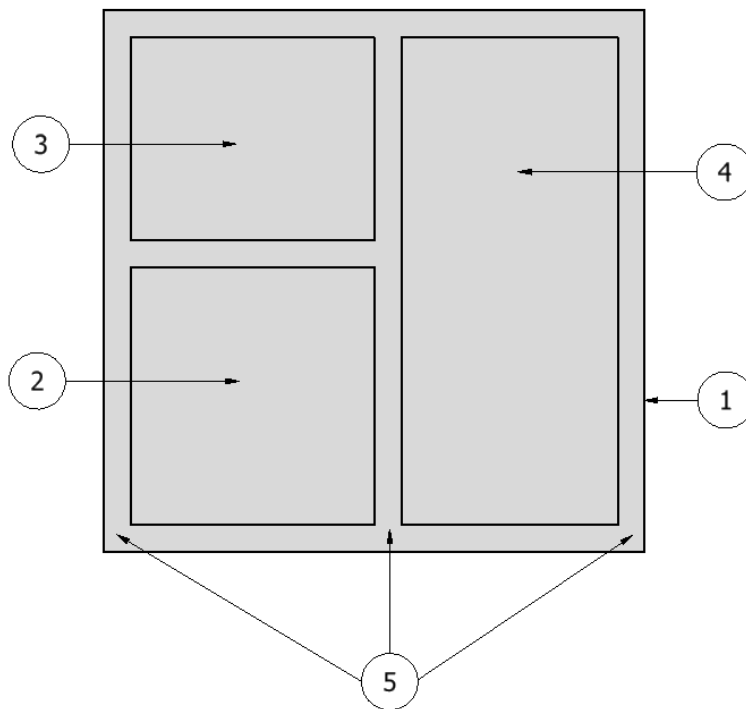
Figure 5.26: Top view indicating the feature numbers

Table 5.8: Dimensional checklist

Dimensional Checklist					
Feature Number	*Description of Feature*	*CAD Dimensions (mm)*			
		Length (L)	*Width (W)*	*Height (H)*	*Thickness (t)*
1	Outer Wall Dimensions	190	190	35	-
2	Room 1 Dimensions	90	85	27	-
3	Room 2 Dimensions	85	70	27	-
4	Room 3 Dimensions	170	75	25	-
5	Constant Wall Thickness	-	-	-	10

Table 5.9 illustrates the dimensional checklist analysis for Feature 1. The measured dimensions were compared to the expected CAD dimensions, and any errors between the two were computed. Figliola et al. [78] defined accuracy as the closeness of a measured value to the true value. Equation 5.5 described the error (e) as the difference between the measured value and the reference value. Equation 5.6 described the accuracy (A) with respect to the reference value [78].

$$e = Measured\ Value - Reference\ Value \tag{5.5}$$

$$A = \frac{|e|}{Reference\ Value} \times 100 \tag{5.6}$$

The dimensions of the produced features were measured upon completing the milling cycle and were re-measured 24 hours after machining to determine the stability. Equation 5.7 described the stability of the produced features, where the re-measured dimension was computed 24 hours after the feature had been produced.

$$Stability = |Measured\ Dimension - Remeasured\ Dimension| \tag{5.7}$$

Figure 5.24 was utilised to specify the tolerance grade for each measured dimension.

Table 5.9: Dimensional checklist for Feature 1

Dimensional Checklist - Feature 1						
Length						
Test Number	CAD Length (mm)	Measured Length (mm)	Length Error (mm)	Accuracy (%)	Stability (mm)	Tolerance Grade
1	190	189.6	0.4	0.211	0	Medium
2	190	189.6	0.4	0.211	0.1	Medium
3	190	189.5	0.5	0.263	0.1	Medium
4	190	189.6	0.4	0.211	0	Medium
5	190	189.4	0.6	0.316	0.1	Coarse
Width						
Test Number	CAD Width (mm)	Measured Width (mm)	Width Error (mm)	Accuracy (%)	Stability (mm)	Tolerance Grade
1	190	189.5	0.5	0.263	0	Medium
2	190	189.7	0.3	0.158	0	Medium
3	190	189.6	0.4	0.211	0	Medium
4	190	189.4	0.6	0.316	0.1	Coarse
5	190	189.6	0.4	0.211	0.1	Medium
Height						
Test Number	CAD Height (mm)	Measured Height (mm)	Height Error (mm)	Accuracy (%)	Stability (mm)	Tolerance Grade
1	35	34.5	0.5	1.429	0	Coarse
2	35	34.4	0.6	1.714	0.1	Coarse
3	35	34.5	0.5	1.429	0	Coarse
4	35	34.4	0.6	1.714	0.1	Coarse
5	35	34.6	0.4	1.143	0	Coarse

From Table 5.9, the maximum dimensional error obtained in producing Feature 1 was the 0.6 mm height error, which resulted in an accuracy error of 1.714%. It was noted that the maximum change in stability experienced by the produced dimensions was 0.1 mm. This 0.1 mm could have been the result of human error in reading the measurement provided by the 200 mm vernier caliper. Since the PU foam was allowed to cure for 60 minutes after deposition before any subtractive manufacturing was executed, the foam could have expanded to its total volume within this timeframe. Fifty-three percent of the dimensions illustrated in Table 5.9 fell within the medium tolerance grade, while the remaining 47% were classified as coarse. Since the focus of this research project was HM with minimised material wastage, these tolerance grades were deemed acceptable. The overall performance of the developed system was discussed later.

Equation 5.8 described the sample mean value ($\bar{x}$) of the data set, where N represented the number of measurements performed and x_i represented the value of the ith iteration. The sample mean provided an estimate of the true mean value (x') [78].

$$\bar{x} = \frac{1}{N}\sum_{i=1}^{N} x_i \tag{5.8}$$

Equation 5.9 defined the sample variance (s_x^2), where the sample variance represented the probable measure of the variation found in the data set [78].

$$s_x^2 = \frac{1}{N-1}\sum_{i=1}^{N} (x_i - \bar{x})^2 \tag{5.9}$$

From this sample variance, the standard deviation (s_x) was computed using Equation 5.10 [78].

$$s_x = \sqrt{s_x^2} = \left(\frac{1}{N-1}\sum_{i=1}^{N} (x_i - \bar{x})^2\right)^{1/2} \tag{5.10}$$

Equation 5.11 defined the standard deviation of the means ($s_{\bar{x}}$). The standard deviation of the means indicated how well a measured value represented an entire data set when a small sample size was analysed.

$$s_{\bar{x}} = \frac{s_x}{\sqrt{N}} \tag{5.11}$$

Equation 5.12 defined the precision interval of a measurement at a given probability ($P\%$) [78].

$$x_i = \bar{x} \pm t_{v,P} s_x \ (P\%) \tag{5.12}$$

Where

$$v = N - 1 \tag{5.13}$$

Where v represented the degrees of freedom of the data set and $t_{v,P}$ represented a coverage factor. The value of $t_{v,P}$ was obtained from the Student's t distribution table provided by Figliola et al. [78]. Refer to Appendix E1 for the Student's t distribution table, where a coverage factor is obtained based on the degrees of freedom and the probability of the data set [78].

In the absence of systematic errors, Equation 5.14 defined the true mean value of the data set [78].

$$x' = \bar{x} \pm t_{v,P}\bar{s_x} \tag{5.14}$$

Repeatability was defined as the ability of a measurement system to repeatedly produce the same output value for identical input conditions [78]. Equation 5.15 defined the system's repeatability error (%Re) [78].

$$\%Re = \frac{2s_x}{FSD} \times 100 \tag{5.15}$$

Where FSD represented the full-scale range of the measurement instrument. For this research, a vernier caliper was utilised to measure the dimensions of the produced parts.

Using Equation 5.8, Equation 5.10, Equation 5.11, Equation 5.12, Equation 5.13, Equation 5.14 and Equation 5.15, the mean, standard deviation, standard deviation of the means, degrees of freedom, coverage factor, true mean and repeatability error for Feature 1 were determined for the values shown in Table 5.9. The resulting values can be seen in Table 5.10.

Table 5.10: Statistical analysis for Feature 1

Statistical Analysis for Feature 1			
	Measured Length	*Measured Width*	*Measured Height*
Mean (mm)	189.54	189.56	34.48
Standard Deviation (mm)	0.0894	0.1140	0.0837
Standard Deviation of the Means (mm)	0.0400	0.0510	0.0374
N	5	5	5
Sum (mm)	947.7	947.8	172.4
v	4	4	4
$t_{4,95}$	2.776	2.776	2.776
True mean x' (mm ± mm)	189.54 ± 0.111	189.56 ± 0.142	34.48 ± 0.104
Repeatability Error (%)	0.0894	0.1140	0.0837

A box and whisker plot displays a five-number summary of a data set, namely the minimum, first quartile, mean, third quartile, and the maximum [79]. The box and whisker plots created to represent the data gathered in Table 5.9 and Table 5.10 can be seen in Figure 5.27, Figure 5.28, and Figure 5.29. The X marker represented the mean value.
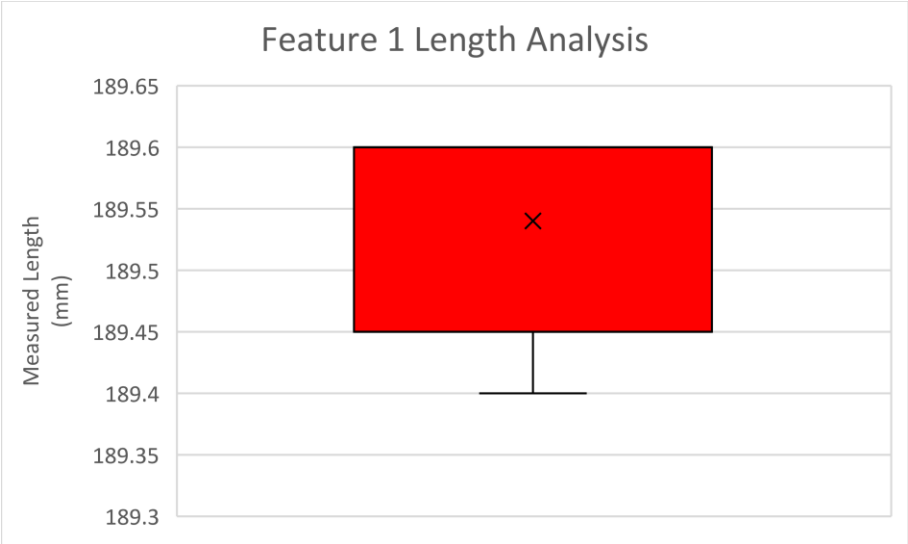
Figure 5.27: Feature 1 measured length box and whisker plot
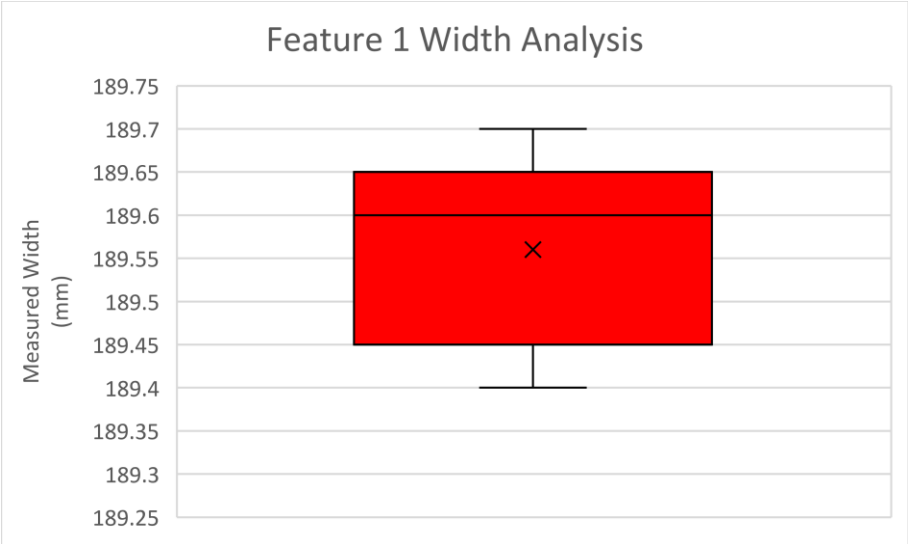
Figure 5.28: Feature 1 measured width box and whisker plot
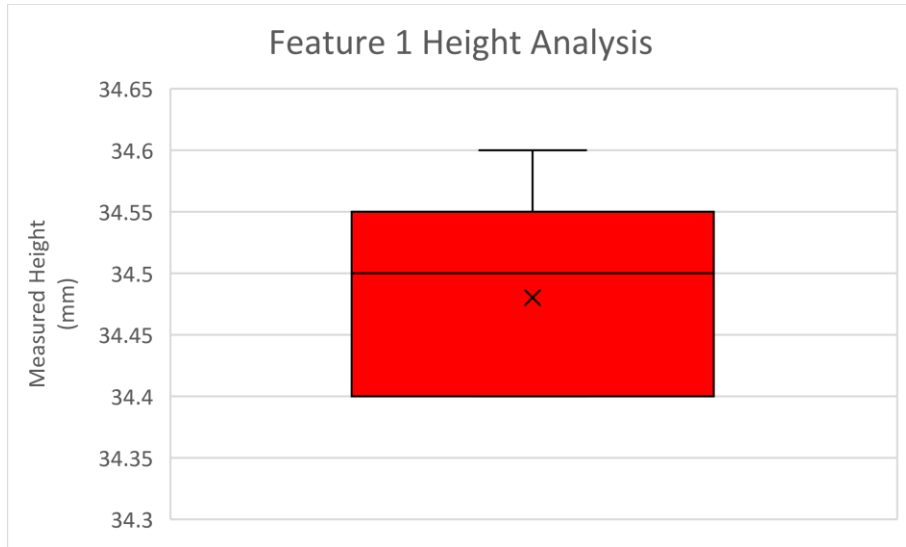
Figure 5.29: Feature 1 measured height box and whisker plot

Chauvenet's criterion was utilised to identify and eliminate possible outliers from the data set. A measurement was regarded as an outlier if the condition defined by Equation 5.16 was satisfied [78].

$$\left(1 - 2 \times P(z_0)\right) < \frac{1}{2N} \tag{5.16}$$

Where

$$z_0 = \frac{|x_i - \bar{x}|}{s_x} \tag{5.17}$$

Table 5.9 and Table 5.10, along with Equation 5.16 and Equation 5.17, were used to determine whether any of the measurements taken were possible outliers. The value of $P(z_0)$ was obtained from the normal error function table provided by Figliola et al. [78]. Refer to Appendix E2 for the normal error function table. The results for the outlier detection for Feature 1 can be seen in Table 5.11.

Table 5.11: Chauvenet's criterion for outlier detection for Feature 1

Outlier Detection for Feature 1 - Length				
Test Number	$(x_i - \bar{x})^2$ _(mm)_	z_0	$P(z_0)$	_Outlier?_
1	0.0036	0.67	0.2486	No
2	0.0036	0.67	0.2486	No
3	0.0016	0.45	0.1736	No
4	0.0036	0.67	0.2486	No
5	0.0196	1.57	0.4418	No
Outlier Detection for Feature 1 - Width				
Test Number	$(x_i - \bar{x})^2$ _(mm)_	z_0	$P(z_0)$	_Outlier?_
1	0.0036	0.53	0.2019	No
2	0.0196	1.23	0.3907	No
3	0.0016	0.35	0.1368	No
4	0.0256	1.40	0.4192	No
5	0.0016	0.35	0.1368	No
Outlier Detection for Feature 1 - Height				
Test Number	$(x_i - \bar{x})^2$ _(mm)_	z_0	$P(z_0)$	_Outlier?_
1	0.0004	0.24	0.0948	No
2	0.0064	0.96	0.3315	No
3	0.0004	0.24	0.0948	No
4	0.0064	0.96	0.3315	No
5	0.0144	1.43	0.4236	No

From Table 5.11, it was found that no outliers were present for the data set.

Refer to Appendix E3, E4 and E5 for the dimensional checklists, statistical analysis (including the box and whisker plots), and outlier detection for features 2, 3, 4 and 5, respectively.

5.2.5.2 Effects of Process Parameters

The subsequent testing stage involved the independent adjustment of the process parameters such as the spindle speed, feed rate, depth of cut and stepover distance to determine the effects of each parameter change. The factor-level table for the CNC milling parameters can be seen in Table 5.12. The random test strategy implemented to determine the effects of the various process parameters on the material removal rate (R_{MR}) and surface finish of the produced parts can be seen in Table 5.13.

Equation 5.18 defined the R_{MR} of the system, where w represented the width of cut, d represented the depth of cut, and f_r represented the feed rate [9].

$$R_{MR} = wdf_r \tag{5.18}$$

Since the focus of this research was not the surface finish of the produced parts, and a surface roughness tester was not available, the surface finish was determined by visual inspection. Examples of fine, medium, and coarse surface finishes were illustrated in Figure 5.30, Figure 5.31, and Figure 5.32, respectively. The machining marks were more visible in the coarse surface finish than the fine and medium surface finishes. Additionally, the sizes of the voids increased as the surface finish grade decreased.
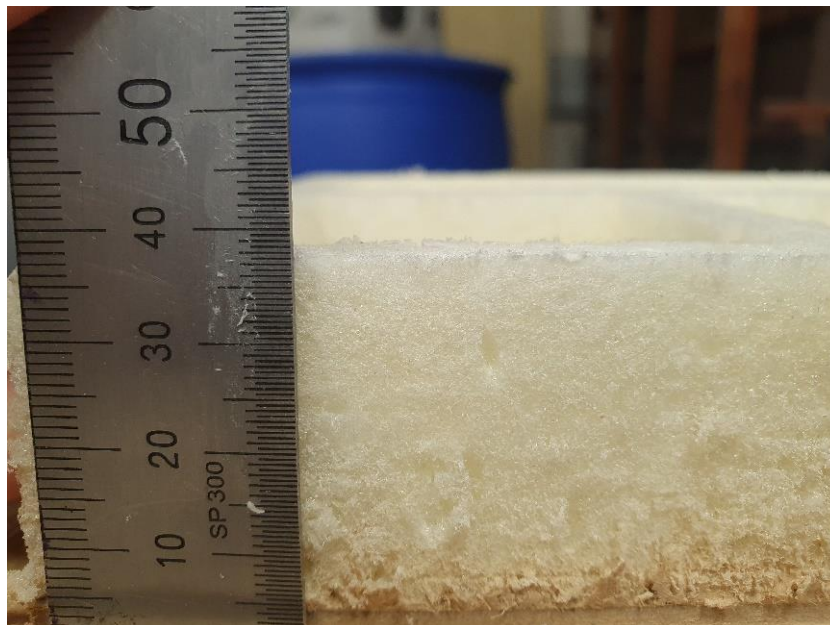
Figure 5.30: Example of a fine surface finish
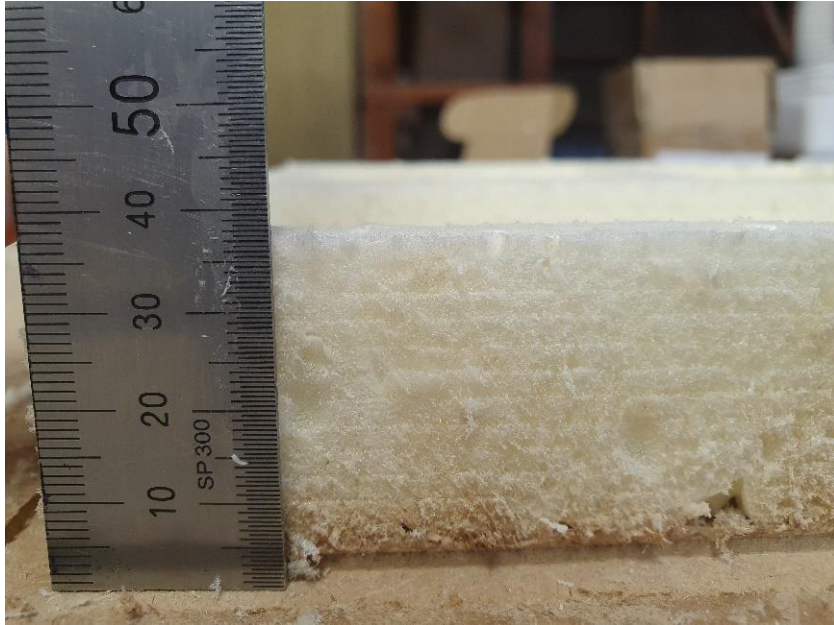
Figure 5.31: Example of a medium surface finish

Figure 5.32: Example of a coarse surface finish

Table 5.12: Factor-level table for CNC milling

Factor	Level		
	1	2	3
Spindle Speed (A) (RPM)	8000	12000	14000
Feed Rate (B) (mm/min)	3000	4000	5000
Depth of Cut (C) (mm)	3	4	5
Width of Cut (D) (mm)	5.5	6.5	7.5

Table 5.13: Random test strategy to determine the effects on R_{MR} and surface finish

Test Number	Factor A	Factor B	Factor C	Factor D	R_{MR} (mm^3/min)	Surface Finish - Visual Inspection
1	8000	3000	3	5.5	49500	Medium
2	12000	4000	4	6.5	104000	Fine
3	14000	5000	5	7.5	187500	Medium
4	12000	3000	5	5.5	82500	Fine
5	8000	5000	4	6.5	130000	Coarse
6	12000	4000	5	7.5	150000	Fine
7	8000	4000	4	5.5	88000	Coarse
8	8000	3000	5	7.5	112500	Medium
9	14000	4000	3	5.5	66000	Fine
10	12000	3000	5	6.5	97500	Fine

From Table 5.13, Test Number 6 provided the most effective material removal rate whilst maintaining a fine surface finish. The spindle speed and feed rate parameters had a significant effect on the visual surface finish of the produced parts. It was noted that the surface finish tended to improve with an increase in spindle speed, whilst an increase in the feed rate and depth of cut provided a rougher surface finish. These deduced relationships between the process parameters and their effects on the surface finish of the produced parts concur with the findings of Chahal et al. [80]. If the part's surface finish was not a priority, the process parameters utilised in Test Number 3 could be implemented. The significant material removal rate of 187500 mm^3/min would substantially decrease the cycle time and produce a working prototype rapidly.

5.2.5.3 Material Wastage

The density of the PU foam was required to determine the mass of the PU foam model. Referring to Appendix B2, the estimated density of the Sika Boom PU foam was 22 kg/m^3 [81]. Cubes were modelled and produced utilising the developed HM system to obtain a more precise density of the PU foam. The cubes with known volume were weighed and used to determine the average density of the foam. The average density was computed to be 24 kg/m^3. The iProperties feature within Autodesk Inventor was utilised to determine the theoretical mass of the model based on the predetermined PU foam density of 24kg/m^3. As shown in Figure 5.33, the theoretical mass of the PU foam VTOL model was 5.5124g.
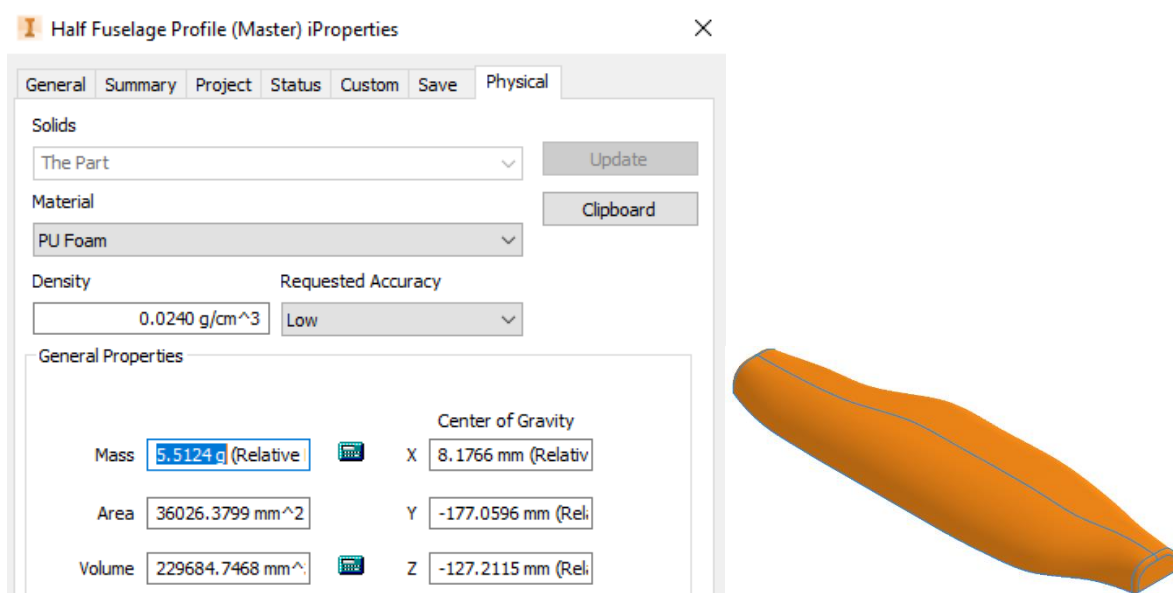
Figure 5.33: Theoretical mass of the PU foam VTOL fuselage model

A bounding box was created to determine the minimum theoretical stock material required to produce the VTOL fuselage model using stand-alone conventional manufacturing processes. A bounding box creates a rectangular boundary around the CAD model that perfectly matches the model's X, Y and Z dimensions. Once the bounding box had been generated, the theoretical stock material was computed by removing the section from the bounding box that would be avoided during the subtractive processes to produce the VTOL fuselage model. As shown in Figure 5.34, the theoretical mass of the PU foam VTOL fuselage stock material was 8.6367g.
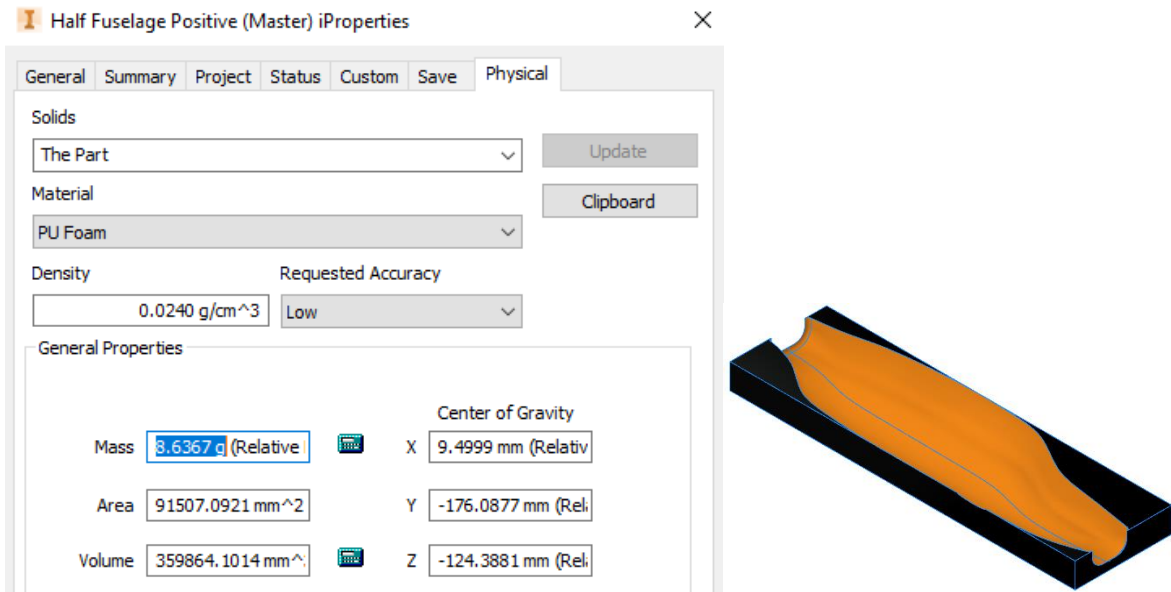
Figure 5.34: Theoretical mass of the PU foam VTOL fuselage's stock material

The minimum theoretical material wastage for the 260 mm VTOL fuselage was calculated to be 36.175%, as shown in Table 5.14.

Table 5.14: 260 mm long VTOL fuselage theoretical material wastage

Theoretical Material Wastage - 260 mm Long VTOL Fuselage		
Mass of Stock Material (g)	*Mass of Model (g)*	*Material Wastage (%)*
8.6367	5.5124	**36.175**

The method to determine the minimum theoretical material wastage for the 260 mm VTOL fuselage model was repeated for the 190x190x35 mm high house model. As shown in Figure 5.35 and Figure 5.36, the theoretical mass of the house model and the house model's stock material was 13.861g and 30.324g, respectively.
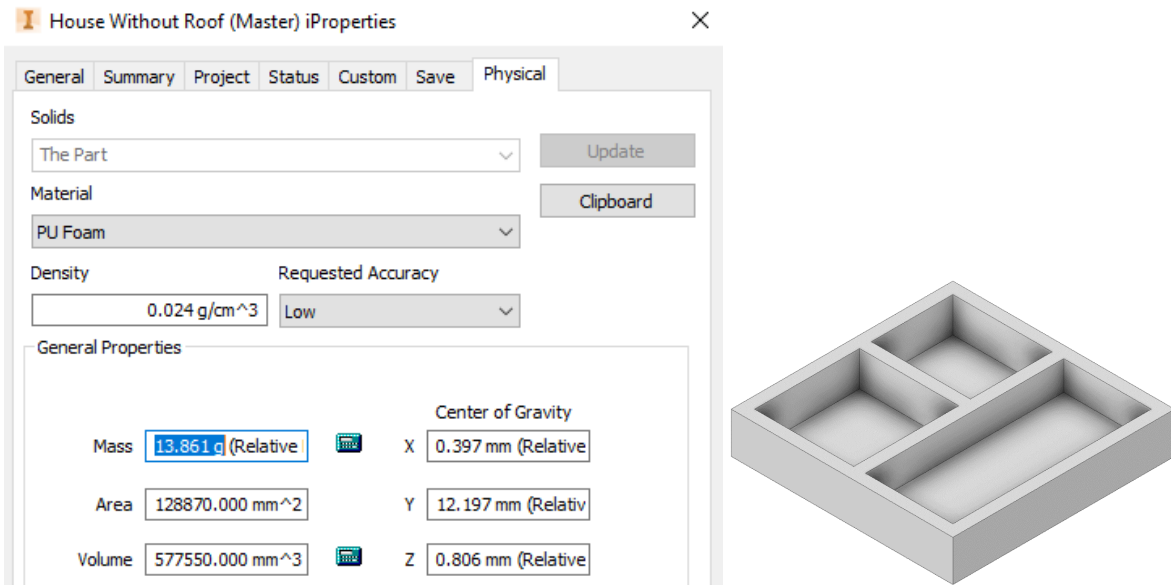
Figure 5.35: Theoretical mass of the house model
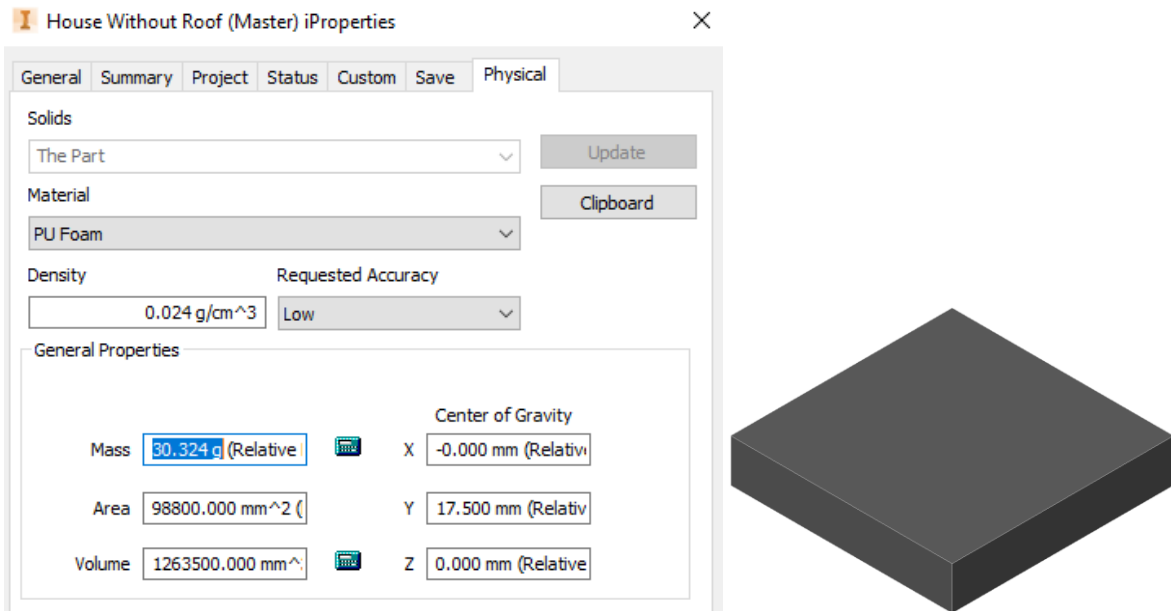
Figure 5.36: Theoretical mass of the house model's stock material

The minimum theoretical material wastage for the 190x190x35 mm high house model was calculated to be 54.290%, as shown in Table 5.15.

Table 5.15: 190x190x35 mm house model theoretical material wastage

Theoretical Material Wastage - 190x190x35 mm House Model		
Mass of Stock Material (g)	Mass of Model (g)	Material Wastage (%)
30.324	13.861	**54.290**

The mass of the machined model was subtracted from the mass of the deposited stock material to determine the experimental material wastage. The stock material was deposited utilising the procedure described in Section 5.2.4. The results gathered for the experimental material wastage in producing the VTOL fuselage and the house models can be seen in Table 5.16 and Table 5.17, respectively. Figure 5.37 illustrates the theoretical and experimental material wastage comparison for the VTOL fuselage and house models. For the experimental analysis, the mean material wastage values were used.

Table 5.16: 260 mm long VTOL fuselage experimental material wastage

Experimental Material Wastage - 260 mm Long VTOL Fuselage Model			
Test Number	*Mass of Deposited Stock Material (g)*	*Mass of Machined Model (g)*	*Material Wastage (%)*
1	8	5.4	32.500
2	7.5	5.3	29.333
3	7.4	5.4	27.027
4	7.2	5.3	26.389
5	6.8	5.4	20.588
Mean Material Wastage (%)			**27.167**

Table 5.17: 190x190x35 mm house model experimental material wastage

Experimental Material Wastage - 190x190x35 mm High House Model			
Test Number	*Mass of Deposited Stock Material (g)*	*Mass of Machined Model (g)*	*Material Wastage (%)*
1	21.2	13.7	35.377
2	22.1	13.8	37.557
3	21.8	13.8	36.697
4	21.3	13.8	35.211
5	21.5	13.7	36.279
Mean Material Wastage (%)			**36.224**
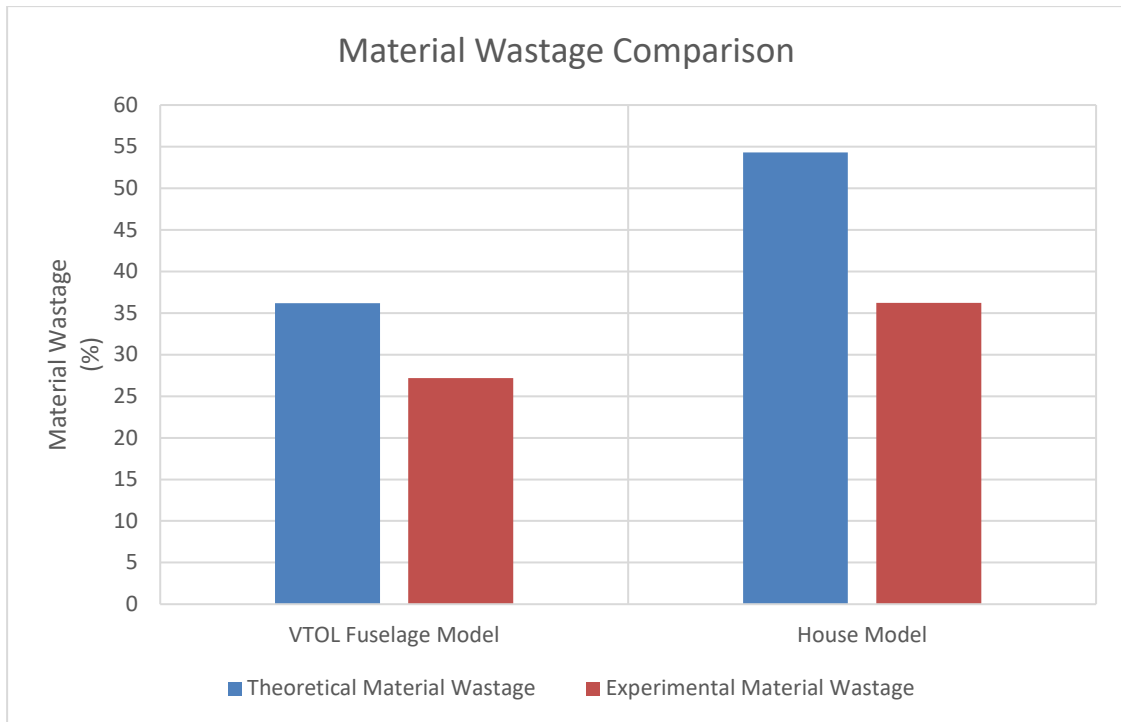
Figure 5.37: Material wastage comparison for the VTOL fuselage and house models

From Table 5.16 and Table 5.17, it was noted that the mean material wastage for the 260 mm long VTOL fuselage and the 190x190x35 mm high house models was 27.167% and 36.224%, respectively. From Figure 5.37, it was noted that the theoretical material wastage in producing both models using stand-alone conventional manufacturing processes, such as milling, was more significant than the experimentally obtained material wastage utilising the developed HM system. The reduction in material wastage comparison between the developed system and conventional manufacturing processes was quantified later in this chapter.

5.2.5.4 Cycle Time Comparison

The final testing stage compared the cycle time to produce the 260 mm long VTOL fuselage, as shown in Figure 5.33, utilising the developed HM system versus a commercially available FDM 3D printer, like the Creality Ender-5 Plus [82]. Three combinations of process settings were tested to compare the cycle times of the two platforms, namely coarse, medium, and fine settings. The various combinations utilised for the Creality Ender-5 Plus 3DP can be seen in Table 5.18.

Table 5.18: Creality Ender-5 Plus 3DP settings

Settings	Creality Ender-5 Plus Settings			
	Layer Height (mm)	Infill Percentage (%)	Infill Pattern	Printing Speed (mm/s)
Coarse Settings	0.3	25	Rectilinear	55
Medium Settings	0.2	50	Rectilinear	55
Fine Settings	0.1	75	Rectilinear	55

The individual processes of the developed HM system were separated, and the time taken to perform each was considered to determine the overall cycle time. First, the time taken to deposit the PU foam via an additive facing toolpath was computed. The PU foam was allowed to cure for 60 minutes after deposition before any subtractive manufacturing was executed. The cycle time for the combined deposition and curing processes can be seen in table 5.19. Second, the time taken to execute the surface rough pocket toolpath for various combinations of process settings can be seen in Table 5.20. Finally, the cycle time of the various surface finish parallel toolpaths can be seen in Table 5.21.

Table 5.19: PU foam deposition and curing cycle time

Settings	PU Foam Deposition		
	Feed Rate (mm/min)	Max Stepover (mm)	Cycle Time (minutes: seconds)
	2000	12	60:49

Table 5.20: Surface rough pocket cycle time for various settings

Settings	Surface Rough Pocket				
	Spindle Speed (RPM)	Feed Rate (mm/min)	Max Stepdown (mm)	Stepover Distance (mm)	Cycle Time (minutes: seconds)
Coarse Settings	14000	5000	5	7.5	04:28
Medium Settings	14000	4000	4	6.5	06:14
Fine Settings	14000	3000	3	5.5	11:12

Table 5.21: Surface finish parallel cycle time for various settings

Settings	Surface Finish Parallel			
	Spindle Speed (RPM)	Feed Rate (mm/min)	Max Stepover (mm)	Cycle Time (minutes: seconds)
Coarse Settings	14000	5000	1.5	03:58
Medium Settings	14000	4000	1	07:00
Fine Settings	14000	3000	0.5	17:48

The toolpath statistics feature within CIMCO Edit was used to determine the cycle time for both the HM system and the Ender-5 Plus 3DP. Figure 5.38 illustrates the toolpath statistics of the surface finish parallel toolpath using the fine settings combination.

Figure 5.38: Cycle time of the surface finish parallel toolpath using fine settings

The cycle time comparison between the two platforms can be seen in Table 5.22. In addition, the cycle times for various combinations of settings for the two platforms were plotted and can be seen in Figure 5.39.

Table 5.22: Cycle time comparison between a commercially available 3D printer and the developed HM system

Settings	Cycle Time (minutes: seconds)	
	Creality Ender-5 Plus	HM System
Coarse Settings	275:00	69:15
Medium Settings	596:00	74:03
Fine Settings	2375:00	89:49
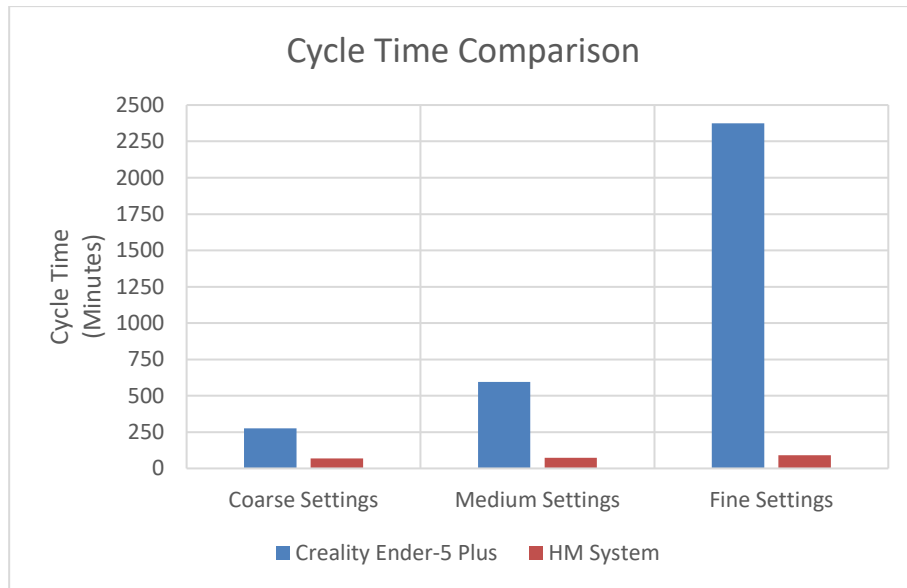
Figure 5.39: Cycle time comparison between the two platforms for various combinations of settings

From Table 5.22 and Figure 5.39, it was noted that the cycle time of the Creality Ender-5 Plus was significantly greater than that of the developed HM system for all three combinations of process settings. The cycle time provided by the CIMCO Edit toolpath statistics feature is often lower than the actual cycle time; however, the software was used to determine the cycle time for both platforms to remove any bias towards the developed system. The process settings utilised for the 3DP's coarse, medium, and fine settings were subjective, and the reduction in cycle time might not have been as significant had these three combinations of settings been defined differently. The reduction in cycle time comparison between the developed system and the Ender-5 Plus 3DP was quantified later in this chapter.

5.3 Overall System Performance

To quantify the dimensional accuracy of the developed HM system, the mean length, width, and height errors were computed by determining the averages of the corresponding errors from Table 5.9 and Appendix E3. The values of these mean errors and their corresponding axis can be seen in Table 5.23. As stated in Section 1.5, the dimensional accuracy of the developed HM system would be limited by the positional accuracy of the CNC machine itself. During the milling processes, it was noted that the cutting tool experienced a significant amount of deflection. This deflection could have been caused by the lack of rigidity experienced by the CNC milling spindle motor mounting assembly. Dépincé et al. [83] suggested that the deflection of the cutting tool during milling was the primary cause of machining errors.

Table 5.23: Developed HM system dimensional accuracy

	Mean Length Error	*Mean Width Error*	*Mean Height Error*
Value (mm)	0.395	0.27	0.415
Corresponding Axis	X	Y	Z

Referring to Table 5.10 and Appendix E4, the maximum repeatability error was 0.3701%. Similar to the dimensional accuracy, the tool deflection experienced during the milling processes directly influenced the repeatability error obtained during testing.

Figure 5.30, Figure 5.31, and Figure 5.32, along with Table 5.13, indicated that the developed HM system could produce fine, medium, and coarse surface finishes (upon visual inspection) at varying material removal rates. From Table 5.13, it was noted that a significant material removal rate of 150000 mm^3/min was possible whilst maintaining a fine surface finish. Using the factor-level table in Table 5.12 to implement the random test strategy shown in Table 5.13 removed any bias towards specific process parameters, which could have skewed the produced data.

As depicted in Figure 5.37, the reduction in material wastage in producing the VTOL fuselage and house models using the developed HM system was 9.008% and 18.066%, respectively. The standard PU foam sheet sizes need to be factored in to quantify further the reduction in material wastage of the developed HM system. The smallest standard sheet size of PU foam supplied by Rigifoam, a local manufacturer and supplier of PU foam, is 2440x1220xthickness mm, where the available thickness ranges from 10 mm to 500 mm [84]. Therefore, if a considerably smaller model than the standard sheet size were to be manufactured, a saw or a hot wire cutter would be required to cut the stock material of the model. If multiple parts are produced from the standard sheet, the material wastage would not be as significant. However, the material wastage would be significantly greater if a single part was needed that did not utilise the entire sheet size. Additionally, the material wastage would increase exponentially if the height of the part to be manufactured was substantially less than the PU foam block's standard thickness.

Figure 5.39 illustrates the cycle time comparison between the two platforms for various combinations of settings. The coarse settings combination provided the lowest percentage reduction in the cycle time at a value of 74.82%, while the fine settings combination provided a 96.22% reduction in cycle time. The complex surfaces of the VTOL's fuselage contributed substantially to the cycle time of the 3DP's layer-by-layer additive manufacturing technique. Therefore, the reduction in cycle time for a less complex part would not be as high as the 96.22% obtained.

Finally, Figure 5.40, Figure 5.41, and Figure 5.42 illustrate the various models produced using the developed HM system during this research project. The mass of the PU VTOL stock material and the mass of the PU VTOL machined model can be seen in Figure 5.43 and Figure 5.44, respectively. The stock material was created by executing the additive facing toolpath utilising the undersize containment boundary, as shown in Figure 5.23. The mass of the PU house machined model can be seen in Figure 5.46, whereby the initial stock material was additively deposited along the walls, as shown in Figure 5.45.

Figure 5.40: Two house models produced using the developed HM system

Figure 5.41: Three house models and nine calibration cubes produced using the developed HM system

Figure 5.42: Four scaled-down VTOL fuselage models produced using the developed HM system

Figure 5.43: Mass of PU VTOL stock material

Figure 5.44: Mass of PU VTOL machined model

Figure 5.45: PU house model additively deposited along the walls

Figure 5.46: Mass of PU house machined model

5.4 Chapter Conclusion

Chapter 5 discussed the results gathered from testing the developed HM platform. First, the theoretical analysis determined the minimum theoretical movement of the machine's carriage along the X, Y and Z axes. This theoretical movement was used to indicate the dimensional accuracy that could be expected from the experimental analysis that followed. Next, the experimental analysis of the system detailed in Section 5.2.4 was divided into four sections, namely dimensional accuracy, repeatability and stability, effects of process parameters, material wastage, and cycle time comparison. Next, the results gathered and the relationships deduced from evaluating each subsection were discussed. Finally, the overall performance of the developed HM system was discussed and quantified by highlighting the key findings of the individual subsections.

Chapter 6

Conclusion and Future Recommendations

This chapter concluded this research project. The performance of the combined additive and subtractive manufacturing platform developed in this dissertation was discussed, and recommendations for future research were proposed.

6.1 Conclusion

This research aimed to develop a combined additive manufacturing and machining platform for large-scale prototyping for minimising material wastage. Furthermore, the findings sought to provide a cost and time-efficient alternative to the current methods of HM currently used in industry.

The evaluation of the developed HM by machining platform was divided into four sections to quantify the overall system performance and determine each section's effectiveness. The four sections evaluated were dimensional accuracy, repeatability and stability, the effects of process parameters, material wastage, and a cycle time comparison.

The dimensional accuracy evaluation found that the developed platform was capable of producing parts with a dimensional accuracy of 0.395 mm in X, 0.27 mm in Y, and 0.415 mm in Z. The maximum stability error recorded was 0.1 mm, which indicated that the produced features had not expanded or collapsed upon completion of the machining cycles within the elapsed 24-hour timeframe. In addition, the maximum repeatability error recorded was 0.3701%. This 0.3701% indicated that the developed system could repeatedly produce the same output for identical input conditions with a low probability for random errors.

Although not a primary focus for this research, the effects of process parameters on the material removal rate and a visual surface finish inspection were performed. It was found that a fine surface finish could be obtained for varying combinations of machining process parameters and material removal rates. For example, a fine surface finish was obtained utilising a significant material removal rate of 150000 mm³/min. The interchangeability between the additive and subtractive processes of the developed HM system allowed for the PU foam to be re-deposited and re-machined continuously. This interchangeability was particularly beneficial when the produced models contained large voids or high levels of porosity.

Two separate models were used to evaluate the reduction in material wastage capabilities of the developed platform. First, the scaled-down VTOL fuselage model yielded a 9.008% reduction in material wastage compared to a stand-alone machining process. Second, the house model produced an 18.066% reduction in material wastage. The house model yielded a 9.058% greater reduction in material wastage than the VTOL fuselage model, owing to the house model's thin walls and deep pocket features. Therefore, the percentage reduction in material wastage was directly dependant on the shape of the model produced. Due to the porosity of the PU foam, the mass of the models produced using the developed system was marginally less than the theoretically calculated mass.

A cycle time comparison was performed between the developed HM platform and a commercially available 3D printer. Three categories of process settings were defined for both systems, namely coarse, medium, and fine settings. The system developed in this research yielded a 96.22% reduction in cycle time for the fine settings category compared to the Ender-5 Plus 3DP. As with the reduction in material wastage, the reduction in cycle time was directly dependant on the geometry of the model to be produced.

In conclusion, the developed additive manufacturing and machining platform was capable of repeatedly producing large, full-scale models that were dimensionally accurate, stable, and complied with the ISO 2768 standard. Furthermore, the developed HM system reduced material wastage and cycle time compared to stand-alone conventional manufacturing techniques. Therefore, the overall performance of the developed system, along with the results produced utilising the system, supported the proposed research objective and hypothesis for this research project.

6.2 Recommendations for Future Research

Recommendations on how the performance of the developed system could be improved upon for future iterations included:

- ➢ Develop a vacuum clamping system to replace the installed workholding technique, as shown in Figure 3.8. A vacuum clamping system would allow for the safe clamping of complex geometries and remove the need to use a clamping kit to secure the workpiece. Additionally, the full size of the cutting bed could be utilised without the risk of colliding with the fixture clamps.

- ➢ Although the system described in Section 5.2.4 and utilised to perform the data analysis for this research project yielded desirable results, the cost-volume ratio of an individual can of one-part moisture curing expanding PU foam was significant compared to the cost-volume ratio of the liquid PU foam detailed in Appendix B1. Therefore, further testing and modifications to the dosing system developed in Section 3.1.3 could yield improved results and a reduction in the operating cost of the developed HM platform.

- ➢ Adding a misting system to the developed platform would enhance the expansion and curing of the PU foam [85]. In addition, the misting could be applied between each deposited layer to ensure maximum adhesion is achieved.

- ➢ Specialised cutting tools explicitly made for milling PU foam would improve the machined parts' accuracy, surface finish, and level of detail. FROGTools, a division of Streamline Automation Ltd, manufacture CNC foam cutting tools capable of producing detailed features at significant cutting depths [86]. FROGTools produce three types of foam cutting tools: end mill, ball end, and ball end tapered. Whilst the end mill and the ball end mill are standard cutting tools, the tapered end mill is uncommon and allows for intricate features to be produced. Furthermore, the flute lengths of the cutting tools utilised in this research project were considerably shorter than those produced by FROGTools. A longer flute length would allow for deep features to be produced without the shank of the cutting tool rubbing against the material and diminishing the surface finish.

- ➢ Develop an extraction system to remove the swarf during machining and prevent both the workpiece and the cutting tool from overheating. This swarf removal would increase the tool life and produce a smoother surface finish.

- ➢ Minimise the deflection of the cutting tool during milling by increasing the rigidity of the CNC milling spindle motor mounting assembly. As stated in Section 5.3, the deflection of the cutting tool during milling was a primary cause of machining errors. Therefore, this deflection experienced during milling would need to be addressed before the long flute length cutting tools produced by FROGTools could be utilised.

➢ The reduction in the material wastage achieved by the developed system was computed by comparing the mass of the deposited stock material to the mass of the machined model. A volume comparison, instead of mass comparison, between the deposited and machined models could provide a more accurate indication of the reduction in material wastage compared to stand-alone manufacturing techniques. For example, a standard block of PU foam, supplied by a manufacturer such as Rigifoam, would possess a more consistent density throughout the block due to the controlled forming of the foam. Therefore, the standard foam block would contain fewer voids than the method utilised in this research. A volume comparison before and after the standard block was machined would provide an accurate indication of the material wastage, which would indicate the cost-effectiveness of the process. This reduction in material wastage and cost-effectiveness could be compared to the system developed in this research by experimentally computing a volume comparison between the additively deposited stock material and the finished product.

➢ The deposition shown in Figure 5.45 should be optimised to further reduce the material wastage due to the unanticipated overgrowing of the foam. A possible solution could be to develop a finer nozzle outlet that could deposit thinner foam sections rather than the large beads depicted in Figure 5.45. The large beads displayed a tendency to sag when multiple layers were deposited on top of one another.

References

1.   Bouwer G. Measuring South Africa's economic growth. 2012;1–4.

2.   Stats SA. Gross domestic product 4th quarter 2019 [Internet]. 2020 [cited 2020 Oct 13]. Available from: http://www.statssa.gov.za/publications/P0441/GDP 2019 Q4 (Media presentation).pdf

3.   Stats SA. Quarterly Labour Force Survey [Internet]. [cited 2020 Oct 13]. Available from: http://www.statssa.gov.za/publications/P0211/P02112ndQuarter2020.pdf

4.   Zalk N. Thinking through the role of manufacturing in economic growth and employment generation in South Africa. Econ3x3. 2014 Feb;

5.   Bhorat H, Rooney C. State of Manufacturing in South Africa. Development Policy Research Unit. 2017 Mar;

6.   Williams G, Cunningham S, De Beer D. Advanced Manufacturing and Jobs in South Africa : An Examination of Perceptions and Trends. International Conference on Manufacturing-Led Growth for Employment and Equality. 2014;(May):1–36.

7.   Attiah E. The Role of Manufacturing and Service Sectors in Economic Growth: An Empirical Study of Developing Countries. European Research Studies Journal. 2019;112–27.

8.   Haraguchi N, Cheng CFC, Smeets E. The Importance of Manufacturing in Economic Development: Has This Changed? World Development. 2017;93:293–315.

9.   Groover MP. Fundamentals of modern manufacturing: materials, processes, and systems. John Wiley & Sons; 2020.

10.   Karbon D, Herr T. G-Code and M-Code: What Do They Mean In CNC Machining? [Internet]. [cited 2020 Oct 19]. Available from: https://www.steckermachine.com/blog/g-code-m-code#:~:text=M-Code — The Organizer of,vary by the specific machine.

11.   CNC Machining [Internet]. [cited 2020 Nov 15]. Available from: https://allekiskiind.com/services/machining-services/cnc-machining/

12.   Different Types of Lathe Cutting Tools for Turning, Boring, Facing, Chamfering and More Operations | CNCLATHING [Internet]. [cited 2020 Nov 15]. Available from: https://www.cnclathing.com/guide/different-types-of-lathe-cutting-tools-for-turning-boring-facing-chamfering-and-more-operations-cnclathing

13.   Astakhov VP. Geometry of Single-point Turning Tools and Drills: Fundamentals and Practical Applications. Springer Science & Business Media. 2010.

14. Rapid prototyping [Internet]. [cited 2020 Oct 13]. Available from: https://engineeringproductdesign.com/knowledge-base/rapid-prototyping-techniques/

15. Chua CK, Leong KF, Lim CS. Rapid prototyping: principles and applications. World Scientific Publishing Company; 2010.

16. Chartier T, Badev A. Rapid Prototyping of Ceramics. Handbook of Advanced Ceramics: Materials, Applications, Processing, and Properties: Second Edition. Elsevier; 2013. 489–524 p.

17. Campbell I, Diegel O, Kowen J, Wohlers T. Wohlers Report 2017 3D Printing and Additive Manufacturing State of the Industry: Annual Worldwide Progress Report. Wohlers Associates; 2017.

18. Grimm T. User's Guide to Rapid Prototyping. Society of Manufacturing Engineers; 2004.

19. Plug Construction Guide [Internet]. [cited 2021 Sep 16]. Available from: https://www.fibreglast.com/product/Plug-Construction-Guide/Learning_Center

20. PLUGS & MOULDS [Internet]. [cited 2021 Sep 16]. Available from: http://compositeplus.ee/plugs-and-moulds/

21. Freitag D, Wohlers T, Phillippi T. Rapid Prototyping: State of the Art. 2003;

22. Hull CW. Apparatus for Production of Three-Dimensional Objects By Stereolithography. Patent. United States; 638905, 1984.

23. Yuan B, Zhou SY, Chen XS. Rapid Prototyping Technology and its Application in Bone Tissue Engineering. Journal of Zhejiang University. 2017;

24. Stereolithography [Internet]. [cited 2020 Dec 5]. Available from: https://www.3dsystems.com/on-demand-manufacturing/stereolithography-sla

25. Nayar S, Bhuminathan S, Bhat W. Rapid prototyping and stereolithography in dentistry. Journal of Pharmacy and Bioallied Sciences. 2015;7(April):S216–9.

26. Chua CK, Wong CH, Yeong WY. Standards, Quality Control, and Measurement Sciences in 3D Printing and Additive Manufacturing. Academic Press. 2017.

27. Prusa J. Basics of 3D printing. Journal of Chemical Information and Modeling. 2020;

28. Melchels FPW, Feijen J, Grijpma DW. A review on stereolithography and its applications in biomedical engineering. Biomaterials. 2010;31(24):6121–30.

29. Crump SS. Apparatus and Method for Creating Three-Dimensional Objects. Patent. United States; 5121329, 1992.

30.   Palermo E. Fused Deposition Modeling: Most Common 3D Printing Method [Internet]. 2013 [cited 2021 Mar 27]. Available from: https://www.livescience.com/39810-fused-deposition-modeling.html

31.   Ambrosi A, Pumera M. 3D-printing technologies for electrochemical applications. Chemical Society Reviews. 2016;45(10):2740–55.

32.   Mohamed OA, Masood SH, Bhowmik JL. Optimization of fused deposition modeling process parameters: a review of current research and future prospects. Advances in Manufacturing. 2015;42–53.

33.   Deckard CR, Beaman JJ, Darrah JF. Method for Selective Laser Sintering With Layerwise Cross-Scanning. United States; 5155324, 1992.

34.   Touri M, Kabirian F, Saadati M, Ramakrishna S, Mozafari M. Additive Manufacturing of Biomaterials – The Evolution of Rapid Prototyping. Advanced Engineering Materials. 2019;21(2).

35.   Czelusniak T, Amorim FL. Selective laser sintering of carbon fiber–reinforced PA12: Gaussian process modeling and stochastic optimization of process variables. International Journal of Advanced Manufacturing Technology. 2020;110.

36.   Gibson I, Rosen D, Stucker B, Khorasani M. Additive Manufacturing Technologies. New York: Springer; 2021.

37.   Awad A, Fina F, Goyanes A, Gaisford S, Basit AW. 3D printing: Principles and pharmaceutical applications of selective laser sintering. International Journal of Pharmaceutics. 2020;586(June):119594.

38.   Sachs E, Haggerty J, Cima M, Williams P. Three-Dimensional Printing Techniques. United States; 5204055, 1993.

39.   Wohlers T, Gornet T. History of additive manufacturing. Wohlers Report. 2014;

40.   3D PRINTING - ADDITIVE [Internet]. [cited 2020 Oct 19]. Available from: https://make.3dexperience.3ds.com/processes/binder-jetting

41.   Shahrubudin N, Lee TC, Ramlan R. An overview on 3D printing technology: Technological, materials, and applications. Procedia Manufacturing. 2019;35:1286–96.

42.   Lee JY, An J, Chua CK. Fundamentals and applications of 3D printing for novel materials. Applied Materials Today. 2017;7:120–33.

43.   Pham D, Dimov SS. Rapid manufacturing: the technologies and applications of rapid prototyping and rapid tooling. Springer Science & Business Media. 2012.

44. Feygin M. Apparatus and Method for Forming an Integral Object From Laminations. United States; 4752352, 1988.

45. Guo N, Leu MC. Additive manufacturing: Technology, applications and research needs. Frontiers of Mechanical Engineering. 2013;8(3):215–43.

46. Rahmati S. Direct Rapid Tooling [Internet]. Vol. 10, Comprehensive Materials Processing. Elsevier; 2014. 303–344 p. Available from: http://dx.doi.org/10.1016/B978-0-08-096532-1.01013-X

47. Singh R, Singh S, Hashmi MSJ. Implant Materials and Their Processing Technologies. Reference Module in Materials Science and Materials Engineering. Elsevier Ltd.; 2016. 1–31 p.

48. Dev Singh D, Mahender T, Raji Reddy A. Powder bed fusion process: A brief review. Materials Today: Proceedings [Internet]. 2021;46:350–5. Available from: https://doi.org/10.1016/j.matpr.2020.08.415

49. Calignano F, Manfredi D, Ambrosio EP, Iuliano L, Fino P. Influence of process parameters on surface roughness of aluminum parts produced by DMLS. International Journal of Advanced Manufacturing Technology. 2013;67(9–12):2743–51.

50. Sealy MP, Madireddy G, Williams RE, Rao P, Toursangsaraki M. Hybrid processes in additive manufacturing. Journal of Manufacturing Science and Engineering, Transactions of the ASME. 2018;140(6).

51. Hur J, Lee K, Zhu-Hu, Kim J. Hybrid rapid prototyping system using machining and deposition. CAD Computer Aided Design. 2002;34(10):741–54.

52. Lee WC, Wei CC, Chung SC. Development of a hybrid rapid prototyping system using low-cost fused deposition modeling and five-axis machining. Journal of Materials Processing Technology. 2014;214(11):2366–74.

53. Akula S, Karunakaran KP. Hybrid adaptive layer manufacturing: An Intelligent art of direct metal rapid tooling process. Robotics and Computer-Integrated Manufacturing. 2006;22(2):113–23.

54. Shah J, Snider B, Clarke T, Kozutsky S, Lacki M, Hosseini A. Large-scale 3D printers for additive manufacturing: design considerations and challenges. International Journal of Advanced Manufacturing Technology. 2019;104(9–12):3679–93.

55. Cincinnati Incorporated. Big Area Additive Manufacturing 3D Printer [Internet]. [cited 2020 Oct 19]. Available from: https://www.e-ci.com/baam

56. Roschli A, Gaul KT, Boulger AM, Post BK, Chesser PC, Love LJ, et al. Designing for Big Area Additive Manufacturing. Additive Manufacturing. 2019;25:275–85.

57.   Hyrel 3D. Hydra 16A [Internet]. [cited 2021 Jan 15]. Available from: https://www.hyrel3d.com/portfolio/hyrda16a/

58.   BLB Industries. The Biggest Machines for Industrial Applications [Internet]. [cited 2020 Oct 19]. Available from: https://blbindustries.se/

59.   Zmorph. Zmorph 3D Printers That Deliver [Internet]. [cited 2021 Jan 15]. Available from: https://zmorph3d.com/

60.   Changzhou Huajiang Electrical Co. Ltd. 3KW/ER20/ 220V-380V Air cooled square [Internet]. [cited 2021 Apr 18]. Available from: http://www.huajiang.cn/content/?40.html

61.   ISCAR Cutting Tools - Metal Working Tools - Grade : IC908 [Internet]. [cited 2021 Jun 6]. Available from: https://www.iscar.com/eCatalog/Grade.aspx?grade=IC908&item=5921254&fnum=121&mapp=ML

62.   Peristaltic & Rotodynamic Pump [Internet]. [cited 2021 Apr 18]. Available from: https://pumps-pumpingequipments.blogspot.com/2016/11/peristaltic-hose-rotodynamic-pumps.html

63.   Reducing Pulsation in Peristaltic Pumping Systems [Internet]. [cited 2021 Apr 18]. Available from: https://www.coleparmer.com/tech-article/reducing-pulsation-peristaltic-pumping

64.   Peristaltic pumps – advantages and applications [Internet]. [cited 2021 Apr 18]. Available from: https://www.manufacturingchemist.com/news/article_page/Peristaltic_pumps_advantages_and_applications/74693

65.   Peristaltic Pump Dosing Pump Peristaltic Liquid Pump, Adjustable Flow rate 66ml/min to 320ml/min GROTHEN G728-2 [Internet]. [cited 2021 Apr 18]. Available from: https://www.aliexpress.com/item/4000081307018.html

66.   Aranjo B, Soori PK, Talukder P. Stepper motor drives for robotic applications. 2012 IEEE International Power Engineering and Optimization Conference, PEOCO 2012 - Conference Proceedings. 2012;(June).

67.   DIY Electronics [Internet]. [cited 2021 May 5]. Available from: https://www.diyelectronics.co.za/store/

68.   Micro Robotics [Internet]. [cited 2021 May 5]. Available from: https://www.robotics.org.za/

69.   Pololu [Internet]. [cited 2021 May 5]. Available from: https://www.pololu.com/

70.   Bolton W. Mechatronics: Electronic Control Systems in Mechanical Engineering. Seventh Ed. Pearson Education; 2019.

71.   Arduino [Internet]. [cited 2021 May 5]. Available from: https://www.arduino.cc/

72.   Teensy USB Development Board [Internet]. [cited 2021 May 5]. Available from: https://www.pjrc.com/teensy/

73.   Industry Showcase | Mastercam [Internet]. [cited 2021 May 5]. Available from: https://www.mastercam.com/industry-showcase/

74.   Jamal Y. Sheikh-Ahmad. Machining of Polymer Composites. Springer Science & Business Media. 2009.

75.   Beckhoff Information System [Internet]. [cited 2021 Jul 10]. Available from: https://infosys.beckhoff.com/english.php?content=../content/1033/tf5100_tc3_nc_i/9231169547.html&id=

76.   Beckhoff AM8100 Operating Instructions [Internet]. [cited 2021 Aug 24]. Available from: https://download.beckhoff.com/download/document/motion/am8100_ba_en.pdf

77.   William. ISO 2768 – General Geometrical Tolerances and Technical Drawings [Internet]. [cited 2020 Oct 19]. Available from: https://www.plianced.com/compliance-wiki/iso-2768-general-geometrical-tolerances-and-technical-drawings/

78.   Figliola RS, Beasley DE. Theory and Design for Mechanical Measurements. Seventh Ed. John Wiley & Sons; 2019.

79.   Box Plot Review [Internet]. [cited 2021 Oct 5]. Available from: https://www.khanacademy.org/math/statistics-probability/summarizing-quantitative-data/box-whisker-plots/a/box-plot-review

80.   Chahal M, Singh V, Garg R, Kumar S. To Estimate The Range Of Process Parameters For Optimization Of Surface Roughness & Material Removal Rate In CNC Milling. International Journal of Engineering Trends and Technology. 2013;4(10):4556–63.

81.   Sika Boom Expanding Polyurethane Foam [Internet]. [cited 2021 Sep 12]. Available from: https://zaf.sika.com/dms/getdocument.get/7e68b160-8099-39eb-9c3a-63f7e1f71e9e/Sika Boom.pdf

82.   Ender-5 Plus 3D Printer [Internet]. [cited 2021 Sep 15]. Available from: https://www.creality.com/goods-detail/ender-5-plus-3d-printer

83.   Dépincé P, Hascoët JY. Active integration of tool deflection effects in end milling. Part 2. Compensation of tool deflection. International Journal of Machine Tools and Manufacture. 2006;46(9):945–56.

84.   Rigifoam [Internet]. [cited 2021 Sep 22]. Available from: https://www.rigifoam.com/

85.   How to use Expanding Foam [Internet]. [cited 2021 Sep 10]. Available from: https://www.topline.ie/blog/how-to-guides/how-to-use-expanding-foam

86.   SPECIALIZED FOAM CNC ROUTER BITS [Internet]. [cited 2021 Jun 11]. Available from: https://www.frog3d.com/frogtools

Appendix A1 – AM Summary Table

AM Technology	Method	Typical Materials	Applications	Advantages	Disadvantages
Vat Photopolymerisation	SLA	– UV-curable (photopolymer) resins	– Concept models – Medical models – Casting patterns	– Smooth surface finish – High dimensional accuracy – Large parts can be produced	– Only photopolymer resins may be used – Requires support structures – Post-processing is required – Operator exposed to toxic liquid resins
Material Extrusion	FDM	– Thermoplastics (PLA, ABS, PET)	– Concept models – Functional prototypes – Jigs & fixtures	– Simple – Low-cost – Numerous thermoplastic materials are available – Scalability	– Visible layers – Complex geometries require support structures – The introduced heat may cause unpredictable shrinkage or distortion
Powder Bed Fusion	SLS/DMLS	– Thermoplastics – Metals – Ceramics	– Form-fit testing – Investment casting – Metal tooling	– Numerous materials are available – The powder is self-supporting (Polymer AM) – Complex geometries can be produced with up to 95% density (DMLS)	– Comparatively expensive process – Large amount of power is consumed when operating the CO2 laser
Binder Jetting	3DP	– Metals – Ceramics – Glass – Sand	– Product visualisation – Casting patterns	– Rapid – Relatively low-cost process – Wide variety of materials – No support structures are required	– Rough surface finish – Infiltration process needed for post-processing – Powder removal may prove challenging for complex geometries
Sheet Lamination	LOM	– Paper – Ceramic-filled tapes – Composites	– Replicas – Rapid tooling – Patterns for sand casting	– Rapid process – No support structures are required – Parts experience minimal deformation or warpage	– Not suited for complex geometries – Large amount of material wastage

Appendix B1 – PU Foam Technical Data Sheets

RESICHEM (PTY)LTD
SUPERIOR URETHANE FOAM SYSTEMS

ECOSPRAY RS3030

ECOSPRAY RS3030 is a self-extinguishing rigid polyurethane spray system for the insulation of roofing, walling, vessels and tanks. The foam has a good surface finish with excellent cell structure and good inter-laminar adhesion. The system uses ECOMATE® as the blowing agent which has zero Ozone Depleting Potential, zero Global Warming Potential and is VOC compliant. It is ideally processed through high pressure impingement mixing, airless spray dispensing equipment such as Gusmer, Probler, Intergun, etc.

TYPICAL PHYSICAL PROPERTIES

Resin (polyol blend)	Appearance	Brown Liquid
	Density	1.15 g/ml
	Viscosity @ 20°C	700 ± 50 mPa.s
Isocyanate	Composition	Technical Grade MDI
	Appearance	Dark Brown Liquid
	Density	1.22 - 1.23 g/ml
	Viscosity	250 ± 50 mPa.s

FORMULATION
100 pbm ECOSPRAY RS3030
107 pbm Resinate 200
100 : 100 (v/v)

TYPICAL REACTION PROFILE
Hand Mix @ 1000 RPM. Reef Altitude; 20ºC

Cream Time	2 - 4 seconds
Gel Time	10 - 12 seconds
Rise Time	24 - 26 seconds
Tack Free	13 - 16 seconds
Free Rise Density (core)	24 - 26 (reef)
	27 - 30 kg/m³ (coastal)
Typical Applied Density (core)	30 - 35 kg/m³ (reef)
	33 - 38 kg/m³ (coastal)
Typical Compressive strength	> 200 kPa
Typical k Factor	0.025 w/m.K (@ mean temperature of 22°C)

PRODUCT DATA SHEET

RESINATE 200

Application and Description

Resinate 200 is a liquid, dark brown mixture of diphenylmethane-4,4'-diisocyanate (MDI) with isomers and homologues of higher functionality. It is used in conjunction with polyols to produce rigid polyurethane foams it is also used in isocyanurate foam, paint, adhesives, structural foam, cellular integral skin foam, automotive bumper and interior parts, high-resilience foam and synthetic wood, etc. Due to its unique composition structure, RESINATE 200 can provide better flowability. It is, therefore, particularly suitable for the production which require strict flowability of systems.

Typical Physical and Chemical Properties

Appearance:	dark brown liquid
NCO Content:	30.2 – 32.5 by weight
Viscosity at 25°C:	150-250 mPa.S
Acidity:	Max 200 ppm HCl
Hydrolysable Chlorine:	$\leqslant 0.2\%$
Density at 20°C	± 1.23 g/cm^3

Packaging
Drums and IBC's.

Appendix B2 – Sika Boom PU Foam Density

Technical Data

Chemical Base	Polyurethane
Density	~ 22 kg / m³
Skinning Time	About 10 minutes at 23 °C
Curing Rate	5 – 10 hours depending on atmospheric temperature and humidity.

Appendix C1 – NEMA 17 (1.7A, 0.4 Nm) Stepper Motor Detail
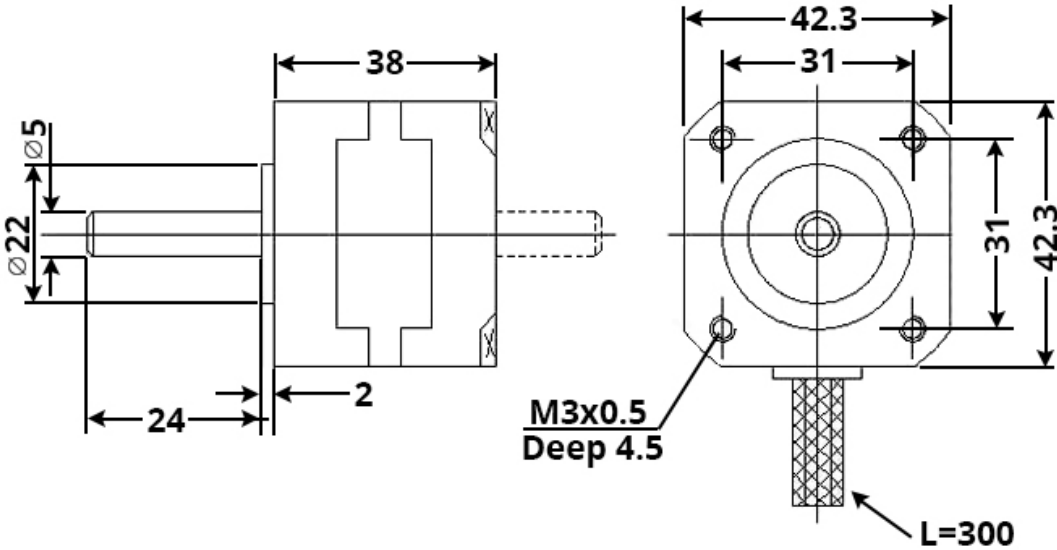
Appendix C2 – Pololu DRV8825 Wiring Diagram
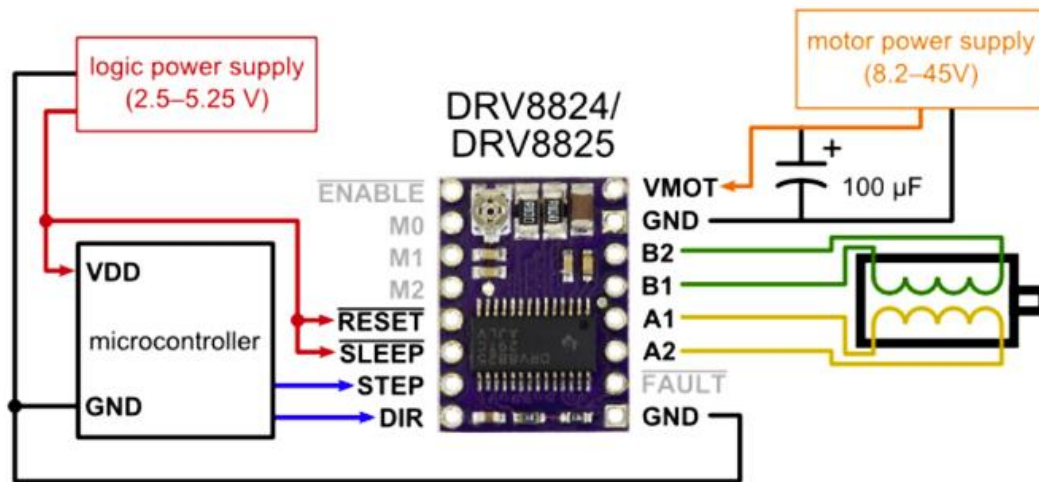
Appendix D1 – Dosing System Code

```
#include <U8g2lib.h>
#include "FastAccelStepper.h"

// Pin Definition
#define dirPinStepper 35          // Direction Pin of Stepper Motor 1's DRV8825
#define stepPinStepper 23          // Step Pin of Stepper Motor 1's DRV8825
#define dirPinStepper2 16          // Direction Pin of Stepper Motor 2's DRV8825
#define stepPinStepper2 17          // Step Pin of Stepper Motor 1's DRV8825
#define RatioPin 27          // Analog input pin for Ratio Potentiometer
#define FlowPin 14          // Analog input pin for FlowRate Potentiometer
#define stopPin 33          // Digital Input pin for Start/Stop switch
#define enablePin 5          // Enable pin connected to both DRV8825's
#define sleep 4          // Sleep pin connected to both DRV8825's
#define reset 19          // Reset pin connected to both DRV8825's


// Instantiation of Screen Object and FastAccelStepper Engine
U8G2_SH1106_128X64_NONAME_F_HW_I2C u8g2(U8G2_R0, /* reset=*/ U8X8_PIN_NONE);     //
Instantiation of Display object, using SH1106 Driver and a hardware I2C port

FastAccelStepperEngine engine = FastAccelStepperEngine();          // Instantiation of
FastAccelStepperEngine which assigns relevant resources like interrupts to use with
                              // FastAccelStepper objects

// Instantiation of FastAccelStepper Objects
FastAccelStepper *stepper = NULL;
FastAccelStepper *stepper2 = NULL;

void setup()
{
  // Declaring digital pins as inputs or outputs
  pinMode(stopPin, INPUT_PULLUP);     // stopPin uses internal pullup resistor to avoid false
readings due to noise
  pinMode(sleep, OUTPUT);
  pinMode(reset, OUTPUT);

  // DRV8825 sleep and reset pins need to be set HIGH for the drive to be enabled
  digitalWrite(sleep, HIGH);
  digitalWrite(reset, HIGH);

  // Initialising all FastAccelStepper Objects and assigning relevant pins to them
  engine.init();
  stepper = engine.stepperConnectToPin(stepPinStepper);
  stepper2 = engine.stepperConnectToPin(stepPinStepper2);

  if (stepper && stepper2)     // // If both steppers were able to connect to their assigned
stepPins
  {
    stepper->setDirectionPin(dirPinStepper);
    stepper->setAcceleration(500);     // Sets max acceleration value for stepper in pulses/s^2
    stepper->setEnablePin(enablePin);
```

```cpp
    stepper2->setDirectionPin(dirPinStepper2);
    stepper2->setAcceleration(500);   // Sets max acceleration value for stepper2 in pulses/s^2
    stepper->enableOutputs();        // Enables outputs for both steppers (enable pins are
bridged)
  }

  Serial.begin(9600);              // Open serial port for debugging purposes

  u8g2.begin();

  u8g2.clearBuffer();        // clear the internal memory
  u8g2.setFont(u8g2_font_nine_by_five_nbp_tr); // choose a suitable font
  u8g2.drawStr(2, 12, "Peristaltic     Pump"); // write something to the internal memory
  u8g2.sendBuffer();         // transfer internal memory to the display       // transfer internal
memory to the display
  delay(2000);
}

float readPots(int PotPin)              // Reads analog value from a Potentiometer and returns a
percentage value
{
 //Testing Oversampling for less noisy potentiometer readings (Takes 8 samples and averages
them)

 float sample_count = 0;
 int interval = 10;
 int start_millis = millis();
 double sum = 0;
 while(sample_count < 50)
 {
  sum += analogRead(PotPin);
  while((millis() - start_millis) < interval);
  sample_count++;
 }

 float avg_reading = sum/sample_count;
 float out = (avg_reading) / 4096;
 if (out <= 0)
 {
  out = 0.01;
 }         // Calculate percentage of maximum analog value given by reading
 else if(out>= 1)
 {
  out = 0.98;
 }
 return out;


}
```

```cpp
bool shouldConstrain(float mot)          // Checks if the motor is assigned a speed above its
maximum value or below zero, returns true if the value is not realistic
{
 if (mot >= 4300 || mot <= 0)
 {
  return true;
 }
 else
 {
  return false;
 }
}

float constrainSpeed(float upper, float lower, float val)      // Constrains commanded motor
speed between an upper and lower bound
{
 float constrainedVal = 0;
 if (val >= upper)
 {
  constrainedVal = upper;
  return constrainedVal;
 }
 else if (val <= lower)
 {
  constrainedVal = lower;
  return constrainedVal;
 }
 else
 {
  constrainedVal = val;
  return constrainedVal;
 }
}

void displayScreen(float ratio, float flow, float scale)     // Displays the overall flowrate and ratio
between steppers, a third scaling parameter is passed to account
{                                      //  for the relationship between pulses/second and volumetric
flowrate
  int flowrate = flow*scale;
  u8g2.clearBuffer();        // clear the internal memory
  u8g2.setFont(u8g2_font_nine_by_five_nbp_tr); // choose a suitable font

  u8g2.drawStr(0, 10, "Speed");
  u8g2.setCursor(50, 10);
  u8g2.print(flowrate, 0);

  u8g2.drawStr(0, 34, "Ratio");
  u8g2.setCursor(50, 34);
  u8g2.print((ratio*100), 0);

  u8g2.sendBuffer();
```

```
}

void stopStart(bool stop, double mot1, double mot2)     // Checks state of start/stop switch and
enables/disables stepper outputs accordingly
{
  if(stop)
 {
  Serial.println("Outputs disabled");
  stepper->disableOutputs();
  stepper->stopMove();
  stepper2->stopMove();
 }
 else
 {
  Serial.println("Outputs enabled");
  stepper->enableOutputs();
  stepper->setSpeedInHz(mot1);
  stepper2->setSpeedInHz(mot2);
  stepper->runForward();
  stepper2->runForward();
 }
}

void updateFlow(int &mot1, int &mot2, float &flow, float &ratio)    // Checks that no motor
speed command exceeds its max speed, if max is exceeded the max value is assigned and
{                                       // both motors are scaled to maintain the demanded ratio

 bool constrain1 = shouldConstrain(mot1);
 bool constrain2 = shouldConstrain(mot2);

 int ratioInt = ratio*100;
 if (ratioInt > 99)
  ratioInt = 99;
 if (constrain1)
 {
  mot1 = round(constrainSpeed(4300, 0, mot1));
  mot2 = round((mot1 - (((float)ratioInt/100.0) * mot1)) / ((float)ratioInt/100.0));
  flow = mot1 + mot2;

 }
 if (constrain2)
 {
  mot2 = round(constrainSpeed(4300, 0, mot2));
  mot1 = round((((float)ratioInt/100.0) * mot2) / (1.0 - ((float)ratioInt/100.0)));
  flow = mot1 + mot2;
 }
}
```

```
void loop()
{
  //Read Analog values from flowrate and ratio potentiometers
  Serial.println(analogRead(FlowPin));         // Calculates flowrate as a % of maximum flowrate
  float flow = readPots(FlowPin)*8600;
                                               // (Max flowrate corresponds to 8600 pulses per
second - 4300 pulses to each stepper),
                                               // Percentage is varied by potentiometer

  float ratio = readPots(RatioPin);     // Calculates the ratio of the overall flow as a percentage
(e.g. 50% means 1:1 mixing)


  int mot1 = ratio * flow;                            // Calculates "Speed" to send to motor 1
(Speed is in pulses per second here)
  int mot2 = (1 - ratio) * flow;


  updateFlow(mot1, mot2, flow, ratio);         // Assign speeds to steppers according to
demanded flowrate and ratio

  stopStart((digitalRead(stopPin)),mot1, mot2);

  displayScreen(ratio, flow, 1);
}
```

Appendix D2 – Dosing System Calibration Sequence Code

```
#include "FastAccelStepper.h"

// Pin Definition
#define dirPinStepper 35          // Direction Pin of Stepper Motor 1's DRV8825
#define stepPinStepper 23          // Step Pin of Stepper Motor 1's DRV8825
#define dirPinStepper2 16          // Direction Pin of Stepper Motor 2's DRV8825
#define stepPinStepper2 17         // Step Pin of Stepper Motor 1's DRV8825
#define RatioPin 27               // Analog input pin for Ratio Potentiometer
#define FlowPin 14                // Analog input pin for FlowRate Potentiometer
#define stopPin 33                // Digital Input pin for Start/Stop switch
#define enablePin 5               // Enable pin connected to both DRV8825's
#define sleep 4                  // Sleep pin connected to both DRV8825's
#define reset 19                  // Reset pin connected to both DRV8825's


FastAccelStepperEngine engine = FastAccelStepperEngine();        // Instantiation of
FastAccelStepperEngine which assigns relevant resources like interrupts to use with
                                // FastAccelStepper objects

// Instantiation of FastAccelStepper Objects
FastAccelStepper *stepper = NULL;
FastAccelStepper *stepper2 = NULL;

// Time variables
float currentMillis;

void setup()
{
  // Declaring digital pins as inputs or outputs
  pinMode(stopPin, INPUT_PULLUP);      // stopPin uses internal pullup resistor to avoid false
readings due to noise
  pinMode(sleep, OUTPUT);
  pinMode(reset, OUTPUT);

  // DRV8825 sleep and reset pins need to be set HIGH for the drive to be enabled
  digitalWrite(sleep, HIGH);
  digitalWrite(reset, HIGH);

  // Initialising all FastAccelStepper Objects and assigning relevant pins to them
  engine.init();
  stepper = engine.stepperConnectToPin(stepPinStepper);
  stepper2 = engine.stepperConnectToPin(stepPinStepper2);
```

```
  if (stepper && stepper2)         // If both steppers were able to connect to their assigned
stepPins
    {
      stepper->setDirectionPin(dirPinStepper);
      stepper->setAcceleration(500);    // Sets max acceleration value for stepper in pulses/s^2
      stepper->setEnablePin(enablePin);

      stepper2->setDirectionPin(dirPinStepper2);
      stepper2->setAcceleration(500);    // Sets max acceleration value for stepper2 in pulses/s^2
      stepper->enableOutputs();        // Enables outputs for both steppers (enable pins are
bridged)
    }
    Serial.begin(9600);             // Open serial port for debugging purposes
}

void runTestSequence()
{
    Serial.println("Test Sequence Started");
    stepper->enableOutputs();        // Enable outputs to start calibration sequence
    stepper->setSpeedInHz(400);      // Speed is set to x pulses/second with an acceleration of y
pulses/s^2 - this should yield a z second(s) ramp until constant rpm is achieved
    stepper2->setSpeedInHz(400);
    currentMillis = millis();        // Save current millis count
    stepper->runForward();           // Start turning stepper motors
    stepper2->runForward();

    while ((millis() - currentMillis) < 60800);    // Let motors run for x seconds
    Serial.println("Outputs disabled");
    stepper->disableOutputs();               // Disable stepper motors
    stepper->stopMove();                     // Stop all commanded moves for stepper
    stepper2->stopMove();                    // Stop all commanded moves for stepper2
    Serial.println("Test Sequence Finished");
}

void loop()
{
    Serial.println("Do you want to run calibration?: ");
    String inString = Serial.readString(); // Read Input from Serial Monitor

    if(inString.indexOf("yes")>=0)        // If input == yes, run for b seconds at x pulses per second
with both motors
    {
      runTestSequence();
    }
    delay(1000);

}
```

Appendix D3 – RC Servo Code

```
#include <Servo.h>

#define trigger 7              // Declare GPIO pin assigned to trigger pin
#define servo_pin 3            // Declare GPIO pin assigned to servo signal wire.
Servo nozzle;

void setup()
{
  pinMode(trigger, INPUT);         // Declare trigger pin connected to PLC IO card as a digital
input.
               // Create an instance of a servo object called nozzle
  nozzle.attach(servo_pin);        // Attach servo object to analog output pin
}

void loop()
{
  if (digitalRead(trigger))         // Check if digital input attached to PLC IO card is HIGH
  {
    nozzle.writeMicroseconds(2000);    // Turn servo to pull nozzle down.
  }
  else
  {
    nozzle.writeMicroseconds(1000);    // Turn servo to release nozzle.
  }
}
```

Appendix E1 – Student's t Distribution Table

Table 4.4   Student's *t* Distribution (Two-Tailed)

ν	t_{50}	t_{90}	t_{95}	t_{99}
1	1.000	6.314	12.706	63.657
2	0.816	2.920	4.303	9.925
3	0.765	2.353	3.182	5.841
4	0.741	2.132	2.776	4.604
5	0.727	2.015	2.571	4.032
6	0.718	1.943	2.447	3.707
7	0.711	1.895	2.365	3.499
8	0.706	1.860	2.306	3.355
9	0.703	1.833	2.262	3.250
10	0.700	1.812	2.228	3.169
11	0.697	1.796	2.201	3.106
12	0.695	1.782	2.179	3.055
13	0.694	1.771	2.160	3.012
14	0.692	1.761	2.145	2.977
15	0.691	1.753	2.131	2.947
16	0.690	1.746	2.120	2.921
17	0.689	1.740	2.110	2.898
18	0.688	1.734	2.101	2.878
19	0.688	1.729	2.093	2.861
20	0.687	1.725	2.086	2.845
21	0.686	1.721	2.080	2.831
30	0.683	1.697	2.042	2.750
40	0.681	1.684	2.021	2.704
50	0.680	1.679	2.010	2.679
60	0.679	1.671	2.000	2.660
∞	0.674	1.645	1.960	2.576

Appendix E2 – Probability Values for Normal Error Function Table

Table 4.3 Probability Values for Normal Error Function: One-Sided Integral Solutions for

$$P(z_1) = \frac{1}{\sqrt{2\pi}} \int_0^{z_1} e^{-\beta^2/2} d\beta$$

$z_1 = \dfrac{x_1 - x'}{\sigma}$	0.00	0.01	0.02	0.03	0.04	0.05	0.06	0.07	0.08	0.09
0.0	0.0000	0.0040	0.0080	0.0120	0.0160	0.0199	0.0239	0.0279	0.0319	0.0359
0.1	0.0398	0.0438	0.0478	0.0517	0.0557	0.0596	0.0636	0.0675	0.0714	0.0753
0.2	0.0793	0.0832	0.0871	0.0910	0.0948	0.0987	0.1026	0.1064	0.1103	0.1141
0.3	0.1179	0.1217	0.1255	0.1293	0.1331	0.1368	0.1406	0.1443	0.1480	0.1517
0.4	0.1554	0.1591	0.1628	0.1664	0.1700	0.1736	0.1772	0.1809	0.1844	0.1879
0.5	0.1915	0.1950	0.1985	0.2019	0.2054	0.2088	0.2123	0.2157	0.2190	0.2224
0.6	0.2257	0.2291	0.2324	0.2357	0.2389	0.2422	0.2454	0.2486	0.2517	0.2549
0.7	0.2580	0.2611	0.2642	0.2673	0.2794	0.2734	0.2764	0.2794	0.2823	0.2852
0.8	0.2881	0.2910	0.2939	0.2967	0.2995	0.3023	0.3051	0.3078	0.3106	0.3133
0.9	0.3159	0.3186	0.3212	0.3238	0.3264	0.3289	0.3315	0.3340	0.3365	0.3389
1.0	0.3413	0.3438	0.3461	0.3485	0.3508	0.3531	0.3554	0.3577	0.3599	0.3621
1.1	0.3643	0.3665	0.3686	0.3708	0.3729	0.3749	0.3770	0.3790	0.3810	0.3830
1.2	0.3849	0.3869	0.3888	0.3907	0.3925	0.3944	0.3962	0.3980	0.3997	0.4015
1.3	0.4032	0.4049	0.4066	0.4082	0.4099	0.4115	0.4131	0.4147	0.4162	0.4177
1.4	0.4192	0.4207	0.4222	0.4236	0.4251	0.4265	0.4279	0.4292	0.4306	0.4319
1.5	0.4332	0.4345	0.4357	0.4370	0.4382	0.4394	0.4406	0.4418	0.4429	0.4441
1.6	0.4452	0.4463	0.4474	0.4484	0.4495	0.4505	0.4515	0.4525	0.4535	0.4545
1.7	0.4554	0.4564	0.4573	0.4582	0.4591	0.4599	0.4608	0.4616	0.4625	0.4633
1.8	0.4641	0.4649	0.4656	0.4664	0.4671	0.4678	0.4686	0.4693	0.4699	0.4706
1.9	0.4713	0.4719	0.4726	0.4732	0.4738	0.4744	0.4750	0.4756	0.4761	0.4767
2.0	0.4772	0.4778	0.4783	0.4788	0.4793	0.4799	0.4803	0.4808	0.4812	0.4817
2.1	0.4821	0.4826	0.4830	0.4834	0.4838	0.4842	0.4846	0.4850	0.4854	0.4857
2.2	0.4861	0.4864	0.4868	0.4871	0.4875	0.4878	0.4881	0.4884	0.4887	0.4890
2.3	0.4893	0.4896	0.4898	0.4901	0.4904	0.4906	0.4909	0.4911	0.4913	0.4916
2.4	0.4918	0.4920	0.4922	0.4925	0.4927	0.4929	0.4931	0.4932	0.4934	0.4936
2.5	0.4938	0.4940	0.4941	0.4943	0.4945	0.4946	0.4948	0.4949	0.4951	0.4952
2.6	0.4953	0.4955	0.4956	0.4957	0.4959	0.4960	0.4961	0.4962	0.4963	0.4964
2.7	0.4965	0.4966	0.4967	0.4968	0.4969	0.4970	0.4971	0.4972	0.4973	0.4974
2.8	0.4974	0.4975	0.4976	0.4977	0.4977	0.4978	0.4979	0.4979	0.4980	0.4981
2.9	0.4981	0.4982	0.4982	0.4983	0.4984	0.4984	0.4985	0.4985	0.4986	0.4986
3.0	0.49865	0.4987	0.4987	0.4988	0.4988	0.4988	0.4989	0.4989	0.4989	0.4990

Appendix E3 – Dimensional Checklists for Features 2, 3, 4 and 5.

Dimensional Checklist - Feature 2					
Length					
Test Number	*CAD Length (mm)*	*Measured Length (mm)*	*Length Error (mm)*	*Accuracy (%)*	*Stability (mm)*	*Tolerance Grade*
1	90	89.8	0.2	0.222	0.2	Medium
2	90	89.6	0.4	0.444	0	Coarse
3	90	90.2	0.2	0.222	0.1	Medium
4	90	90.1	0.1	0.111	0.1	Fine
5	90	90.2	0.2	0.222	0	Medium
Width					
Test Number	*CAD Width (mm)*	*Measured Width (mm)*	*Width Error (mm)*	*Accuracy (%)*	*Stability (mm)*	*Tolerance Grade*
1	85	84.9	0.1	0.118	0	Fine
2	85	84.8	0.2	0.235	0.1	Medium
3	85	85	0	0.000	0.1	Fine
4	85	84.7	0.3	0.353	0	Medium
5	85	84.8	0.2	0.235	0	Medium
Height					
Test Number	*CAD Height (mm)*	*Measured Height (mm)*	*Height Error (mm)*	*Accuracy (%)*	*Stability (mm)*	*Tolerance Grade*
1	27	26.5	0.5	1.852	0	Coarse
2	27	26.5	0.5	1.852	0.1	Coarse
3	27	26.7	0.3	1.111	0.1	Coarse
4	27	26.6	0.4	1.481	0	Coarse
5	27	26.5	0.5	1.852	0	Coarse

Dimensional Checklist - Feature 3					
Length					
Test Number	CAD Length (mm)	Measured Length (mm)	Length Error (mm)	Accuracy (%)	Stability (mm)	Tolerance Grade
1	85	84.7	0.3	0.353	0.1	Medium
2	85	84.4	0.6	0.706	0	Coarse
3	85	84.5	0.5	0.588	0	Coarse
4	85	84.6	0.4	0.471	0	Coarse
5	85	84.9	0.1	0.118	0	Fine
Width					
Test Number	CAD Width (mm)	Measured Width (mm)	Width Error (mm)	Accuracy (%)	Stability (mm)	Tolerance Grade
1	70	69.7	0.3	0.429	0	Medium
2	70	69.8	0.2	0.286	0	Medium
3	70	70.4	0.4	0.571	0.3	Coarse
4	70	70.2	0.2	0.286	0	Medium
5	70	69.5	0.5	0.714	0	Coarse
Height					
Test Number	CAD Height (mm)	Measured Height (mm)	Height Error (mm)	Accuracy (%)	Stability (mm)	Tolerance Grade
1	27	26.8	0.2	0.741	0.1	Fine
2	27	26.6	0.4	1.481	0.1	Coarse
3	27	26.6	0.4	1.481	0.1	Coarse
4	27	26.7	0.3	1.111	0	Coarse
5	27	26.6	0.4	1.481	0	Coarse

Dimensional Checklist - Feature 4						
Length						
Test Number	CAD Length (mm)	Measured Length (mm)	Length Error (mm)	Accuracy (%)	Stability (mm)	Tolerance Grade
1	170	169.7	0.3	0.176	0.1	Medium
2	170	169.6	0.4	0.235	0.2	Medium
3	170	169.5	0.5	0.294	0	Medium
4	170	169.4	0.6	0.353	0	Coarse
5	170	169.2	0.8	0.471	0.1	Coarse
Width						
Test Number	CAD Width (mm)	Measured Width (mm)	Width Error (mm)	Accuracy (%)	Stability (mm)	Tolerance Grade
1	75	74.9	0.1	0.133	0	Fine
2	75	75.1	0.1	0.133	0.1	Fine
3	75	74.8	0.2	0.267	0	Medium
4	75	74.7	0.3	0.400	0.1	Medium
5	75	74.9	0.1	0.133	0.1	Fine
Height						
Test Number	CAD Height (mm)	Measured Height (mm)	Height Error (mm)	Accuracy (%)	Stability (mm)	Tolerance Grade
1	25	24.5	0.5	2.000	0	Coarse
2	25	24.5	0.5	2.000	0.1	Coarse
3	25	24.7	0.3	1.200	0.2	Coarse
4	25	24.7	0.3	1.200	0.1	Coarse
5	25	24.8	0.2	0.800	0	Medium

			Dimensional Checklist - Feature 5			
			Thickness			
Test Number	CAD Thickness (mm)	Measured Thickness (mm)	Thickness Error (mm)	Accuracy (%)	Stability (mm)	Tolerance Grade
1	10	10.1	0.1	1.000	0	Fine
2	10	10.2	0.2	2.000	0	Medium
3	10	10	0	0.000	0.1	Fine
4	10	10.1	0.1	1.000	0	Fine
5	10	10.2	0.2	2.000	0.1	Medium

Appendix E4 – Statistical Analysis for Features 2, 3, 4 and 5.

Statistical Analysis for Feature 2			
	Measured Length	_Measured Width_	_Measured Height_
Mean (mm)	89.98	84.84	26.56
Standard Deviation (mm)	0.2683	0.1140	0.0894
Standard Deviation of the Means (mm)	0.1200	0.0510	0.0400
_N_	5	5	5
Sum (mm)	449.9	424.2	132.8
_v_	4	4	4
_$t_{4,95}$_	2.776	2.776	2.776
True mean x' (mm ± mm)	89.98 ± 0.333	84.84 ± 0.142	26.56 ± 0.111
Repeatability Error (%)	0.2683	0.1140	0.0894

Feature 2 Length Analysis

Feature 2 Width Analysis

Feature 2 Height Analysis
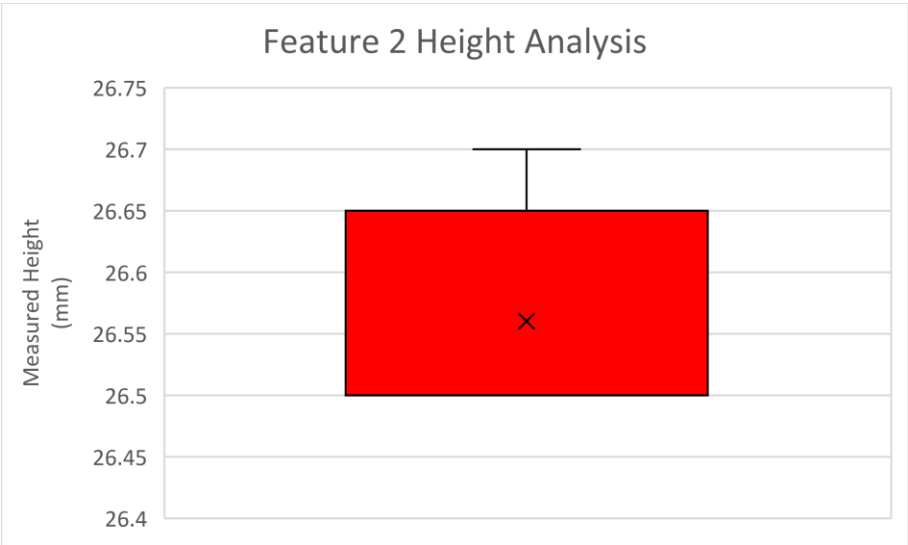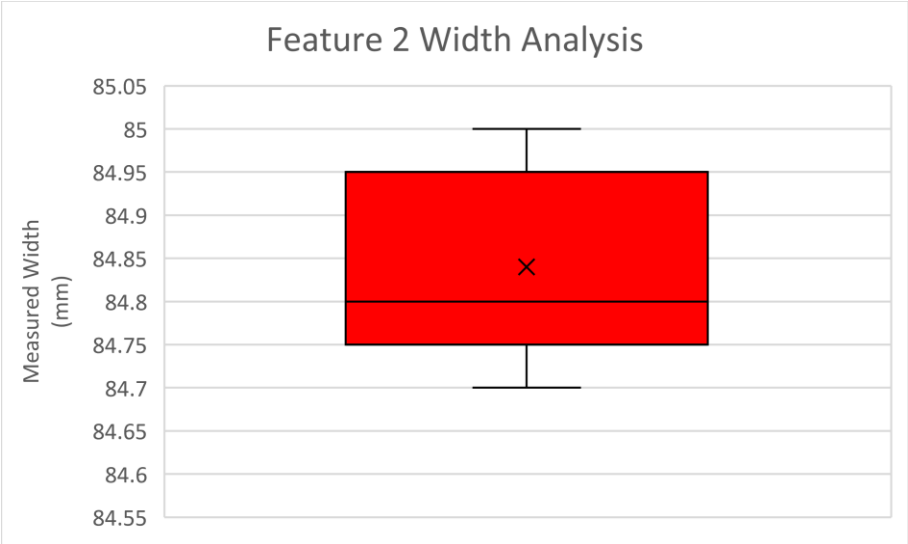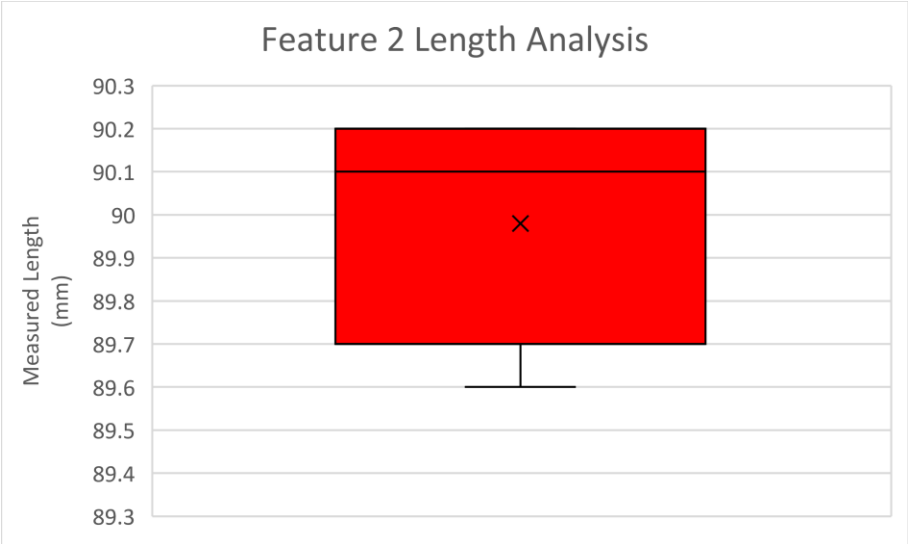
Statistical Analysis for Feature 3			
	Measured Length	_Measured Width_	_Measured Height_
Mean (mm)	84.62	69.92	26.66
Standard Deviation (mm)	0.1924	0.3701	0.0894
Standard Deviation of the Means (mm)	0.0860	0.1655	0.0400
_N_	5	5	5
Sum (mm)	423.1	349.6	133.3
_v_	4	4	4
$t_{4,95}$	2.776	2.776	2.776
True mean x' (mm ± mm)	84.62 ± 0.239	69.92 ± 0.46	26.66 ± 0.111
Repeatability Error (%)	0.1924	0.3701	0.0894

Feature 3 Length Analysis

Feature 3 Width Analysis

Feature 3 Height Analysis
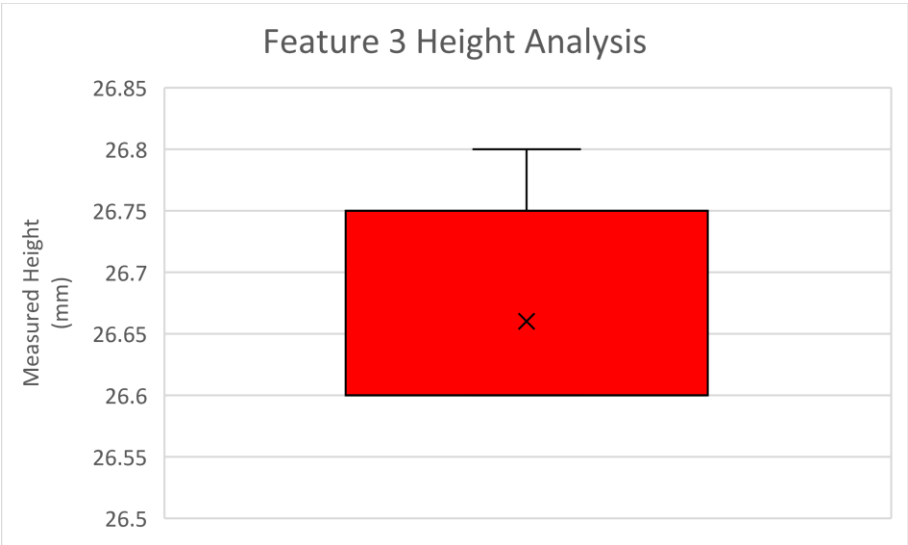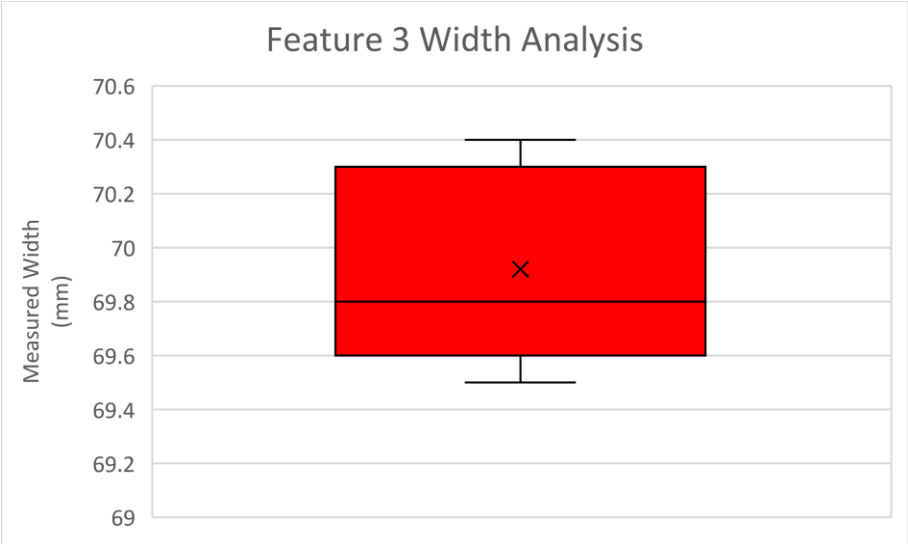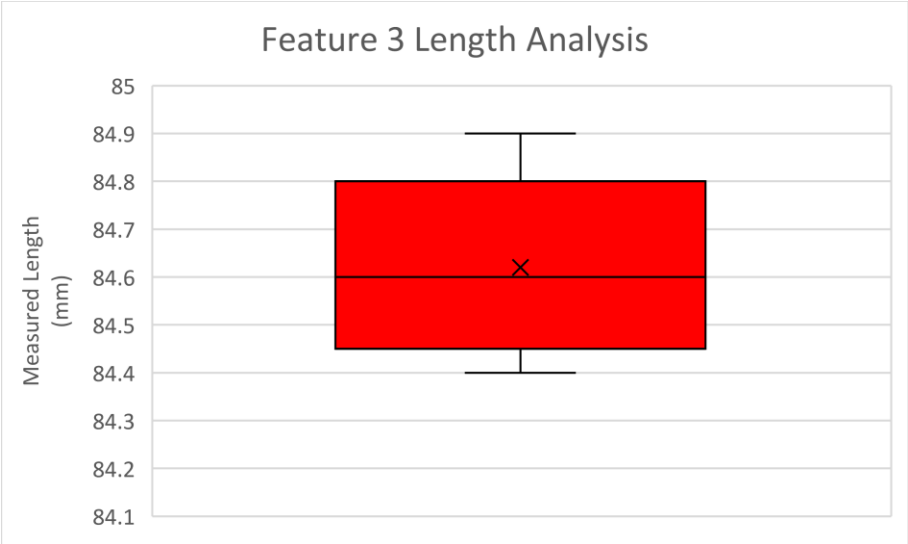
Statistical Analysis for Feature 4			
	Measured Length	_Measured Width_	_Measured Height_
Mean (mm)	169.48	74.88	24.64
Standard Deviation (mm)	0.1924	0.1483	0.1342
Standard Deviation of the Means (mm)	0.0860	0.0663	0.0600
_N_	5	5	5
Sum (mm)	847.4	374.4	123.2
_v_	4	4	4
$t_{4,95}$	2.776	2.776	2.776
True mean x' (mm ± mm)	169.48 ± 0.239	74.88 ± 0.184	24.64 ± 0.167
Repeatability Error (%)	0.1924	0.1483	0.1342

Feature 4 Length Analysis

Feature 4 Width Analysis

Feature 4 Height Analysis
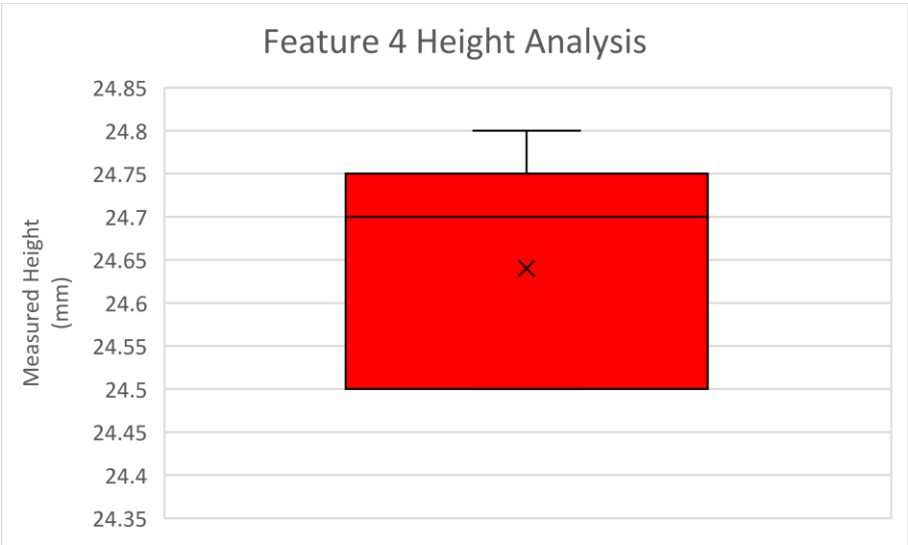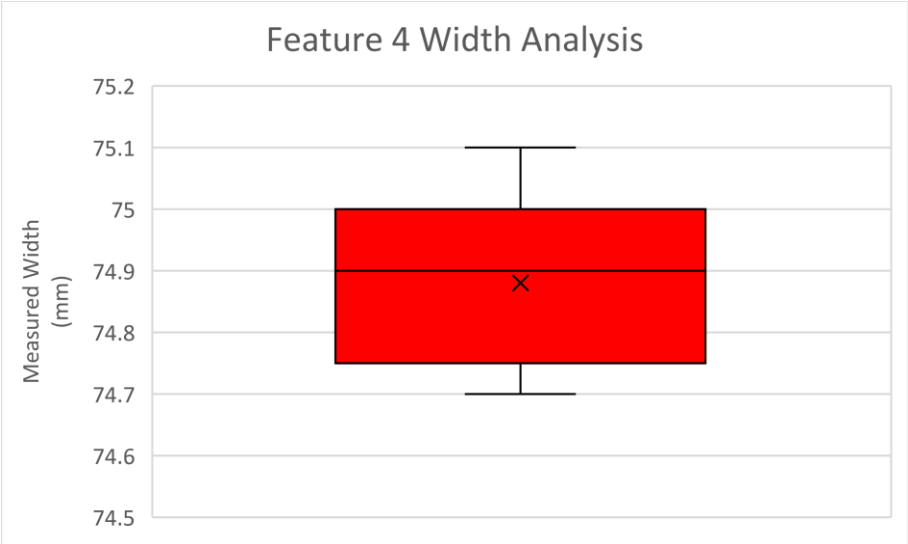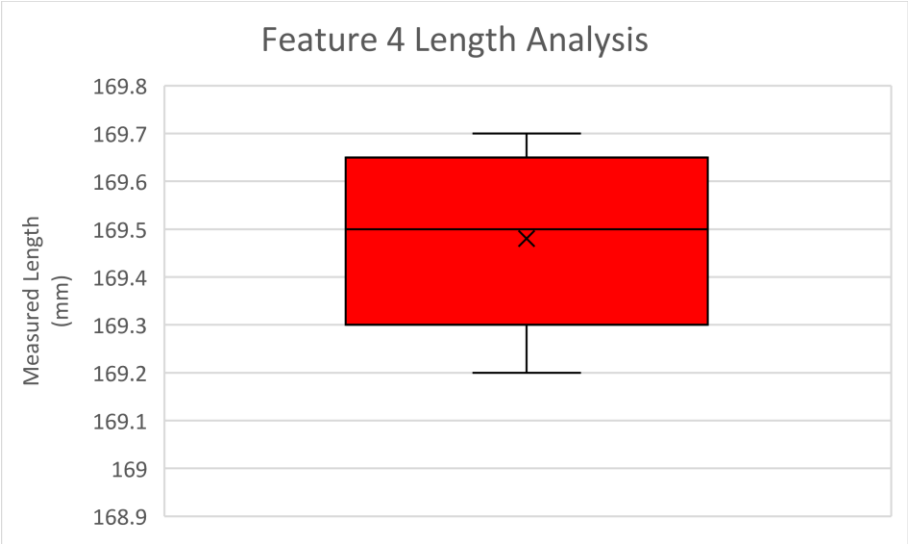
Statistical Analysis for Feature 5	
	Measured Thickness
Mean (mm)	10.12
Standard Deviation (mm)	0.0837
Standard Deviation of the Means (mm)	0.0374
N	5
Sum (mm)	50.6
v	4
$t_{4,95}$	2.776
True mean x' (mm ± mm)	10.12 ± 0.104
Repeatability Error (%)	0.0837

Feature 5 Thickness Analysis
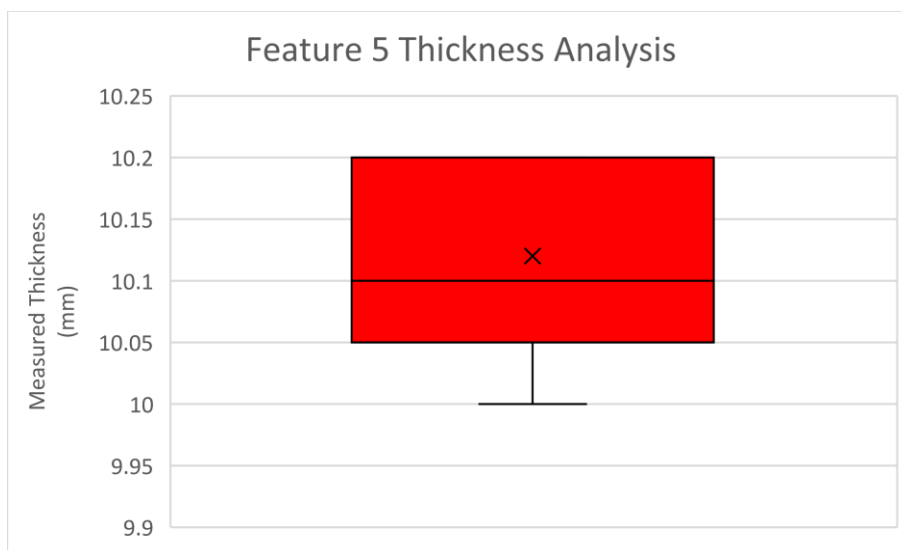
Appendix E5 – Outlier Detection for Features 2, 3, 4 and 5.

Outlier Detection for Feature 2 - Length				
Test Number	_$(x_i - \bar{x})^2$ (mm)_	_z_0_	_P(z_0)_	_Outlier?_
1	0.0324	0.67	0.2486	No
2	0.1444	1.42	0.4222	No
3	0.0484	0.82	0.2939	No
4	0.0144	0.45	0.1736	No
5	0.0484	0.82	0.2939	No
Outlier Detection for Feature 2 - Width				
Test Number	_$(x_i - \bar{x})^2$ (mm)_	_z_0_	_P(z_0)_	_Outlier?_
1	0.0036	0.53	0.2019	No
2	0.0016	0.35	0.1368	No
3	0.0256	1.40	0.4192	No
4	0.0196	1.23	0.3907	No
5	0.0016	0.35	0.1368	No
Outlier Detection for Feature 2 - Height				
Test Number	_$(x_i - \bar{x})^2$ (mm)_	_z_0_	_P(z_0)_	_Outlier?_
1	0.0036	0.67	0.2486	No
2	0.0036	0.67	0.2486	No
3	0.0196	1.57	0.4418	No
4	0.0016	0.45	0.1736	No
5	0.0036	0.67	0.2486	No

Outlier Detection for Feature 3 - Length				
Test Number	$(x_i - \bar{x})^2$ *(mm)*	z_0	$P(z_0)$	*Outlier?*
1	0.0064	0.42	0.1628	No
2	0.0484	1.14	0.3729	No
3	0.0144	0.62	0.2324	No
4	0.0004	0.10	0.0398	No
5	0.0784	1.46	0.4279	No
Outlier Detection for Feature 3 - Width				
Test Number	$(x_i - \bar{x})^2$ *(mm)*	z_0	$P(z_0)$	*Outlier?*
1	0.0484	0.59	0.2224	No
2	0.0144	0.32	0.1255	No
3	0.2304	1.30	0.4032	No
4	0.0784	0.76	0.2764	No
5	0.1764	1.13	0.3708	No
Outlier Detection for Feature 3 - Height				
Test Number	$(x_i - \bar{x})^2$ *(mm)*	z_0	$P(z_0)$	*Outlier?*
1	0.0196	1.57	0.4418	No
2	0.0036	0.67	0.2486	No
3	0.0036	0.67	0.2486	No
4	0.0016	0.45	0.1736	No
5	0.0036	0.67	0.2486	No

Outlier Detection for Feature 4 - Length				
Test Number	_$(x_i - \bar{x})^2$ (mm)_	_z_0_	_$P(z_0)$_	_Outlier?_
1	0.0484	1.14	0.3729	No
2	0.0144	0.62	0.2324	No
3	0.0004	0.10	0.0398	No
4	0.0064	0.42	0.1628	No
5	0.0784	1.46	0.4279	No
Outlier Detection for Feature 4 - Width				
Test Number	_$(x_i - \bar{x})^2$ (mm)_	_z_0_	_$P(z_0)$_	_Outlier?_
1	0.0004	0.13	0.0517	No
2	0.0484	1.48	0.4306	No
3	0.0064	0.54	0.2054	No
4	0.0324	1.21	0.3869	No
5	0.0004	0.13	0.0517	No
Outlier Detection for Feature 4 - Height				
Test Number	_$(x_i - \bar{x})^2$ (mm)_	_z_0_	_$P(z_0)$_	_Outlier?_
1	0.0196	1.04	0.3508	No
2	0.0196	1.04	0.3508	No
3	0.0036	0.45	0.1736	No
4	0.0036	0.45	0.1736	No
5	0.0256	1.19	0.383	No

Outlier Detection for Feature 5 - Thickness				
Test Number	_$(x_i - \bar{x})^2$ (mm)_	_z_0_	_$P(z_0)$_	_Outlier?_
1	0.0004	0.24	0.0948	No
2	0.0064	0.96	0.3315	No
3	0.0144	1.43	0.4236	No
4	0.0004	0.24	0.0948	No
5	0.0064	0.96	0.3315	No